UNIVERSITY OF CALIFORNIA
RIVERSIDE

Unconventional Seed-Mediated Growth of Non-Spherical Plasmonic Nanostructures

A Dissertation submitted in partial satisfaction
of the requirements for the degree of

Doctor of Philosophy

in

Chemistry

by

Ji Feng

December 2018

Dissertation Committee:
Dr. Yadong Yin, Chairperson
Dr. Ming Lee Tang
Dr. De-en Jiang

The Dissertation of Ji Feng is approved:

Committee Chairperson

University of California, Riverside

Acknowledgments

I would like to express my most profound gratitude to my advisor, Prof. Yadong Yin, for his academic advice and direction. I am ever grateful to him, and I am lucky to have the opportunity to work under his guidance. His insightful and knowledgeable guidance helps me to explore the mystery of nanoworld, and his wise and enlightened insight helps me to understand the real big world better.

I am also very thankful to my other committee members, Prof. Ming Lee Tang, and Prof. De-en Jiang, for their time spent in my final defense and valuable comments on my dissertation.

I would like to thank my project collaborators: Dr. Jinxing Chen, Dr. Wenshou Wang, Dr. Dongdong Xu, Dr. Chuanbo Gao, Dr. Yifan Ye, Dr. Haizhou Liu, and Gongde Chen and I learned a lot from them. I am much indebted to many past and current members of Yin group for providing a rich working experience, intellectual stimulation, and friendship: Dr. Le He, Dr. Michael Dahl, Dr. Mingsheng Wang, Dr. Yiding Liu, Dr. Yaocai Bai, Dr. Lishun Fu, Dr. Wenjing Xu, Dr. Xiaojing Wang, Zhiwei Li, Fan Yang, Rashed Aleisa, Dr. Yoon Jae Lee, Dr. Anirban Das, Qingsong Fan, Chaolumeng Wu, Dr. Yongqing Wang, Dr. Aiwei Tang, Dr. Dawei Wang, Dr. Shichuan Li, Dr. Chunyu Zhou, Dr. Mingfu Gong, Dr. Aiqin Gao, Dr. Yun Liu, Shuai Zhou, Lan Peng, Panpan Xu, Wenwen Yin, Bo Li, Xiaojun Zeng, Zhouhui Xia, Zhenyuan Liu et al. I would also like to thank the undergraduate and high school students who have worked and are working with me right now: Angel Kuo, Jin Jung, Tianyu Su, and Guy Moore. I thank Dr. Krassimir N. Bozhilov, Dr. Mathias Rommelfanger, and Dr. Michael Pigeon for

assistance in using facilities in CFAMM; Dr. Dan Borchardt for assistance in using optical facilities in Chemistry department. I also would like to thank Dr. Kevin Simpson for his help and guidance during my teaching.

I am incredibly grateful to my family for their support and understanding, which make this thesis possible. My thanks also go to my friends Dr. Guoxiang Hu, Dr. Yufei Ni, Dr. Yaokai Duan, and Yue Jin for their valuable help.

Dedication

To Shufang, Peng and Lyuye.

ABSTRACT OF THE DISSERTATION

Unconventional Seed-Mediated Growth of Non-Spherical Plasmonic Nanostructures

by

Ji Feng

Doctor of Philosophy, Graduate Program in Chemistry
University of California, Riverside, December 2018
Dr. Yadong Yin, Chairperson

Noble metal nanostructures with tunable localized surface plasmon resonance (LSPR) frequency have attracted significant attention due to their broad applications in chemical sensing, photothermal therapy, and energy conversion. Because the resonance is sensitive to the particle geometry, a significant amount of efforts have been made to develop non-spherical metal nanostructures which provide access to many interesting plasmonic absorption and scattering phenomena that are not seen in spherical ones. Although conventional wet chemical methods have been proved to be powerful for the synthesis of non-spherical nanostructures, it still has limitations of being only applicable to specific materials and lacking effective mechanisms for controlling the orientation of the nanostructures collectively. In this dissertation, we discuss our unconventional methods for the synthesis of non-spherical plasmonic nanostructures.

Firstly, we developed a seed-mediated growth for creating secondary structures of Au on spherical Au seeds. The formation of nanoislands is induced by modifying the seeds with Pt to create a mismatched surface for metal deposition. The number of the islands on each seed can be controlled by adjusting the reaction parameters from three

aspects: the strain energy, the degree of oxidative ripening and the diffusion of metal precursors on the surface of the metal seed. It is worth noting that ligand-assisted ripening, should be considered as an important factor to tune the structure of the nanoparticle. By integrating all the important parameters, Au satellite structure, dimers, trimers and tetramers were obtained. It is worth noting that the Au dimers synthesized by using this method is of controllable particle size, high purity, well-defined structures and unique optical property, which has not been reported previously.

Through the study of the optical properties of dimers, we found out that the plasmonic resonance of dimers could be separated into two modes: a transverse mode and a longitudinal mode, which can be excited by light polarized along the short side and the long side of the dimers, respectively. The two modes correspond with light absorption at different wavelengths, which have never been carefully studied and utilized before. The key to split the resonant mode of dimers is to control their orientation under polarized light. To control the orientation of the dimer structures, we developed a stepwise seeded growth method for the synthesis of self-registered anisotropic plasmonic nanostructures. The synthesis requires using colloidal nanoparticle as substrates for the assembly of the metal seeds, and precise control over the exposure of the metal seeds by surface passivation. The anisotropic seeded growth of metal nanostructure can be induced by creating a physical barrier on the seeds, which partially passivates the exposed area of the seeds. Au dimers, linear trimers and Au-Ag dimers with distinguishable plasmonic excitation bands have been synthesized. This method is very versatile for the synthesis of other metals and semiconductors, for example, Pd and Cu_2O.

This synthesis method results in rod-like nanostructures perpendicularly registered to the substrates. Taking advantages of this unique feature, we report dynamic tuning of the plasmonic excitation of Au-Au and Au-Ag dimers by controlling their orientation relative to the incident light. Such tuning is enabled by switching the substrate to anisotropic magnetic nanoparticles, whose orientation can be magnetically controlled. By tuning the direction of the magnetic field, we are able to control the excitation of plasmonic modes of the Au-Au dimers and Au-Ag dimers under the incidence of polarized light. The optical switching of Au-Au and Au-Ag dimers exhibits bright colors with high contrast. The nanostructures with orthogonal orientations are fixed in the hydrogel to obtain anti-counterfeiting patterns.

Table of Contents

List of Figures

Chapter 1 Introduction to Seed-Mediated Growth of Non-Spherical Plasmonic Nanostructures

1.1 Overview

Nanomaterials has attracted continuous attention from the beginning of its discovery. When the size of the material is brought down to the nanometer scale, many properties of the material will change accordingly. Comparing to their bulk counterparts, nanomaterials have large surface area and high surface energy. Importantly, the localized surface plasmon resonance (LSPR), which is generated by the interaction between the light wave and electrons in the conduction band of a nanoparticle, could bring more applications to the nanomaterials, such as chemical sensing, optoelectronics, catalysis, and photothermal therapy.[1-4] When the material is fixed, the LSPR frequency is highly related to the size, shape, surrounding medium of the nanoparticle, the distance between the nanoparticles and the alignment of anisotropic nanoparticles in the light field.[5-7] In the past decades, LSPR tuning has been widely studied to meet requirement of different applications. Among them, seed-mediated growth, which is a general strategy to synthesize nanocrystals with well-controlled size, shape and composition, plays a major role in the LSPR tuning of nanostructures.

In this chapter, we would like to focus on the well-established theories and recent progress in the field of seed-mediated growth of plasmonic nanostructures. We start with a brief introduction to the rise of nanotechnology and the novel physicochemical properties which have arisen from the nanomaterials, followed by introduction of plasmonic resonance. After that, we will discuss the basic concept of seed-mediated

growth of plasmonic nanostructures. By analyzing the similarity between products and seeds, we divide seed-mediated growth in two method, conventional seed-mediated growth and unconventional seed-mediated growth. The detailed information regarding thesis two synthetic strategies will be discussed in Section 1.2 and 1.3. Although impressive progress has been achieved in nanotechnology, there are some great challenges facing the research community, which will be discussed in Section 1.4. And scope of this dissertation will be displayed in Section 1.5.

1.1.1 History of nanotechnology

Generally, nanotechnology deals with materials at the atomic, molecular or macromolecular level in the length scale of approximately 1-100 nanometers range. It is a complex and highly interdisciplinary science: it integrates chemistry, physics, materials science, engineering, biology, medicine, etc. Although "nanotechnology" is modern terminology, people have been using nanotechnology in their daily lives since very early. For example, in the 4th century, Romans fabricated the dichroic Lycurgus Cup, which could show a different color depending on whether or not light is passing through it.[8] The dichroic effect is achieved by mixing gold-silver alloy nanoparticles in the glass. So that it appears opaque green when lit from outside but translucent red when light shines through the inside. Not only that, in about 6th-15th century, gold nanoparticles have been used to make stained-glass windows with brilliant colors, which have been used to decorate the cathedrals in European. These workers became the earliest researchers in the field of nanotechnology without knowing it.

The first scientific description of nanotechnology is the preparation of "ruby" gold colloids, which was reported by Michael Faraday in 1857.[9] Soon after that, the ideas and concepts of nanotechnology started with a talk entitled "There's Plenty of Room at the Bottom", presented by Richard Feynman at an American Physical Society meeting at the California Institute of Technology in 1959.[10] In his talk, Feynman described a process of writing and reading the Encyclopedia on the head of a pin, and proposed several advantages of making things small into nanometer scale in bioscience, data storage, mechanical engineering and chemical synthesis. He predicted that it should be possible for scientist to design new molecule by arranging atoms one by one, and get an enormously greater range of possible properties that substances can have. Over a decade later, Professor Norio Taniguchi in Tokyo University of Science coined the term nanotechnology to describe semiconductor processes such as thin film deposition and ion beam milling exhibiting characteristic control on the order of a nanometer.[11] With the development of the characterization methods, especially electron microscopy techniques, including transmission electron microscopy (TEM), scanning electron microscopy (SEM), atomic force microscopy (AFM), that modern nanotechnology began. Over the past several decades, the research in nanotechnology has achieved impressive progress, which benefits the human society in many ways. For example, carbon nanotubes have been used to make sports equipment stronger and lighter weight. TiO_2 and ZnO_2 nanoparticles are used in transparent sunscreens to effectively absorb light and make the sunscreen spread more easily over the skin. Silver nanoparticles are used in fabric to kill bacteria and make clothing odor-resistant.

Nowadays, nanotechnology is attracting more and more attention in medicine, cancer diagnose, catalysis, electronics, food packaging, fuel cells, solar cells, and batteries.[12-16] It is believed that nanotechnology is a key technology for the future.

1.1.2 Introduction of surface plasmon resonance

Plasmonic nanostructures have attracted continuous attention due to their wide application in sensing, optoelectronics, catalysis and photothermal therapy.[1, 17] Surface plasmon resonance (SPR) refers to the collective oscillations of the conduction electrons in metallic nanostructures. occurs in two distinct forms: localized SPR (LSPR) and propagating surface plasmon polaritons (SPPs). LSPR occurs when the dimensions of a metallic nanostructure are less than the wavelength of incident light, leading to collective but non-propagating oscillations of surface electrons in the metallic nanostructure.[1] The hot electrons can vibrationally activate adsorbates at the metal surface and catalyze the reactions, such as Suzuki coupling, water splitting, ethylene and propylene epoxidation, NH_3 oxidation, and CO oxidation. Besides, plasmonic nanostructures have been widely investigated for chemical/bio-sensing. It has been demonstrated that nanostructures with edges or sharp tips show advantages for surface-enhanced Raman scattering (SERS), due to the strong enhancement of electric field intensity on the surface of nanocrystals.[18] Moreover, plasmonic nanostructures display considerable photothermal effect, which has been studied in cancer therapy.[19] In addition, plasmonic nanostructures can be engineered to optical nano-antennas, which could enable control and manipulation of optical fields at nanoscale regions.[20]

Mie theory provides calculation for the plasmonic extinction (absorption + scattering) cross section of a metal nanosphere:

$$C_{ext} = \frac{24\pi^2 R^3 \varepsilon_m^{3/2}}{\lambda}\left[\frac{\varepsilon_i}{(\varepsilon_r + 2\varepsilon_m)^2 + {\varepsilon_i}^2}\right]$$

where C_{ext} is the extinction cross section, R is the radius of the nanosphere, and ε_m, ε_r and ε_i are the relative dielectric constant of the medium surrounding the nanosphere, and the real and imaginary part of the dielectric function of the metal.[21] In a situation with a fixed particle size and surrounding media, C_{ext} largely depends on the intrinsic dielectric properties of the metal species. According to the equation, when ε_r is close to $-2\varepsilon_m$, the nanoparticle is expected to have the largest C_{ext}. In addition, the ε_i should be close to zero to maximize the C_{ext}. Such requirement could only be matched with some metal species. Another important factor that need to be considered is the quality factor, which is proportionally related to the strength of the surface plasmon. Taken altogether, some metal nanocrystals show LSPR in visible light range, such as Cu, Ag, Au, and Al, and some are responsive under ultraviolet light irradiation, such as Rh, Pd, and Pt.[22] Among all of the metal species, Ag has the largest quality factor across most of the spectrum from 300 to 1200 nm.[21] The LSPR of Au and Cu are limited to wavelengths higher than 500 and 600 nm, due to interband transition, where electrons are excited to higher energy levels.[21]

It is found that the wavelength of LSPR for a certain metal is highly dependent on the shape of the nanoparticle.[23] For example, the optical property of Au nanospheres and nanorods are quite different. The former shows a strong absorption band in the visible

region of the electromagnetic field at about 520 nm; While the later has two absorption band at both higher and lower wavelength.[5, 24] The optical property of Au non-spherical nanocrystals should be understood by using Gans theory, in which the extinction coefficient γ of randomly oriented particles can be simulated.[25] According to Gans, the extinction coefficient γ can be calculated by the following equation:

$$C_{ext} = \frac{2\pi NV\varepsilon_m^{3/2}}{3\lambda}\sum_j \frac{(1/P_j^2)\varepsilon_i}{(\varepsilon_r + \frac{1-P_j}{P_j}\varepsilon_m)^2 + \varepsilon_i^2}$$

where N is the number of particles per unit volume, V is the volume of each particle. P_j are the depolarization factors for the three axes A, B, C of the rod with A > B = C. P_A, P_B and P_C are defined as:

$$P_A = \frac{1-e^2}{e^2}\left[\frac{1}{2e}\ln\left(\frac{1+e}{1-e}\right) - 1\right]$$

$$P_B = P_C = \frac{1-P_A}{2}$$

where e is related to the aspect ratio of the Au nanorods. Following Gans theory, people have figured out the relationship between the aspect ratio of Au nanorods and the maximum absorption wavelength: λ_{max} = (52.95R - 41.68) ε_m + 466.38. This equation shows that the maximum absorption wavelength of Au nanorods depends only on the aspect ratio R and the dielectric constant of the surrounding medium ε_m.[26-27]

1.1.3 General concept of seed-mediated growth

Seed-mediated growth is an effective method to synthesize metal nanocrystals with well-

defined shape, size, structure and composition.[28-30] In 2001, Murphy and co-workers firstly reported the growth of Au nanorods on Au colloidal nanoparticles.[31] After that, the strategies and mechanism of seed-mediated growth of different plasmonic metal nanostructures has been intensively studied. A flourishing development was seen on the synthesis of metal nanocrystals with high uniformity and well-defined nanostructures, such as nanospheres, nanocubes, octahedrons, tetrahedrons, decahedrons, icosahedrons, bipyramid, nanorods, nanowires, nanoplates, nanoshells and nanosatellites.[32-38]

In general, seed-mediated growth is a two-step synthetic process. The first step is the synthesis of metal nanoparticle seeds. In most of the cases, the seeds can be used without purification. The second step is the growth step, which is performed by injecting a precursor solution into a solution containing the colloidal seeds, reductants, capping agent and stabilizer/surfactants (Figure 1.1).[28] The metal precursor is reduced to form zero-valent atoms, which then heterogeneously nucleate on the surface of the seeds. Continued growth of the seeds results in the formation of well-defined nanocrystals. Comparing with one-step synthesis, which integrates the seeding and growth through direct reduction of metal precursors, the two-step seed-mediated growth show advantages in many aspects: (1) the sizes of the products can be widely tuned by varying the ratio of precursors to the seeds; (2) nanocrystals with predictable morphologies can be synthesized by controlling the reaction conditions in the growth step; (3) a vast number of crystal morphologies can be obtained by the combination of different seeding and growth steps; (4) the mechanism for crystal growth under different reaction conditions can be very well studied. It is obvious that seed-mediated growth has better control over the

growth process by separating the growth step from the nucleation step.

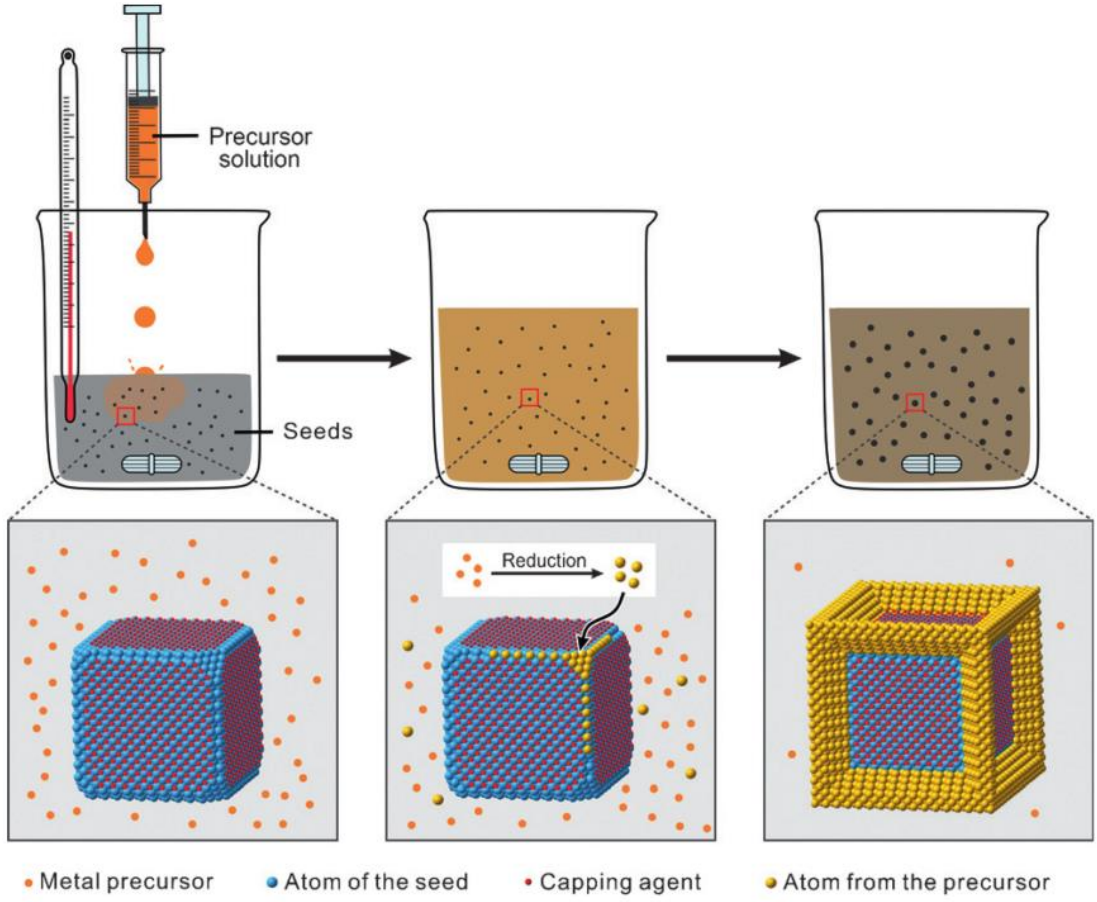

Figure 1.1 General strategy used for the seed-mediated growth of colloidal metal nanocrystals. Copyright © 2017 Wiley-VCH.[28]

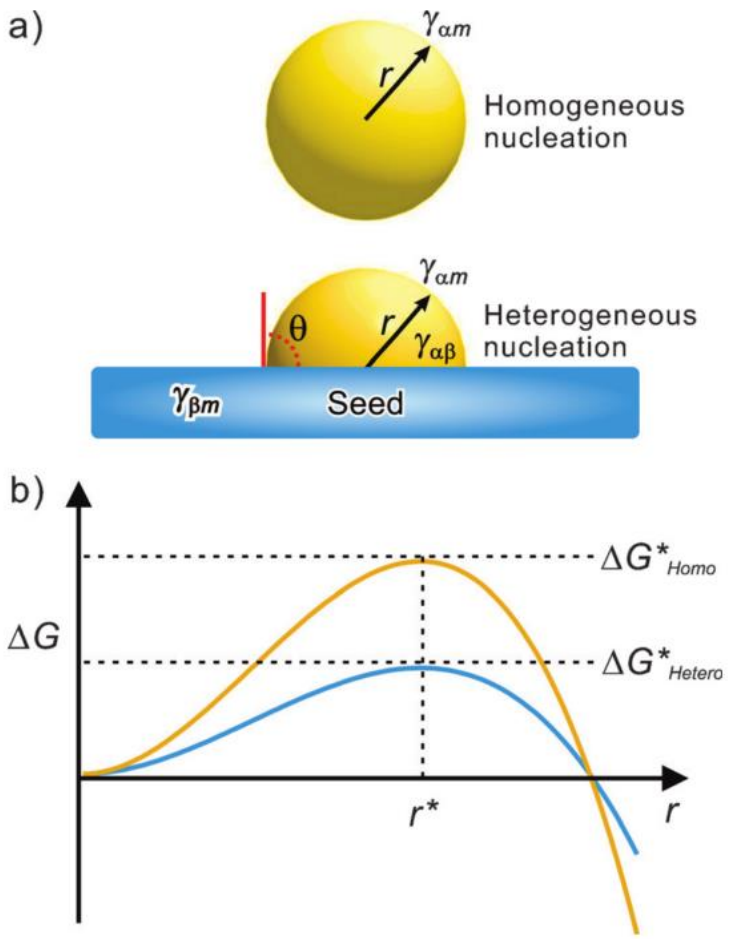

Figure 1.2 Comparison of homogeneous nucleation with heterogeneous nucleation: a) scheme and b) change in Gibbs free energy as a function of size. Copyright © 2017 Wiley-VCH.[28]

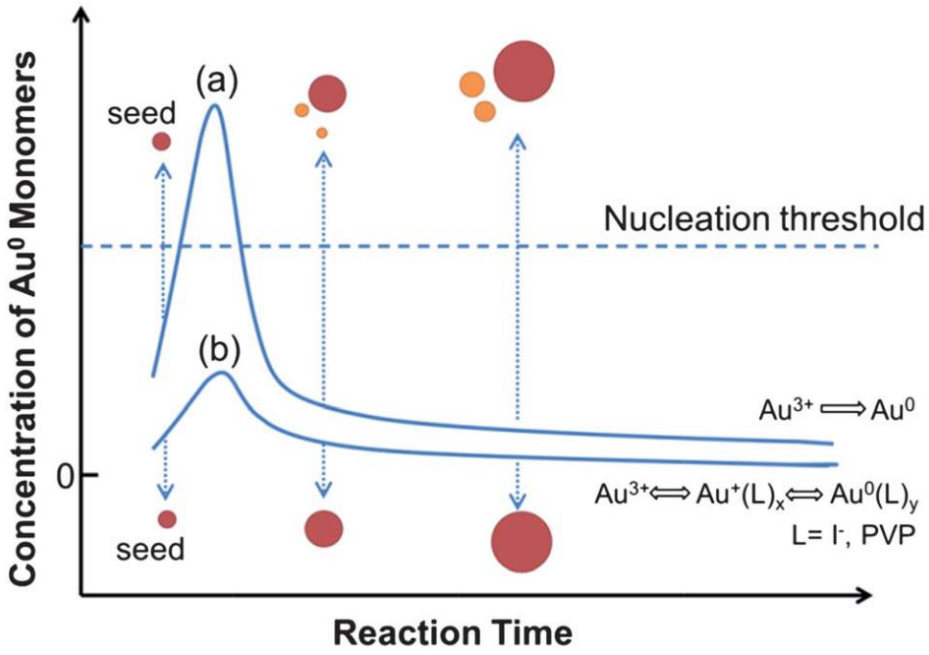

Figure 1.3 Schematic diagram depicting the stages of the growth of Au nanoparticles in a seeded synthesis without (a) and with (b) self-nucleation being suppressed by additional coordinating ligands. Copyright © 2012 The Royal Society of Chemistry.[39]

Some key parameters to a successful seed-mediated growth has been studied in previous reports, such as the internal structure of the seeds, nucleation of the metal precursor in the growth step, effect of ligands, reaction kinetics and diffusions. We will use examples to analyze them in the corresponding paragraphs. Above all, it should be noted that control of the nucleation step is very important to a good seed-mediated growth. Homogeneous nucleation should be avoided in order to prevent the formation of nanocrystals with diverse sizes, shapes, morphologies, and internal structures. As it has been theoretically studied, the free energy of heterogeneous nucleation is lower than the free energy of homogeneous nucleation when the nuclei are of the same sizes, indicating less driving force for heterogeneous nucleation than homogeneous nucleation (Figure 1.2).[28] In another word, the free energy of a successful seed-mediated growth should be kept in between the thresholds of heterogeneous nucleation and homogeneous nucleation. Practically, a seed-mediated growth prefers a reaction system at relatively low temperature and with low concentration of both metal precursors and reductants. Usually, people used a syringe pump to control the injection rate of the precursor into a suspension of seeds and reductants in order to limit the concentration of the metal precursor below the threshold of homogeneous nucleation. A vivid example is the seed-mediated growth of Au nanospheres (Figure 1.3).[39] Firstly, the Au seeds were prepared by quickly reducing $HAuCl_4$ with $NaBH_4$ in the presence of trisodium citrate, which was used as a ligand to provide electrostatic repulsion to stabilize the Au seeds. The following growth step required preparation of a growth solution, which employed polyvinylpyrrolidone (PVP) as the capping agent to stabilize the Au^0 monomers after initial reduction and preventing

interparticle agglomeration, potassium iodide (KI) as an additional coordinating ligand, and ascorbic acid (AA) as a weak reducing agent. It is worth noting that the introduction of KI leads to coordination of I^- with Au^{3+} ions, which effectively decreases the reduction potential of the Au salt. By this means, the equilibrium concentration of Au^0 reduced by AA is greatly decreased. Therefore, the deposition rate of the metal precursor can be greatly reduced to avoid self-nucleation while maintaining a high precursor concentration in the growth solution. Thanks to the use of KI and PVP, the growth solution is transparent and colorless, and could be kept with no change for 1 hour. Au nanospheres with size range from several nanometers to 200 nm could be successfully synthesized by adjusting the volume ratio between the seed solution and the growth solution.

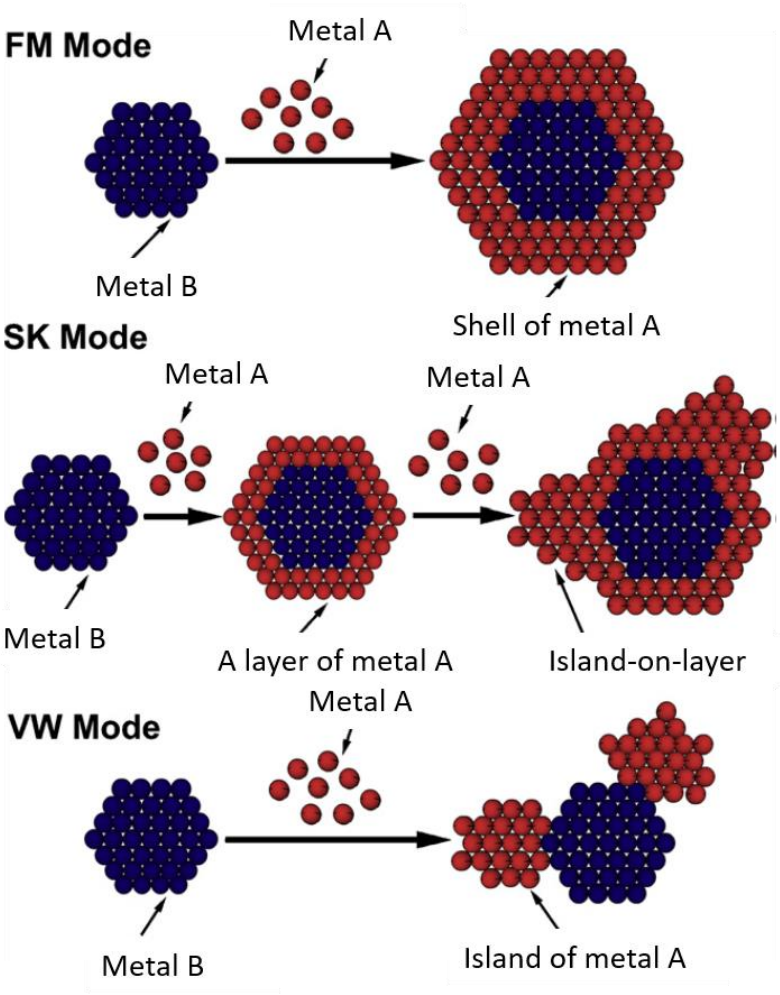

Figure 1.4 Schematic illustration of three different growth modes. Copyright © 2009 Elsevier.[40]

Seed-mediated growth is governed by a set of thermodynamic and kinetic parameters. When deposit metal A on surface of metal B, the deposition mode is largely determined by the surface energies of three interfaces (Figure 1.4): γ_A for surface energy of metal A in solution, γ_B for surface energy of metal B in solution, and γ_i for interfacial energy of metal A and B. The overall excess energy ($\Delta\gamma$) is created to include the contribution of these four energy terms according to the following equation: $\Delta\gamma = \gamma_A + \gamma_i + \gamma_{strain} - \gamma_B$, in which γ_{strain} is the strain energy.[41-42] Depending on the overall excess energy, three type of growth modes have been observed: Frank-van der Merwe (FM) or layer-by-layer mode, Volmer-Weber (VW) or island growth mode, and Stranski-Krastanov (SK) mode. One important factor that need to be considered is the lattice mismatch, which can be calculated according to the following equation: lattice mismatch = $100 \times |(a_B - a_A)/a_B|$, in which a_A and a_B are the lattice constant of metal A and metal B, respectively.[43] This mismatch induces a positive γ_{strain}, which increases rapidly with the growth of nuclei. When the deposited metal has a small lattice mismatch with the seed, and the sum of γ_A, γ_i, and γ_{strain} is smaller than γ_B, layer-by-layer deposition (FM mode) is favorable (negative $\Delta\gamma$). In contrast, $\Delta\gamma$ becomes positive if the system has a large γ_{strain}, or the sum of γ_A, γ_i, and γ_{strain} is bigger than γ_B, leading to deposition of metal A on the high energy sites of metal B (VW mode). SK mode occurs when the system has large γ_{strain}, but initially the sum of γ_A, γ_i, and γ_{strain} is smaller than γ_B, metal A will grow in layer-by-layer fashion first. When the A layers grow thick enough (typically > 3 atomic layers), there will no longer be an energy benefit for wetting, and island growth will take over. The theory of the 'three growth modes' is effective in understanding the formation mechanism

of some complex nanostructures, such as core-shell, dumbbell, and particle-on-particle structures. Nanocrystals grown in VW and SK modes always have different symmetry from the nanocrystal seeds. However, in real application, the nanostructure is also determined by ligands, which greatly affect the energies of the growing surfaces and growth kinetics.

In the following section, we will discuss the seed-mediated synthesis of non-spherical plasmonic metal nanostructures. The synthetic methods are divided into conventional and unconventional methods (Figure 1.5). Here, we classified the synthetic methods based on whether the structure of the product can be predicted by the seed structure. If the structure of the product is derived from the seeds, the synthetic method will be treated as conventional method. In the section of conventional seed-mediated growth, we will discuss several aspects, such as the internal structures of the seeds, the facet-selective deposition by using ligands and Ag underpotential deposition, and control of reaction kinetics. In the section of unconventional seed-mediated growth, we focus our discussion on mainly two parts: surface modification of the seeds and template-assisted seed-mediated growth. In addition, creation of unconventional nanostructures by control of diffusion will also be included. We will limit our discussion to colloidal synthesis. Some methods, such as lithography, chemical vapor deposition, laser irradiation, that are unique but not using solution phase synthesis will not be discussed in this section.[44-46]

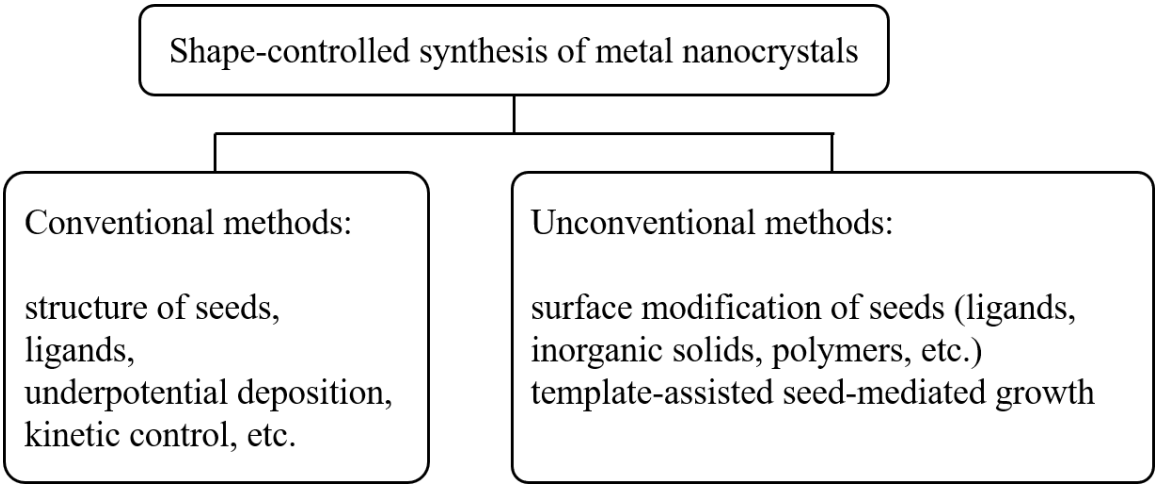

Figure 1.5 Outline of the introduction.

1.2 Conventional Seed-Mediated Growth

The plasmonic properties of metal nanostructures are mainly due to their size, shape and geometrical arrangement. Compared to isotropic spherical particles, anisotropic nanostructures like nanorods, nanoplates, could offer tunability in plasmonic properties by controlling their shapes and geometric arrangement. Conventional seed-mediated growth of plasmonic metal nanocrystals refers to metal nanostructures with structures derived from the seeds. For example, synthesis of Au nanospheres, Ag nanoplates, and Pd nanocubes by using spherical Au seeds, small Ag nanoplates, small Pd nanocubes are considered conventional seeded-growth, because there is no symmetry breaking of the nanoparticle seeds during the growing process. Even there is symmetry breaking during the growth, such as seed-mediated synthesis of Au nanorods, the growth will not be treated as unconventional, because the nanorod structure can be derived from the structure of the seeds. Another example is the facet-selective deposition of Pd on Pd nanocubes, which was observed when controlling the deposition rate and diffusion rate of Pd.[47] However, the growth step is still be considered unconventional, because the structure of the product is derived from the cubic structure of the seeds. The geometries of the plasmonic nanostructures synthesized via conventional seed-mediated growth methods largely depends on the internal structure of seeds and the growth pathways, which includes passivation of some certain facets, and control of the growing kinetics.

1.2.1 Structures of Seeds

The seeds could be single crystalline or polycrystalline or of many crystal defects. This crystal structure of metals, such as Au and Ag, is known as face-centered cubic (fcc) and

has atoms at each corner of the cube and six atoms at each face of the cube. The intrinsic surface energies of an fcc metal increase in the order of $\gamma\{111\} < \gamma\{100\} < \gamma\{110\}$ in vacuum at 0 K in the absence of capping agents.[23] According to Wulff's theorem, a truncated octahedron, which is enclosed by eight {111} and six {100} facets, is the most stable shape of a single crystal fcc metal in an inert gas or vacuum. This truncated octahedron, also called a Wulff polyhedron, is often approximated as a sphere. However, in solution phase synthesis, one may obtain varies metal nanocrystals due to the variations in the synthetic conditions. The fcc structure contains three types of planes with an *abcabcabc* arrangement along the <111> direction. The most common defects in fcc metals are stacking faults and twin defects. Stacking faults occur when the *abcabcabc* stacking pattern of layers of metal atoms is disrupted by a missing or insertion of a layer, for example, *abcab<u>a</u>cabc* (insertion of plane *a*). And a twin plane is formed when this disruption results in a mirroring of the stacking pattern around one of the layers, for example, *abca<u>b</u>acba*. Because the energy barrier to the formation of the twin defects is very low in fcc metals (Cu, Ag and Au), multiple twin defects can occur in a single nanocrystal, increasing the diversity of the seeds.

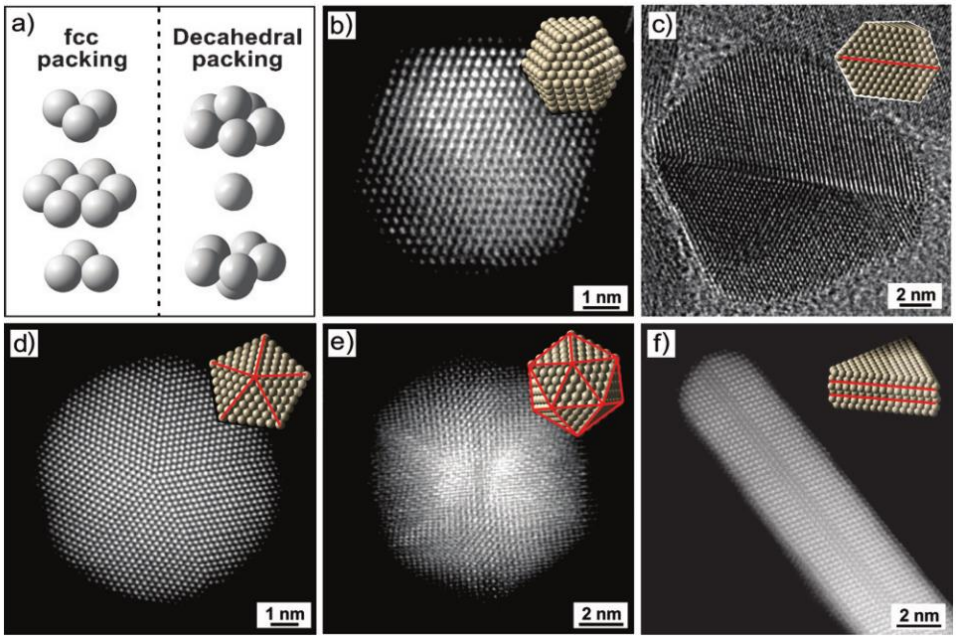

Figure 1.6 a) Schematic representation of fcc packing and decahedral packing. AHAADF-STEM image and the corresponding atomic model of (b) a single-crystal seed, (d, e) multiply twinned seeds and (f) a stacking fault-lined seed. TEM image and the corresponding atomic model of (c) a singly twinned seed. Copyright © 2017 Wiley-VCH.[28]

Formation of metal nanocrystal seeds is a result of thermodynamic and kinetic control. The former regulates the structure of the nanocrystal according to the minimum in Gibbs free energy, which includes minimization of surface and volume free energies, internal defects, and strain energies. The later includes control of the ligand type and reduction rate of the metal ions. In conclusion, there are four kinds of the seeds (Figure 1.6): single-crystal seeds (truncated octahedron, cube, octahedron, tetrahedron, and cuboctahedron), singly twinned seeds (bipyramidal), multiply twinned seeds (decahedral or icosahedral shape) and stacking fault-lined seeds (plate-like).[28]

1.2.2 Facet-Selective Deposition

In the seed-mediated growth, the major role of ligands in the synthesis of plasmonic nanocrystals has been summaries by the 'face-blocking theory', in which a capping agent selectively adsorbed to a particular crystal facet of the growing nanocrystal and slows the growth rate of that facet relative to the others.[48-49] The ligands can be small molecules or polymers. For example, Br^- is for the growth of Ag (100), and PVP is for Au (111) and Ag (100).[50] Zhang et al. reported a seed-mediated growth method for the synthesis of Ag nanoplates with aspect ratio up to 400 (Figure 1.7).[51] The key parameter in the growth step is the use of citrate ligands, which can effectively block the overgrowth of Ag onto the {111} facets and ensure anisotropic growth along the lateral direction. They also demonstrated that similar to citrate, many di- and tricarboxylate compounds whose two nearest carboxylate groups are separated by two or three carbon atoms, have preferential binding to the {111} facet.[52]

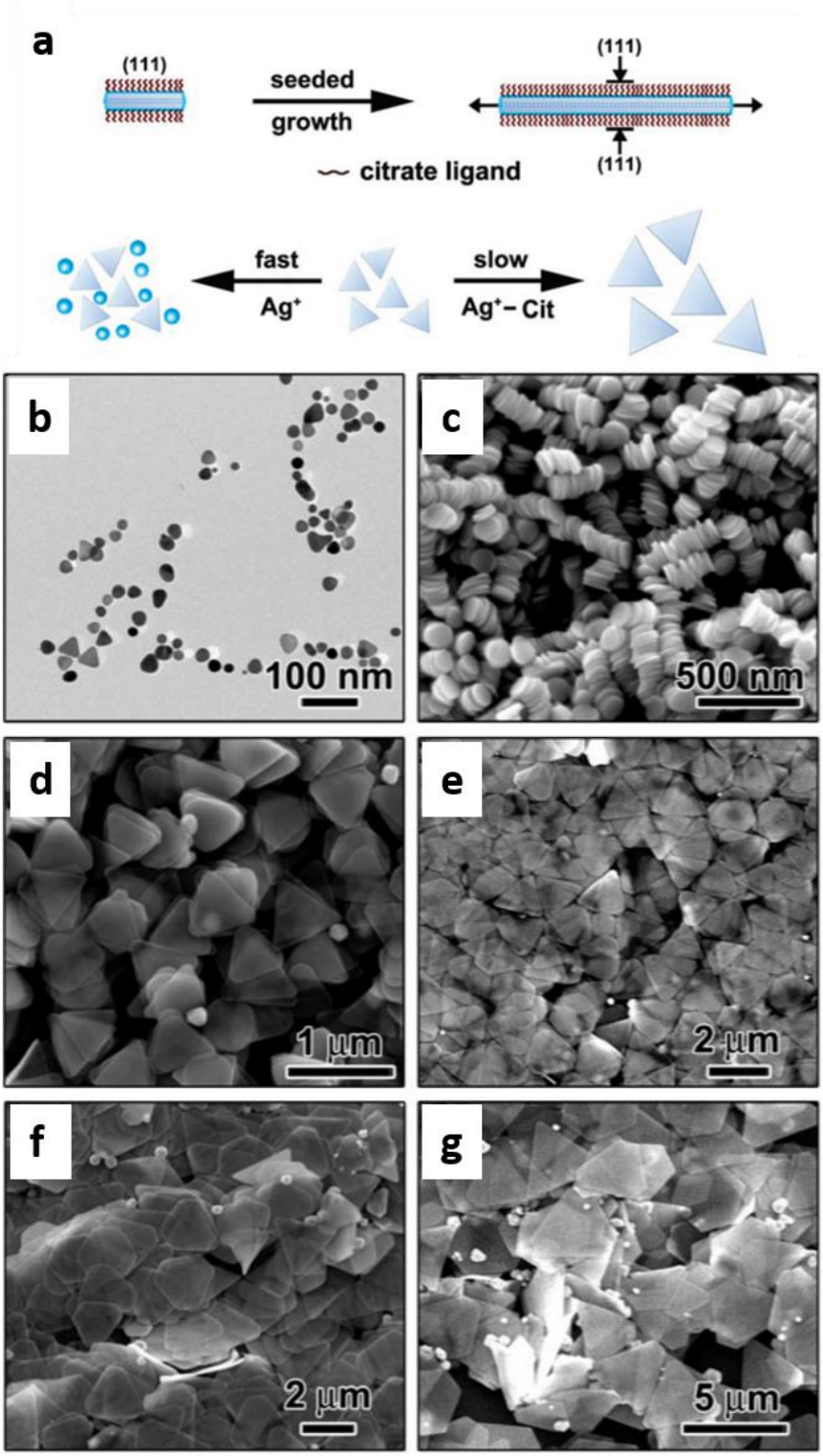
a
(111)
seeded
growth
(111)
(111)
citrate ligand
fast
Ag+
slow
Ag+– Cit
b
100 nm
c
500 nm
d
1 µm
e
2 µm
f
2 µm
g
5 µm

Figure 1.7 (a) Schematic illustration of the anisotropic seeded growth of Ag nanoplates based on selective ligand adhesion and seeded growth at different reaction rates. TEM image (b) and SEM images (c-g) showing the evolution of Ag nanoplates during the stepwise growth process: from original seeds (a) after removal of PVP by centrifuging and washing to larger Ag nanoplates after (b) one, (c) two, (d) four, (e) five, and (f) seven cycles of seeded growth. Copyright © 2010 American Chemical Society.[51]

Another method for facet selective growth is through Ag underpotential deposition (UPD).[53] Ag UPD has been used to create Au nanocrystals with high energy facets. For example, Ag^+ was added as additives in the reduction of $HAuCl_4$ with AA to produce {720}-faceted concave cubic gold nanocrystals.[54] In this case, the strength of reducing agent is not strong enough to reduce Ag^+, due to the low pH value. However, Ag^+ can still be reduced when facilitated by the surface of the nanoparticles, because the surface enables reduction at a potential less negative than the Nernst potential.[55] By depositing onto an Au surface facet, Ag hinders the further deposition of Au on that same facet and stabilizes it, leading to its slowed growth and subsequent retention in the final nanoparticle structure.[56] Personick et al. take advantages of Ag UPD to direct the growth of four different particle morphologies: octahedra with {111} facets, rhombic dodecahedra with {110} facets, truncated di-tetragonal prisms with {310} facets, and concave cubes with {720} facets (Figure 1.8).[57] The preferential passivation of Au facets was realized by adjusting the amount of Ag^+ in the seed-mediated growth process.

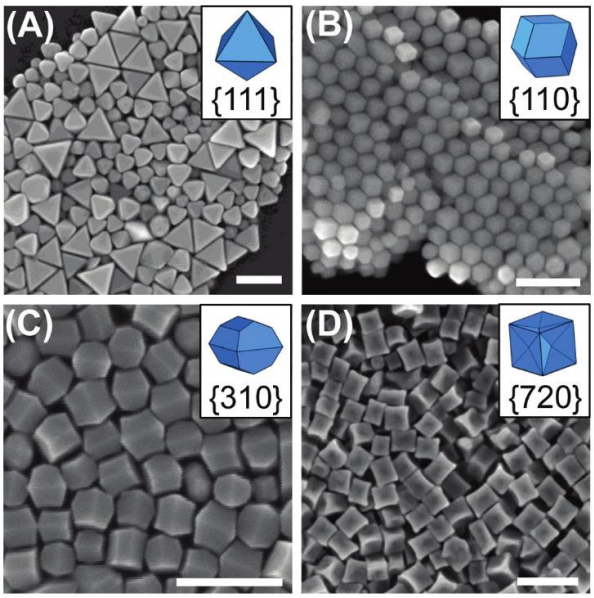

Figure 1.8 SEM images of (A) octahedra, (B) rhombic dodecahedra, (C) truncated ditetragonal prisms, and (D) concave cubes synthesized from reaction solutions containing Ag+/Au3+ ratios of 1:500, 1:50, 1:12.5, and 1:5, respectively. Scale bars: 200 nm. Copyright © 2011 American Chemical Society.[57]

1.2.3 Kinetic Control

Kinetic control refers to the control of reduction rate of metal precursor. Practically, it can be done by: adjusting the rate of precursor decomposition/reduction by adding ligand to form complex with the metal ions; adjusting the strength of reducing agent (changing the type of reducing agent, and adjusting pH); coupling the reduction of metal precursor to an oxidation process; involving Ostwald ripening; adjusting reaction temperature.

Reaction kinetics should be controlled both in the seeding step and the growth step. As we have discussed in section 2.1, when the reduction or decomposition kinetics of the metal precursor is sufficiently fast, the atoms tend to arrange to form single crystalline nanoseeds. In contrast, when the reaction kinetics are kept slow, the system favors formation of multiply twined seeds, because the size of the seeds could be kept small for a long time. As it is known that the multiply twined seeds are enclosed by the low surface energy {111} facets, it will compensate the strain energy caused by twining to achieve lowest total free energy. In this case, the size of the seeds should be kept small, because the surface energy increases with a rapid increase of the particle size, leads to failure in compensation of the strain energy of large seeds. It is also worth noting that considerably low reduction kinetics leads to formation of nuclei and seeds through random hexagonal close packing, together with stacking faults. One example is the formation of plate-like seeds, which is not thermodynamically favored.

Similarly, the low reduction rate of metal precursor favors facet selective deposition in the growth step. Liu et al. performed selective deposition of Au on the edges of Ag octahedra by injecting $HAuCl_4$ solution dropwise with a syringe pump at pH~2, using AA

as the reducing agent.[58] Because the {100} tips and {110} edges of the Ag octahedra having higher surface energies and increased reactivity than the more stable {111} facets, Au atoms would preferentially deposit on the tips and edges under this weak reducing condition.

Xia et al. showed the importance of controlling reaction kinetics in facet-selective growth of metal nanocrystals (Figure 1.9).[47] In this case, Pd nanocubes with slight truncation at corners and edges are used as seeds for the deposition of Pd. Because the truncated facets are relatively clean comparing to the side faces, deposition of Pd are expected to occur on the edges and corners. Taking atom diffusion into consideration, the result can be different with control of the ratio between the rates for atom deposition and surface diffusion ($V_{deposition}/V_{diffusion}$). Practically, the deposition rate was controlled by adjusting the injection rate of Pd precursors, while the diffusion rate was controlled by adjusting the reaction temperature. When the reaction is dominated by deposition, surface diffusion is negligible, and the deposition will happen to the clean facets, resulting in the formation of Pd octapods. On the contrary, when the reaction is dominated by diffusion, the growth will be switched to the <100> and <110> directions, because most of the adatoms at the corners can quickly migrate to edges and side faces of a cubic seed, forming a cuboctahedron as the final product.

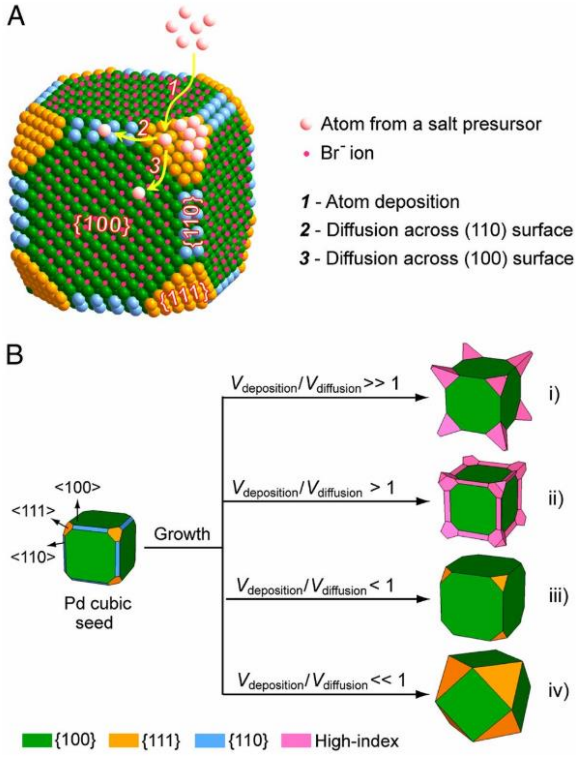

Figure 1.9 Effect of surface diffusion on the growth pattern of a Pd cubic seed. Schematics of (A) three different options for the Pd atoms added to the corner site of a Pd cubic seed whose side faces are capped by Br^- ions, and (B) different pathways and the corresponding shapes or morphologies expected for the growth of a Pd cubic seed under four different conditions. Copyright © 2013 PNAS.[47]

1.3 Unconventional Seed-Mediated Growth

Instantaneous and reversible tuning of the photonic property of metal nanostructures holds great promises for developing novel optoelectronic devices and more effective chemical and biomedical sensors by allowing instant selective excitation or quenching of specific plasmon modes. Although the development of conventional seed-mediated growth produces tremendous structures for the nanocrystal family, it still has limitations on the controlled growth of nanostructures beyond the facets of the seeds. Unconventional seed-mediated growth shows its advantages especially during the growth process using spherical nanocrystals as seeds. Conventionally, when depositing metal A on surface of a spherical seed composed of the same material, the growth will follow a layer-by-layer mode, because of the zero mismatch between the seed and the growing material.[42] Examples can be found in enlargement of Au nanocrystals through seed-mediated growth. Even when some of the facets of the nanocrystal are passivated by the capping ligands, the deposition on the facets still follows the layer-by-layer mode, resulting in facet-selective growth. It will be impossible to grow a nanoparticle of metal A on one side of its seed through conventional seed-mediated growth. However, growth of such nanostructure can be realized by unconventional methods using ligands, inorganics, microemulsions to control the surface properties of the seeds. Seed-mediated growth through unconventional strategies greatly enriched the diversity of the nanostructures, which have more advantages in applications. Also, some unique nanostructures can be used as models for investigation of their optical properties. In this section, we will discuss unconventional seed-mediated growth in two categories: 1) surface modification of seeds;

2) template-assisted seed-mediated growth. The former aims to tune surface properties of seeds by using organic ligands, masks made of polymers, inorganics and metal coordinates. After modification, the symmetry of the seeds will be broken, resulting in anisotropic growth beyond facet-selective growth. The later one employed solid and hollow colloidal nanoparticles as templates, which play a very important role in shaping and reshaping the growth of the nanostructures.

1.3.1 Surface Modification of Seeds

1.3.1.1 Surface Modification of Seeds with Organic Ligands

As we have discussed before, there are two roles of ligands in conventional seed-mediated growth strategies: stabilize the colloidal nanostructures, and direct the growth of some certain facets. Controlling the role of ligand beyond facets remains a big challenge to the synthesis of plasmonic nanostructures. Recent research revealed that the ligands should have more impact in determining the growth modes of the nanocrystals.

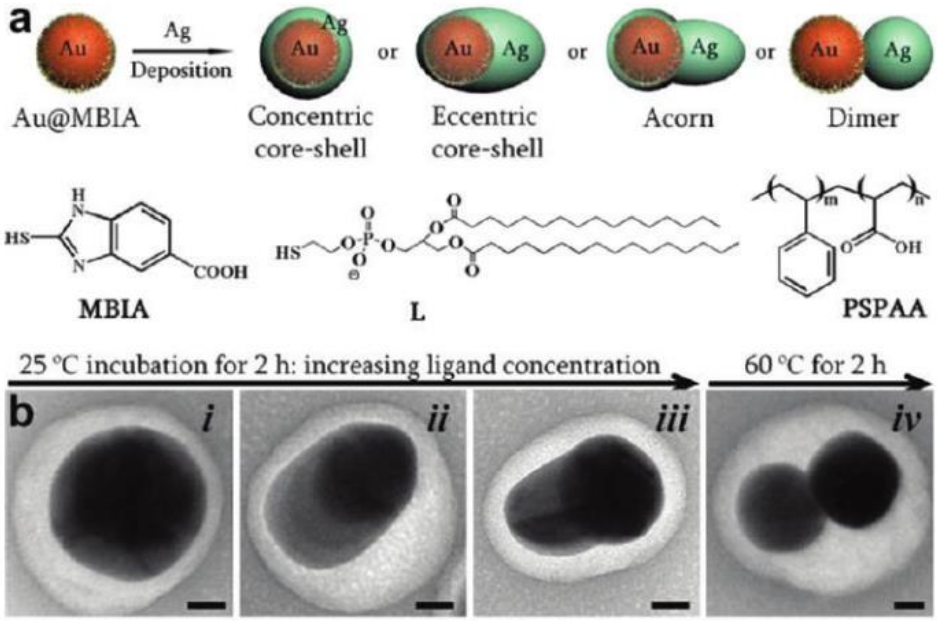

Figure 1.10 (a) Schematics illustrating the Au−Ag hybrid NPs and diagrams of relevant molecules; (b) TEM images of sample i−iv with stained background. Scale bars: 20 nm. Copyright © 2012 American Chemical Society.[59]

Feng et al. reported the synthesis of Au-Ag bimetallic nanostructures by seed-mediated growth of Ag on surface-modified Au nanospheres (Figure 1.10).[59] Because of the matching Au-Ag lattices (lattice parameters are 0.408 and 0.409 nm for Au and Ag, respectively), growth of Ag on an Au nanosphere results in a core-shell nanostructure, following the FM growth mode. The morphology of the Au-Ag nanostructures can be continuously tuned to SK and VW growth modes by varying the ligand condition during the growth of Ag. In a typical synthesis, citrate-stabilized Au nanospheres were incubated with 2-mercaptobenzoimidazole-5-carboxylic acid (MBIA), and used as seeds for the growth of Ag. Importantly, MBIA has both -SH group and -COOH group, which interacts with both Au and Ag species. Hydroquinone was added in the reaction system as a weak reductant, followed by dropwise addition of $AgNO_3$. In this case, the ligands were embedded on surface of the Au nanosphere, and could generated organic defects at the Au-Ag interface. Such defects introduce strain in the metal lattice, resulting in change in the growth modes. Density of the ligands on surface of the Au nanosphere was controlled by adjusting the concentration of the ligands and temperature for surface modification. When the incubation was performed at room temperature, and the concentration of MBIA was increased from 1 to 5, and 20 μM, the Ag nanoparticle shifted from concentric coverage to one side of the nanostructure. It is worth mentioning that the surface of Au was covered with a thin layer of Ag in all of the structures, indicting a SK growth mode. And when the temperature of the surface modification increased to 60 °C, the contact area between Au and Ag could be largely reduced to show a dimer nanostructure. The coating of Ag on the Au nanosphere was barely detectable, showing a VW growth mode.

They also demonstrated that further increasing the incubation temperature to 80 and 100 °C could lead to formation of multiple Ag islands, which was due to the rising difficulty for the nucleation and quickly accumulation of Ag^0 in solution.[60]

Polymers could be modified on plasmonic metal nanostructures to influence the surface diffusion of metal ions in the seed-mediated growth process. Wang et al. reported a very interesting method for tuning the growth pathways by using polyvinylpyrrolidone (PVP) as ligands (Figure 1.11).[61] PVP is a bulky, non-toxic, non-ionic polymer, which has been widely used in the synthesis of colloidal nanoparticles as a stabilizer, a shape-control reagent, and a mild reductant.[62] The interaction between PVP and metal ions is controversial. Some people suggested that the pyrrolidinone groups are perpendicularly adsorbed onto the surface of the metal nanoparticles mainly via the carboxyl group, while other claimed that the coordination between the nitrogen atom in the five-membered ring and the metal ion also contributed.[63-64]

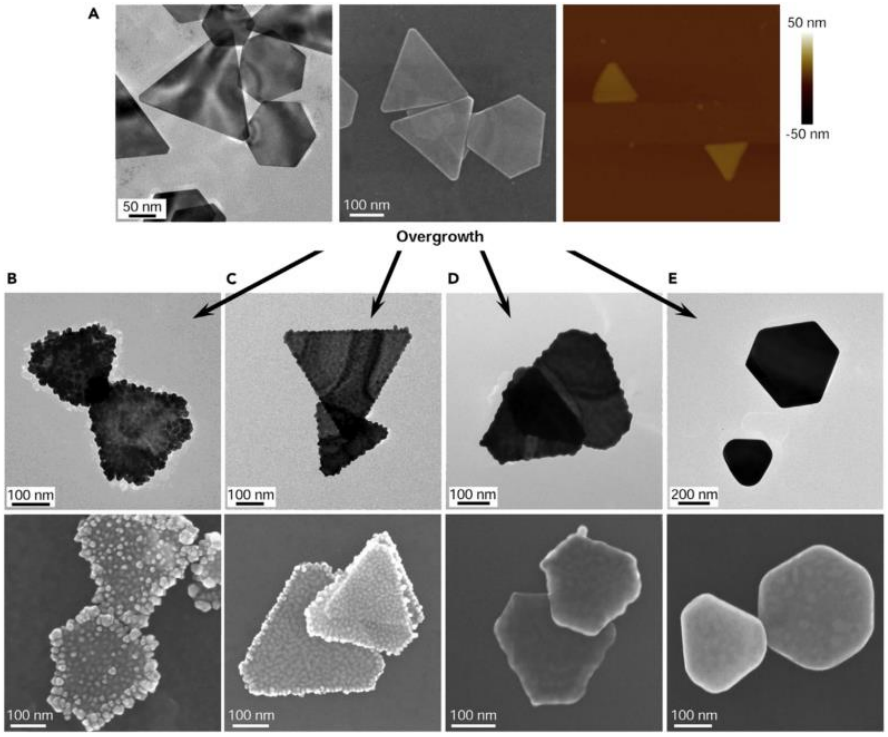

Figure 1.11 Shift of island growth on Au nanoplates to layer-by-layer mode by manipulation of reaction kinetics after PVP modification. The TEM, and SEM, and AFM images (left to right) in (A) reveal the original surfaces of two-dimensional Au nanoplates to be smooth. Overgrowth of the Au nanoplates produces islands on the nanoplates at a relatively high reaction kinetics (B), whereas island deposition (B–D) is gradually transformed to layer-by-layer growth (E) when reaction kinetics are decreased, as demonstrated by TEM, SEM, and AFM analyses (top to bottom). Copyright © 2017 Elsevier Inc.[61]

In this synthesis, the authors show that the growth modes of metal species could be tuned by using strong polymeric binding ligand at a high deposition rate. In a typical seed-mediated growth process, the pre-synthesized Au nanoplates were incubated in a PVP aqueous solution. Then, the seeds solution was mixed with ascorbic acid, which was used as a reducing agent, followed by addition of $HAuCl_4$ as a gold precursor at a fast injection rate. The seed-mediated growth produced quasi-hemispherical Au nanoislands with sizes of 10-20 nm epitaxially grown on the Au nanoplate. The Au nanoislands were highly stable in their synthetic solution. The nanostructure could be maintained for more than 10 days, which could be considered as a stable substrate for SERS applications. Here, the polymeric framework of PVP limits the diffusion of Au^{3+} in the chemical deposition process. It was worth noting that the reaction kinetics had to be controlled in this synthesis, because the nanoislands were formed on the surface of the nanoplates when the atoms were deposited too fast to migrate to other regions. When the reaction kinetics was decreased by decreasing the concentration of ascorbic acid, the injection rate, and the concentration of the Au precursor, the morphologies of the nanostructures changed from a VW mode to a FM mode. Slow reaction kinetics produced Au nanoplates with flat surfaces. This method was versatile for the growth of nanoislands on varies geometries, such as Au nanorods and nanospheres.

1.3.1.2 Surface Modification of Seeds with Masks

Surface modification of plasmonic nanostructures with organic ligands show its power in breaking the symmetry of the metal seeds. However, because the adsorption and desorption of organic ligands on a plasmonic nanostructure is dynamic in solution phase,

it is not easy to precisely control the starting points for the growth of the secondary nanostructure. In contrast, partially masking the surfaces of the seeds with an inert material provides accurate control of the size, shape, and uniformity of the products. There are many materials which could be selected to form the masks, for examples, polymers, inorganic solids, and metal coordinates.

Polymers could be modified on plasmonic nanostructures as masks to prevent the growth of metal nanostructures at some certain sites. Thanks to the quick development of polymer coating on metal nanoparticles, many metal-polymer hybrid nanostructures could be used as seeds for the growth of unconventional nanostructures.[65] For example, Au-PS Janus nanoparticles have been synthesized through free radical polymerization.[66]

It is reported that surface segregation of amphiphilic block copolymers on a planar metal surface can result in micelles with dense cores on some certain areas.[67] This phenomenon has been observed on Au nanostructures to create polymer 'patches'. As suggested in Choueiri et al.'s work, PS transformed from a continuous coating to patches on Au nanospheres, when the decreasing the solvent quality for the PS ligands.[68] Liu et al. reported the synthesis of Au-Pd, and Au-Au nanodimers by using Janus Au-PS nanoparticles as seeds, originated from surface segregation of PEO-PS copolymers on the Au nanospheres.[69]

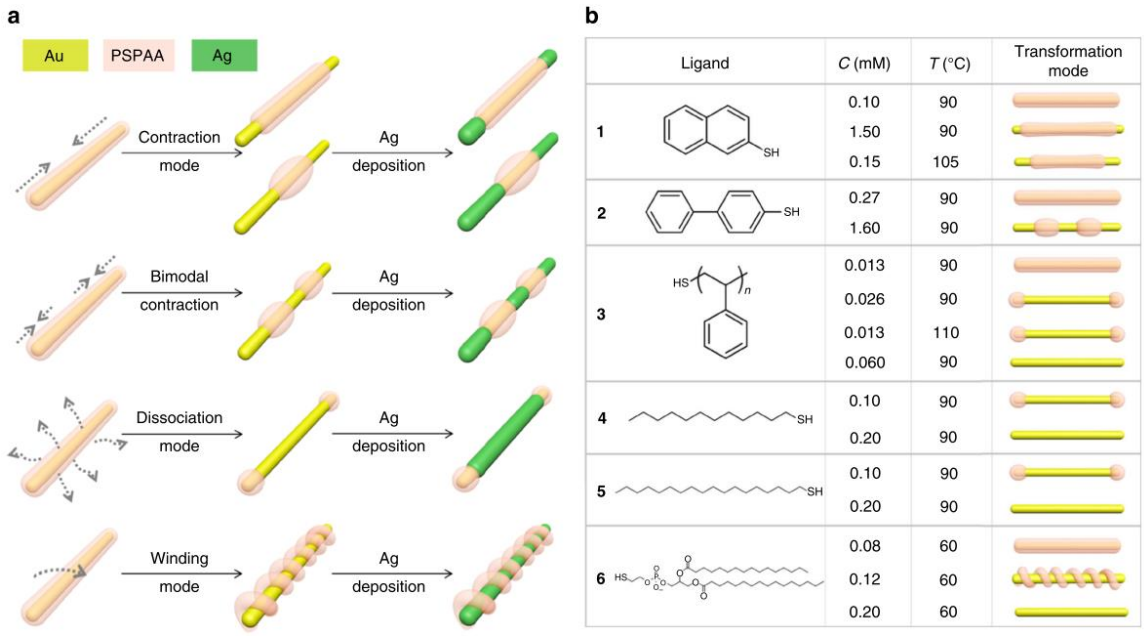

Figure 1.12 Schematics illustrating the four transformation modes of (AuNR-ligand)@PSPAA. a Contraction, bimodal contraction, dissociation, and winding modes (left panel). b The ligand dependence is summarized in the Table on the right panel. Ligands 1–6 are 2-naphthalenethiol, biphenyl-4-thiol, thiol-terminated polystyrene, 1-dodecanethiol, 1-octadecanethiol, and a thiol-ended phospholipid, 2-dipalmitoyl-sn-glycero-3-phosphothioethanol (sodium salt), respectively. C (mM) the concentration of the ligand in the initial encapsulation step, T the temperature used for transforming the (AuNR-ligand)@PSPAA in water. Copyright © 2018 Nature Publishing Group.[70]

Recently, Wang et al. reported a seed-mediated growth of unconventional Au nanostructures by using Au nanorods with transformable polystyrene-block-poly(acrylic acid) (PSPAA) polymeric masks as seeds (Figure 1.12).[70] Different from stationary polymer coating, the shapes of the polymer shells on the Au nanorods can be tuned under different modes of shell transformation, allowing them to direct different growth pathways for the deposition of Ag. In a typical synthesis, the Au nanorods are mixed with PS-PAA and a hydrophobic ligand in dimethyl formamide/H_2O solution, and heated at 110 °C for 2 h to form AuNR-ligand@PS-PAA core-shell nanostructures. The nanostructures were then heated to initiated the shape transformation of the PS-PAA shell, resulting in contraction, bimodal contraction, dissociation and winding of the shell. The modes of shape transformation are highly related to the types of ligands and their concentrations. This method provides a way to deposit Ag and Pd at targeted and arbitrary position of Au nanorods. AuNRs-Ag-Pd trimetallic nanostructures with Pd on the tips and Ag after it could also be synthesized by stepwise contraction and metal deposition. In addition, this method could be used on other plasmonic nanostructures such as Au bipyramids and triangular nanoprisms.

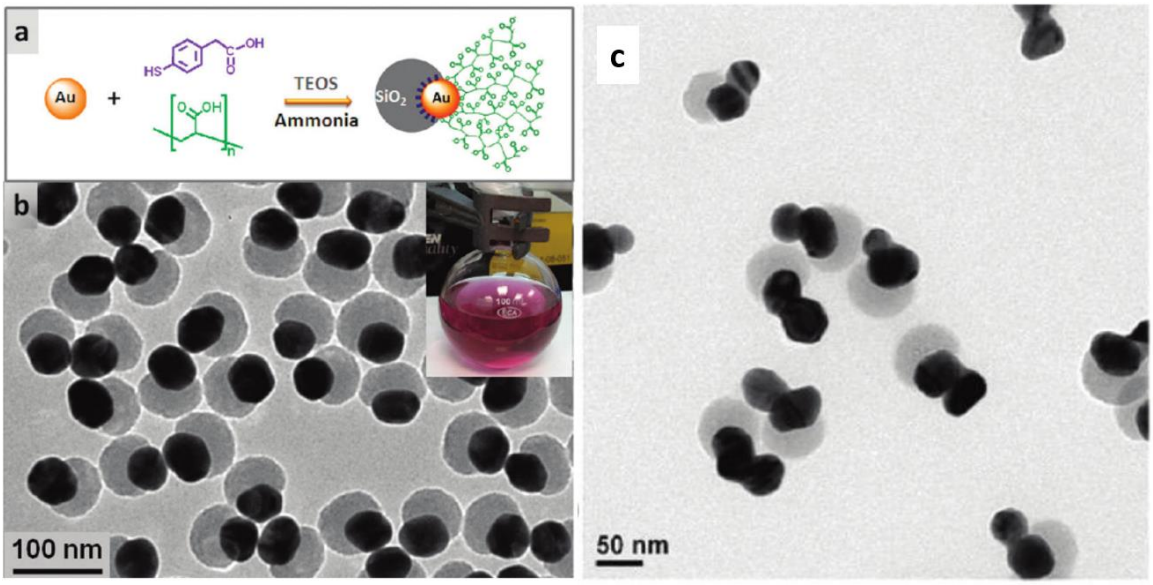

Figure 1.13 (a) Schematic illustration of the ligand competition that led to the formation of Janus Au-SiO_2; (b) TEM image of Janus Au-SiO_2, with [4-MPAA]:[PAA86] = 1:0.129 and [TEOS] = 1.445 mM; inset, a digital photo showing the color of the products. (c) TEM image of the ternary structures AgNS-Au-SiO_2. Copyright © 2010 American Chemical Society.[71]

Inorganic solids, which are inert in seed-mediated growth, can also be used as masks. This strategy requires selective coating of inorganic solids on surface of the metal seeds. When the seed is partially covered by inorganic solids, deposition of the metal precursor will only happen to the exposed area of the seed. There will not be metal deposited on inorganic solids, because the interaction between metal-metal is stronger than that of metal-inorganic solid. Selective deposition of inorganic solids on metal nanocrystals requires carefully control of the surface property of metal by using ligands. Chen et al. first used Janus Au-SiO_2 nanoparticles as seeds for the growth of ternary Ag-Au-SiO_2 nanoparticles (Figure 1.13).[71] The partial coating of SiO_2 on the Au nanosphere was achieved by a sol-gel method using competing ligands, 4-mercaptophenylacetic acid (4-MPAA) and poly(acrylic acid) (PAA), to functionalize the surface of the Au nanospheres. Because 4-MPAA is favorable for silica deposition and PAA is not, having a mixture of the two ligands on surface of the Au nanospheres will decrease the compatibility between Au and SiO_2, resulting in the eccentric silica coating on the Au surface. During the seed-mediated growth step, Ag grew from the exposed area of Au, leading to the formation of ternary Ag-Au-SiO_2 nanostructures. The intrinsic ligand conditions of some anisotropic plasmonic nanostructures were suitable for site-selective silica coating. For example, it is well-known that the density on the sides of the Au nanorods is higher than that on the ends, due to the lower curvature of sides than ends. Taking this into consideration, Wang et al. selectively deposited SiO_2 on sides or ends of Au nanorods, and used these particles as seeds for the growth of various structures.[72] Because of the relatively low density of CTAB at the ends of the Au nanorods, SiO_2 will firstly deposited on the ends, then on the

sides. Controlling the amount of SiO_2 leads to selective deposition only on the ends. On the other hand, selective deposition of SiO_2 only on the sides of the nanorods could be achieved by modifying the nanorods with small amount of methoxypoly(ethylene glycol) (mPEG-SH). Because of the high curvature and the low density of CTAB at the ends, mPEG-SH was modified preferentially on the ends of the nanorods. And due to the larger size of mPEG-SH than that of CTAB, SiO_2 could be firstly deposited on the sides. Transverse growth of the Au@end-SiO_2 and longitudinal growth of the Au@side-mSiO_2 were obtained after the seed-mediated growth.

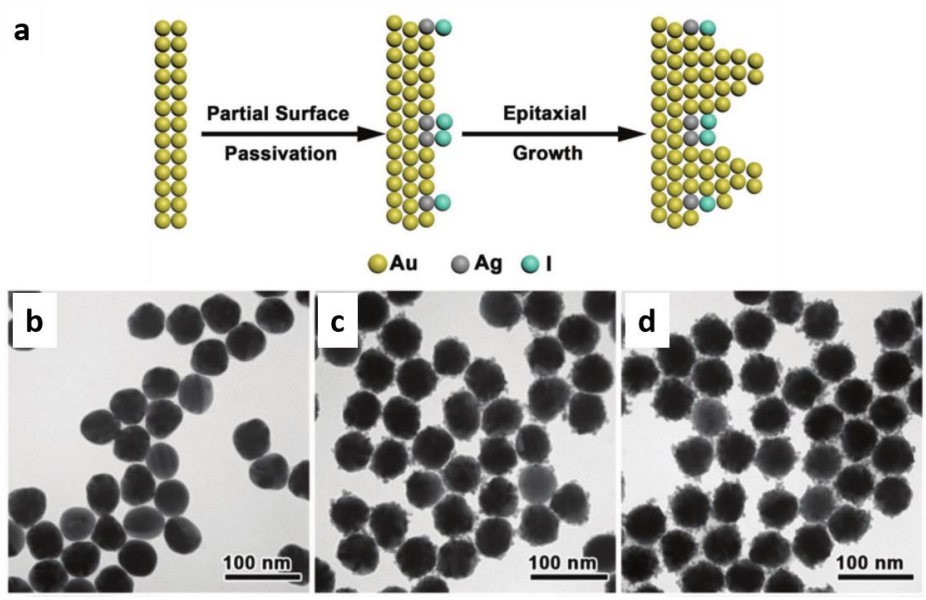

Figure 1.14 (a) A cartoon illustrating the formation of the islands-on-Au nanostructures. (b) TEM images of the AuNSs. (c–d) TEM images of the islands-on-AuNSs with varying densities of the nanoislands by changing the concentration of $HAuCl_4$. Copyright © 2018 WILEY-VCH.[31]

Surface passivation can also be created by depositing metal coordinates on a seed. Fan et al. reported the synthesis of high-density Au-Ag alloy nanoislands as secondary nanostructures on the surface of Au nanocrystals (Figure 1.14).[31] During the seed-mediated growth, Ag was firstly deposited on surface of the Au nanocrystal in a solution containing KI. Because the binding energy of Ag-I is high, the surface is energetically unfavorable for a FM mode growth. Therefore, the metal deposition and convenient migration to these sites are suppressed, which leads to the formation of abundant nanoislands as secondary structures on the surface of the Au nanoparticles. The concentration of KI should be controlled to a low value, because high concentration of KI leads to formation of AuI_4^- complex, which favored FM deposition of Au. It is worth noting that the curvature of the nanoislands would be affected by the concentration of $AgNO_3$, because it altered the surface passivation and kinetics in the crystal growth.

1.3.2 Template-Assisted Seed-Mediated Growth

Template synthesis is a powerful and versatile method for preparing nanomaterials. Pioneered work done by Charles Martin and Martin Moskovits demonstrates the concept of template synthesis to fabricate nanostructures composed of polymers, metals, semiconductors, and other materials by electrochemical deposition using AAO templates.[73-75] The method has been developed to fabricate metal nanocomplex with designed orders and surface properties.[76-77] Nanomaterials synthesized by templating strategies hold a well-defined size, shape and configuration, which usually benefits from the directing effect of the templates.[78] In colloidal synthesis, theoretically, a template can be any substance with nanostructured features. Thus, there are abundant types of

materials that can be taken into consideration, for example, inorganic solids, micelles, emulsions, and etc.

Template-assisted seed-mediated growth of plasmonic nanostructures can be divided into two categories: seed-mediated growth on surface of a template and confined seed-mediated growth inside a template. In the former case, the seeds are dispersed on the surface of the template. After seeded growth, a shell structure is formed, replicating the shape of the template. And in the latter case, the seeds are encapsulated in a shell. The metal precursor in the growth solution penetrates through the shell, and was deposited on the seeds. The template acts as a nanoreactor, which confined the growth of the seeds.

Some people use templates as substrates to stabilize the nanoparticles. This part will not be discussed because the growth of the nanoparticles is independent of the substrates. There are several advantages of template synthesis: 1) the shape of the template helps to synthesize nanostructures which are difficult to achieve by solution phase synthesis; 2) template synthesis usually leads to high yield of products; 3) nanostructures with high uniformity derived from the well-defined template can be synthesized; 4) the space in templates gives room for the fabrication of even more complicated structures.

1.3.2.1 Seed-Mediated Growth on a Template

Up to date, seed-mediated growth on a template has been widely investigated. In this case, the seeds are dispersed on a template at first. During the seed-mediated growth step, the seeds can grow bigger, and finally connected with each other to form a nanoshell structure. It is worth noting that the substrate needs to be modified with ligands which have strong interaction with both the substrate and the metal species in order to

immobilize the seeds. The concept has been demonstrated by Oldenburg et al., who used colloidal silica nanospheres as templates for the synthesis of Au nanoshells.[79] The monodispersed colloidal silica nanospheres with size of 120 nm were synthesized through a modified Stöber method, and modified with APTES to graph the surface of silica with NH_2 groups. Then, gold seeds with size of 1-2 nm were loaded to the modified silica nanospheres. About 30 % of the silica surface could be covered with Au seeds, limited by interparticle Coulomb repulsion. The seed-mediated growth was performed through reducing an aged mixture of chloroauric acid and potassium carbonate by a solution of sodium borohydride. As more Au was deposited on the seeds, the coverage of Au on the silica nanoparticle increase, resulting in the formation of Au nanoshells with about 95 % yield. Formation of nanoshell could greatly broaden the plasmonic excitation of Au nanoparticles to over 800 nm in wavelength, which showed advantages in biomedical applications.

Due to the structure directing effect of the template, the shape of the plasmonic nanostructure depends on the geometry of the colloidal template. In addition, the intrinsic property of the colloidal template can add on to the functionality of the complex structure. For example, magnetic colloidal template can help the nanocomplex to be both photoactivity and magnetic responsive. Wang et al. has reported the synthesis of anisotropic nanoshells by using rod-like templates for information encryption and magnetic-field-direction sensing.[80] In a typical synthesis, Akaganéite (β-FeOOH) nanorods were used as the starting materials which were first coated with a layer of silica, reduced to magnetic state, and loaded with gold seeds. After seed-mediated growth, the

gold nanoparticles formed anisotropic nanoshells, which could exhibit different plasmonic extinction spectra when the incident light was polarized along transverse and longitudinal directions.

1.3.2.2 Confined Seed-Mediated Growth in a Template

A successful confined seed-mediated growth inside a shell template including three steps: (1) seeding of metal nanoparticles in a template; (2) confined seed-mediated growth of metal nanostructures; and (3) removal of the templates. Step (3) is not always necessary.

Generally speaking, growth of non-spherical plasmonic structures requires the use of non-spherical templates. Gao et al. reported the synthesis of metal nanorods with tunable aspect ratio and high purity in tubular silica templates (Figure 1.15).[81] This method is versatile for the synthesis of metal nanorods composed of varies metal species, such as Au, Ag, Pt and Pd. Some of which cannot be obtained by conventional seeded-mediated growth method. The tubular templates were produced by coating uniform nickel-hydrazine rod-like nanocrystals with a layer of silica through a sol-gel process, and selective removal of the nickel-hydrazine templates.[82] Silica nanotubes with tunable aspect ratio could be successfully synthesized by tuning the hydrazine/nickel ratio during the original template synthesis. Taking Au for example, seeding of Au nanoparticles inside a shell template is of great importance to the successful growth of Au nanostructures. If not all the Au seeds are encapsulated inside the template, Au seeds outside the template will have a better chance to grow than the Au seeds inside the template, due to the direct interaction with Au precursors. Another important factor that needs to be controlled is the growth pathways. To address the problem, the inner surface

of the original silica nanotube was modified by introducing a layer of 3-aminopropyltriethoxysilane (APS) to the surface of the nickel-hydrazine nanorods before the deposition of the silica layer. After removal of the nickel-hydrazine nanorods, the amino groups are left on the inner surfaces of the silica nanotubes. Due to the electrostatic and/or coordination interaction between amino groups and $AuCl_4^-$/metallic Au, Au species could be limited to the inner surfaces of the silica nanotubes. After reduction, an Au nanoparticle with size of 4 nm could be successfully loaded inside the tubular template. On the other hand, the growth pathway has to be controlled to limit self-nucleation of Au nanostructures. A low reaction rate was preferred in the growth step. It required using ascorbic acid as a weaker reducing agent. In addition, KI was introduced to lower the reduction rate of $AuCl_4^-$ by forming complex with Au^{3+}. Meanwhile, additional capping ligand, for example, polyvinylpyrrolidone (PVP), was also added to the growth solution to stabilize the atomic monomer species and further delay the self-nucleation. Moreover, metal nanorods with tunable aspect ratio was achieved by controlling the aspect ratio of the silica nanotubes. A series of Au nanotubes with aspect ratio increasing from 3.5 to 5.7, 14.8, and 21 could be synthesized by using silica nanotubes of different dimensions.

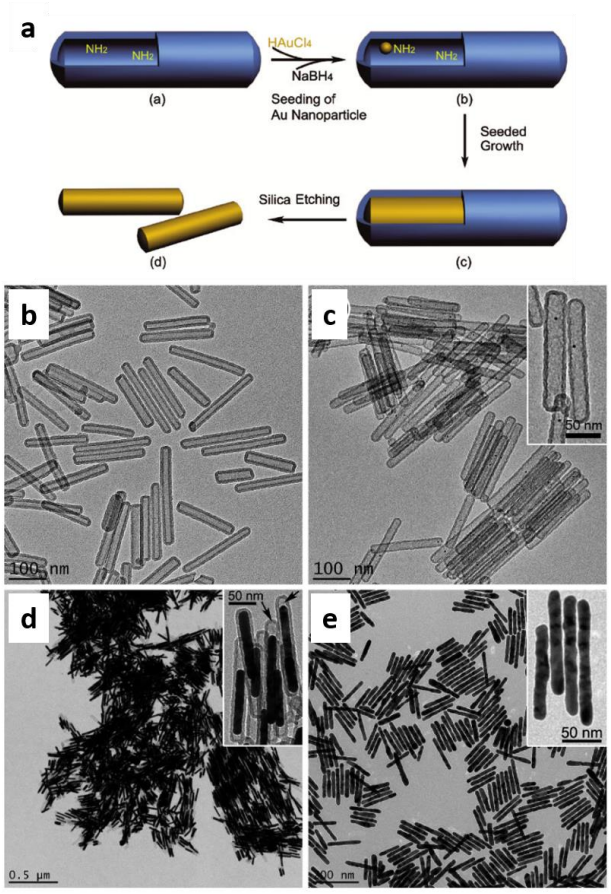

Figure 1.15 (a) A general templating approach to the synthesis of metal nanorods in tubular silica templates. TEM images of the (a) silica nanotubes with inner cavity functionalized with amino groups; (b)Au seed@silica nanotubes; (c)Au nanorod@silica nanotubes after seeded growth; (d) Au nanorods after removal of silica templates. Copyright © 2011 American Chemical Society.[81]

Confined growth could also be achieved in between two inorganic layers. Zhang et al. developed confined growth of thin Au nanoshells in the empty space between Fe_3O_4@SiO_2 nanospheres and a porous shell.[83] A typical synthesis started from the synthesis of superparamagnetic Fe_3O_4 colloidal nanocrystal clusters through a high temperature hydrolysis reaction. The highly responsive superparamagnetic cores were used to broadens the applications of the nanoshells for magnetically guided delivery and magnetic resonance (MR) imaging. The Fe_3O_4 colloidal nanocrystal clusters were coated with a thin layer of SiO_2 and modified with APTES for the attachment of pre-synthesized TSC capped Au nanoseeds with sized of about 15 nm in diameter. After the loading of Au, the nanostructures were coated with another layer of silica to fully encapsulate the Au seeds inside the silica matrix in the presence of PVP. The porosity and pore sizes of the silica shell was tuned by using a 'surface-protected etching' method, using NaOH as the etchant. This process was not only aimed make the Au nanoseeds accessible, but also provided enough space for the formation of a complete shell in the following seed-mediated growth reaction. Finally, the Au nanoshells were formed via overgrowth of the embedded Au nanoseeds. It is worth mentioning that the porous silica shell protected the Au nanoseeds against detachment from the colloidal substrates, leading to high yield of Au nanoshells with complete structures.

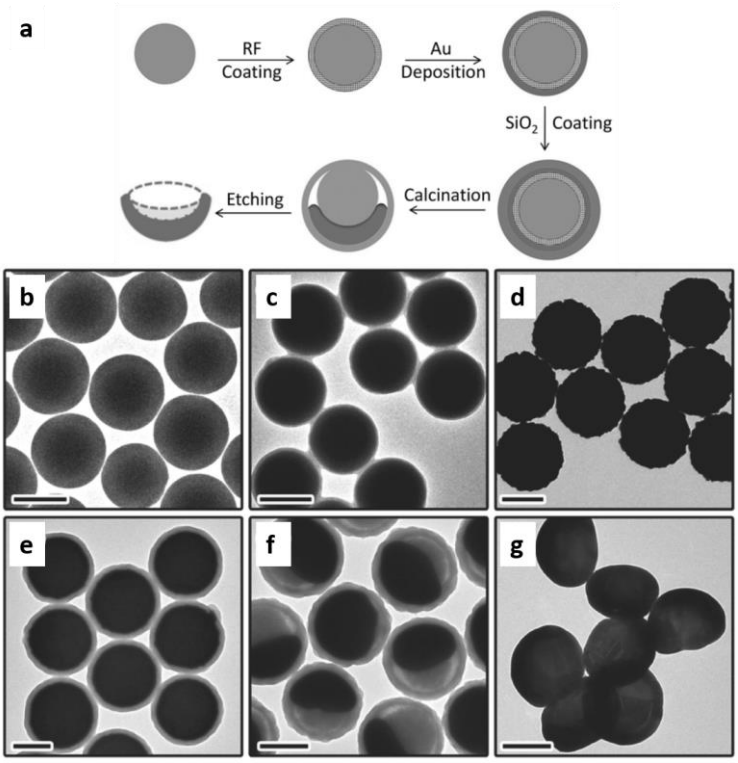

Figure 1.16 (a) Outline of the confined dewetting process for the fabrication of Au nanocups: silica spheres are coated sequentially with RF, Au, and SiO_2 layers, followed by calcination in air to remove RF and dewet Au from SiO_2 surface, and then etching SiO_2 templates to release Au nanocups. TEM images of (b) SiO_2 nanospheres. (c) SiO_2@RF nanospheres. (d) SiO_2@RF@Au nanospheres. (e) SiO_2@RF@Au@SiO_2 nanospheres. (f) SiO_2@RF@Au@SiO_2 nanospheres after calcination in air at 800 °C for 3 h. f) Au nanocups after removal of the SiO_2 templates. All scale bars are 200 nm. Copyright © 2017 WILEY-VCH.[84]

Interestingly, seed-mediated growth in spherical templates could also result in non-spherical structures. Gao et al. reported the synthesis of Au nanocups with tunable dimensions through a confined-space thermal dewetting strategy for OCT imaging (Figure 1.16).[84] The synthesis started with coating a layer of resorcinol formaldehyde resin (RF) on a silica nanosphere through a sol-gel method. Then, the RF layer was modified with APTES, and loaded with 1-2 nm Au seeds. The nanostructure was added into a solution containing Au precursors for the growth of Au nanoshell. After that, an additional layer of silica was coated on the nanostructure as a protector to prevent interparticle aggregation during high-temperature calcination, and also afford confined space for the Au dewetting process. As the dynamics of thermal dewetting is determined by macroscopic hydrodynamic flows, the calcination temperature is a crucial factor for the formation of nanocups. Au nanocups were achieved after thermal dewetting at 800 °C, and released by etching of silica with HF. This high temperature treatment also ensured the complete removal of the RF layer, leaving room for the deformation of the Au nanoshell. It was worth mentioning that the thickness of the RF layer determines the extra space available for thermal dewetting of Au. When the thickness of RF decreased from 25, to 18, and 12 nm, the height of Au nanocups increased and the size of the cup opening decreased. Because of the differences in geometries, the Au nanocups showed very different plasmonic properties from Au nanoparticles and Au nanoshells with the same size. The asymmetric shape and strong extinction of the nanocups at around 1250-1360 nm contributed to a much better backscattering intensity achieved by the nanocups than the nanoshells in response to the OCT light source.

1.4 Challenges

Unconventional seed-mediated growth is an interesting research topic, because it leads to the growth of metal nanocrystals beyond facet control, which will result in a variety of plasmonic nanostructures with unique optical properties. Although many excellent works have been done to tune the growth pathways of metal nanocrystals and discover the chemistry behind the seed-mediated growth, it still remains a challenge to create secondary nanostructures on pre-existing Au or Ag nanocrystals in a controllable manner, which could benefit both application and fundamental study.

Seed-mediated growth of Au or Ag nanocrystals usually results in core-shell nanostructures, due to the tight lattice match in a monometallic or Au/Ag bimetallic system. Growth of secondary nanostructures usually occurs in a bimetallic system with large lattice mismatch and thus poor wettability between the two components. In previous reports, the seeds were modified with strong ligands, masks and inorganic solids for the construction of secondary nanostructures. However, the difficulty in synthesis, and the lack of structural tunability and optical properties limit the application of such methods as general synthetic methods. Therefore, it is highly important to build up a new synthetic system, which provides a universal method for building secondary nanostructures with tunable geometries and optical properties.

Besides the difficulty in synthesis, dynamic tuning of the optical properties of plasmonic nanoparticles with complicated geometry is another challenge. Because dynamic tuning of plasmonic excitation of anisotropic nanostructures holds great promise for developing novel optoelectronic devices and more effective chemical and biomedical

sensors, it is very important to develop a reliable method by allowing instant selective excitation or quenching of specific plasmon modes.

1.5 The Scope of This Dissertation

This dissertation discusses our efforts in the development of unconventional seed-mediated growth method for the synthesis of non-spherical plasmonic metal nanocrystals. The unique optical properties of the non-spherical nanostructures, such as Au-Au dimers and trimers, is investigated, and the application of such nanostructures is demonstrated.

Chapter 1 is the introduction to nanocrystal synthesis. First, the general concept of seed-mediated growth is introduced, followed by discussion of conventional and unconventional methods for the synthesis of metal nanocrystals. Some well-established theories on controlled growth of metal nanocrystals has been discussed.

In Chapter 2, we will introduce our work regarding the unconventional synthesis of non-spherical nanostructures in solution phase. We developed a system, which could be widely applied for the construction of a secondary nanostructure on a metal seed. This method was based on surface modification of the metal seed with another metal species of mismatched lattice, which could induce a positive strain energy to drive the growth of metal follow the island-growth mode. By introducing ligand-assisted oxidative ripening to the system, the number of islands on a metal seed could be controlled. We show the successful preparation of Au satellite structures and dimers with high yield, and the possibility to tune the nanostructure to Au trimers, and tetramers. The key parameters for the synthesis were carefully studied, including the surface strain, the oxidative ripening and the diffusion of metal precursors.

In Chapter 3, we show the template-assisted seed-mediated growth method for the fabrication of rod-like nanostructures. After the successful synthesis of the Au dimer, we studied their unique optical property, and found out that the optical property of such nanostructure was highly related to the connection area and overlapping distance of the two nanospheres. To control the growth of Au dimers with more precision, we borrow the idea from template synthesis, and design our system by making use of colloidal nanoparticles as substrates. In order to create surface anisotropy, we used a non-metal solid, which was inert in the seed-mediated growth of metal nanocrystals to partially cover the surface of the metal seed. So that the secondary structures could only grow from the uncovered areas. By using this template-assisted seed-mediated growth method, we successfully synthesized Au-Au dimers, and heteodimers, such as Au-Ag, Au-Pd, and Au-Cu_2O. Repeating the synthetic procedure resulted in formation of rod-like nanostructure with higher aspect ratio, eg. linear trimers, and tetramers.

Chapter 4 will focus on the study of the angular dependent plasmonic property of Au-Au and Au-Ag dimers, and their application as anticounterfeiting patterns. Thanks to the template-assisted seed-mediated growth, rod-like plasmonic nanostructures, which were self-registered along the surface normal of the colloidal substrates could be obtained. By controlling the orientation of the colloidal substrates rather than the nanorods themselves, we were able to selectively excite different resonant mode of the nanostructures. To demonstrate this unique advantage, we adopted this strategy for growing Au nanorods on the surface of magnetic iron oxide nanorods and nanoplates to produce magnetic/plasmonic nanocomposites whose plasmonic bands can be selectively

excited by controlling the orientation of the magnetic components using external magnetic field. The convenient magnetic control further enabled the creation of thin polymer films containing Au nanorods with defined orientation at different locations, producing polarization dependent color displays that may find potential application in information encryption.

In Chapter 5, we present a conclusion, and discuss any possible future work that can be done as an extension of this dissertation.

1.6 References

1. Li, M.; Cushing, S. K.; Wu, N., Plasmon-enhanced optical sensors: a review. *Analyst* **2015,** *140* (2), 386.
2. Ozbay, E., Plasmonics: Merging Photonics and Electronics at Nanoscale Dimensions. *Science* **2006,** *311* (5758), 189.
3. Zhang, X.; Li, X.; Reish, M. E.; Zhang, D.; Su, N. Q.; Gutiérrez, Y.; Moreno, F.; Yang, W.; Everitt, H. O.; Liu, J., Plasmon-Enhanced Catalysis: Distinguishing Thermal and Nonthermal Effects. *Nano Lett.* **2018,** *18* (3), 1714.
4. Huang, X.; El-Sayed, M. A., Plasmonic photo-thermal therapy (PPTT). *Alexandria Journal of Medicine* **2011,** *47* (1), 1.
5. Chen, H.; Shao, L.; Li, Q.; Wang, J., Gold nanorods and their plasmonic properties. *Chem. Soc. Rev.* **2013,** *42* (7), 2679.
6. Liu, Y.; Han, X.; He, L.; Yin, Y., Thermoresponsive Assembly of Charged Gold Nanoparticles and Their Reversible Tuning of Plasmon Coupling. *Angew. Chem., Int. Ed.* **2012,** *51* (26), 6373.
7. Pérez-Juste, J.; Rodríguez-González, B.; Mulvaney, P.; Liz-Marzán, L. M., Optical Control and Patterning of Gold-Nanorod–Poly(vinyl alcohol) Nanocomposite Films. *Adv. Funct. Mater.* **2005,** *15* (7), 1065.
8. Saito, K.; Setoura, K.; Ito, S.; Miyasaka, H.; Mitsuda, Y.; Tatsuma, T., Plasmonic Control and Stabilization of Asymmetric Light Scattering from Ag Nanocubes on TiO2. *ACS Appl. Mater. Interfaces* **2017,** *9* (12), 11064.
9. Faraday, M., The Bakerian Lecture: Experimental Relations of Gold (and Other Metals) to Light. *Philos. Trans. Royal Soc. London* **1857,** *147*.
10. Feynman, R. P., There's plenty of room at the bottom [data storage]. *Journal of Microelectromechanical Systems* **1992,** *1* (1), 60.
11. Taniguchi, N., On the Basic Concept of Nanotechnology. *Proc. Intl. Conf. Prod. Eng. Tokyo,* **1974**.
12. Krishna, V. D.; Wu, K.; Su, D.; Cheeran, M. C. J.; Wang, J.-P.; Perez, A., Nanotechnology: Review of concepts and potential application of sensing platforms in food safety. *Food Microbiology* **2018,** *75*, 47.
13. Goutam, S.; Omar, N.; Van Den Bossche, P.; Van Mierlo, J., Chapter Two - Review of Nanotechnology for Anode Materials in Batteries. In *Emerging Nanotechnologies in Rechargeable Energy Storage Systems*, Rodriguez-Martinez, L. M.; Omar, N., Eds. Elsevier: Boston, 2017; pp 45.

14. Jianrong, C.; Yuqing, M.; Nongyue, H.; Xiaohua, W.; Sijiao, L., Nanotechnology and biosensors. *Biotechnology Advances* **2004,** *22* (7), 505.
15. Shi, J.; Kantoff, P. W.; Wooster, R.; Farokhzad, O. C., Cancer nanomedicine: progress, challenges and opportunities. *Nat. Rev. Cancer* **2016,** *17*, 20.
16. Liu, Y.; Pharr, M.; Salvatore, G. A., Lab-on-Skin: A Review of Flexible and Stretchable Electronics for Wearable Health Monitoring. *ACS Nano* **2017,** *11* (10), 9614.
17. Yang, X.; Yang, M.; Pang, B.; Vara, M.; Xia, Y., Gold Nanomaterials at Work in Biomedicine. *Chem. Rev.* **2015,** *115* (19), 10410.
18. Feng, J.; Gao, C.; Yin, Y., Stabilization of noble metal nanostructures for catalysis and sensing. *Nanoscale* **2018,** *10* (44), 20492.
19. Chatterjee, H.; Rahman, D. S.; Sengupta, M.; Ghosh, S. K., Gold Nanostars in Plasmonic Photothermal Therapy: The Role of Tip Heads in the Thermoplasmonic Landscape. *J. Phys. Chem. C* **2018,** *122* (24), 13082.
20. Patel, S. K.; Argyropoulos, C., Plasmonic nanoantennas: enhancing light-matter interactions at the nanoscale. *EPJ Applied Metamaterials* **2015,** *2*, 4.
21. Rycenga, M.; Cobley, C. M.; Zeng, J.; Li, W.; Moran, C. H.; Zhang, Q.; Qin, D.; Xia, Y., Controlling the Synthesis and Assembly of Silver Nanostructures for Plasmonic Applications. *Chem. Rev.* **2011,** *111* (6), 3669.
22. Sanz, J. M.; Ortiz, D.; Alcaraz de la Osa, R.; Saiz, J. M.; González, F.; Brown, A. S.; Losurdo, M.; Everitt, H. O.; Moreno, F., UV Plasmonic Behavior of Various Metal Nanoparticles in the Near- and Far-Field Regimes: Geometry and Substrate Effects. *J. Phys. Chem. C* **2013,** *117* (38), 19606.
23. Xia, Y.; Xiong, Y.; Lim, B.; Skrabalak, S. E., Shape-Controlled Synthesis of Metal Nanocrystals: Simple Chemistry Meets Complex Physics? *Angew. Chem., Int. Ed.* **2009,** *48* (1), 60.
24. Yeh, Y.-C.; Creran, B.; Rotello, V. M., Gold nanoparticles: preparation, properties, and applications in bionanotechnology. *Nanoscale* **2012,** *4* (6), 1871.
25. Gans, R., Über die Form ultramikroskopischer Silberteilchen. *Annalen der Physik* **1915,** *352* (10), 270.
26. Link, S.; Mohamed, M. B.; El-Sayed, M. A., Simulation of the Optical Absorption Spectra of Gold Nanorods as a Function of Their Aspect Ratio and the Effect of the Medium Dielectric Constant. *J. Phys. Chem. B* **1999,** *103* (16), 3073.
27. Yan, B.; Yang; Wang, Y., Comment on "Simulation of the Optical Absorption Spectra of Gold Nanorods as a Function of Their Aspect Ratio and the Effect of the Medium Dielectric Constant". *J. Phys. Chem. B* **2003,** *107* (34), 9159.

28. Xia, Y.; Gilroy, K. D.; Peng, H.; Xia, X., Seed-Mediated Growth of Colloidal Metal Nanocrystals. *Angew. Chem., Int. Ed.* **2017,** *56* (1), 60.
29. Gao, C.; Goebl, J.; Yin, Y., Seeded growth route to noble metal nanostructures. *J. Mater. Chem. C* **2013,** *1* (25), 3898.
30. Niu, W.; Zhang, L.; Xu, G., Seed-mediated growth method for high-quality noble metal nanocrystals. *Science China Chemistry* **2012,** *55* (11), 2311.
31. Murphy, C. J.; Thompson, L. B.; Chernak, D. J.; Yang, J. A.; Sivapalan, S. T.; Boulos, S. P.; Huang, J.; Alkilany, A. M.; Sisco, P. N., Gold nanorod crystal growth: From seed-mediated synthesis to nanoscale sculpting. *Curr. Opin. Colloid Interface Sci.* **2011,** *16* (2), 128.
32. Zheng, Y.; Zhong, X.; Li, Z.; Xia, Y., Successive, Seed-Mediated Growth for the Synthesis of Single-Crystal Gold Nanospheres with Uniform Diameters Controlled in the Range of 5–150 nm. *Part. Part. Syst. Char.* **2014,** *31* (2), 266.
33. Niu, W.; Zheng, S.; Wang, D.; Liu, X.; Li, H.; Han, S.; Chen, J.; Tang, Z.; Xu, G., Selective Synthesis of Single-Crystalline Rhombic Dodecahedral, Octahedral, and Cubic Gold Nanocrystals. *J. Am. Chem. Soc.* **2009,** *131* (2), 697.
34. Park, G.; Seo, D.; Jung, J.; Ryu, S.; Song, H., Shape Evolution and Gram-Scale Synthesis of Gold@Silver Core–Shell Nanopolyhedrons. *J. Phys. Chem. C* **2011,** *115* (19), 9417.
35. Wang, Y.-N.; Wei, W.-T.; Yang, C.-W.; Huang, M. H., Seed-Mediated Growth of Ultralong Gold Nanorods and Nanowires with a Wide Range of Length Tunability. *Langmuir* **2013,** *29* (33), 10491.
36. Chen, L.; Hu, H.; Liu, Q.; Ji, F.; Chen, S.; Xu, Y.; Zhang, Q., Halide-free synthesis of Au nanoplates and monitoring the shape evolution process through a marker experiment. *J. Mater. Chem. C* **2016,** *4* (27), 6457.
37. Jiang, Y.; Zhang, Q.; Liu, X.; Chen, Y.; Wang, L.; Fu, J.; Duan, H.; Wang, Y.; Yang, X., Au nanoshell-coated superparamagnetic Fe3O4–silica composite nanoparticles with surface-modification of an activatable cell-penetrating peptide for tumor-targeted multimode bioimaging and photothermal therapy. *RSC Adv.* **2016,** *6* (88), 85587.
38. Jimenez de Aberasturi, D.; Serrano-Montes, A. B.; Langer, J.; Henriksen-Lacey, M.; Parak, W. J.; Liz-Marzán, L. M., Surface Enhanced Raman Scattering Encoded Gold Nanostars for Multiplexed Cell Discrimination. *Chem. Mater.* **2016,** *28* (18), 6779.
39. Gao, C.; Vuong, J.; Zhang, Q.; Liu, Y.; Yin, Y., One-step seeded growth of Au nanoparticles with widely tunable sizes. *Nanoscale* **2012,** *4* (9), 2875.

40. Peng, Z.; Yang, H., Designer platinum nanoparticles: Control of shape, composition in alloy, nanostructure and electrocatalytic property. *Nano Today* **2009,** *4* (2), 143.
41. Peng, Z. M.; Yang, H., Designer platinum nanoparticles: Control of shape, composition in alloy, nanostructure and electrocatalytic property. *Nano Today* **2009,** *4* (2), 143.
42. Bauer, E.; van der Merwe, J. H., Structure and growth of crystalline superlattices: From monolayer to superlattice. *Physical Review B* **1986,** *33* (6), 3657.
43. Chambers, S. A., Epitaxial growth and properties of thin film oxides. *Surf. Sci. Rep.* **2000,** *39* (5), 105.
44. Shen, B.; Linko, V.; Tapio, K.; Pikker, S.; Lemma, T.; Gopinath, A.; Gothelf, K. V.; Kostiainen, M. A.; Toppari, J. J., Plasmonic nanostructures through DNA-assisted lithography. *Science Advances* **2018,** *4* (2).
45. Juluri, R. R.; Rath, A.; Ghosh, A.; Satyam, P. V., Substrate Symmetry Driven Endotaxial Silver Nanostructures by Chemical Vapor Deposition. *J. Phys. Chem. C* **2013,** *117* (25), 13247.
46. Semaltianos, N. G.; Chassagnon, R.; Moutarlier, V.; Blondeau-Patissier, V.; Assoul, M.; Monteil, G., Nanoparticles alloying in liquids: Laser-ablation-generated Ag or Pd nanoparticles and laser irradiation-induced AgPd nanoparticle alloying. *Nanotechnol.* **2017,** *28* (15), 155703.
47. Xia, X.; Xie, S.; Liu, M.; Peng, H.-C.; Lu, N.; Wang, J.; Kim, M. J.; Xia, Y., On the role of surface diffusion in determining the shape or morphology of noble-metal nanocrystals. *PNAS* **2013,** *110* (17), 6669.
48. Pastoriza-Santos, I.; Liz-Marzán, L. M., Colloidal silver nanoplates. State of the art and future challenges. *J. Mater. Chem.* **2008,** *18* (15), 1724.
49. Millstone, J. E.; Hurst, S. J.; Métraux, G. S.; Cutler, J. I.; Mirkin, C. A., Colloidal Gold and Silver Triangular Nanoprisms. *Small* **2009,** *5* (6), 646.
50. Yu, D.; Yam, V. W.-W., Controlled Synthesis of Monodisperse Silver Nanocubes in Water. *J. Am. Chem. Soc.* **2004,** *126* (41), 13200.
51. Zhang, Q.; Hu, Y.; Guo, S.; Goebl, J.; Yin, Y., Seeded Growth of Uniform Ag Nanoplates with High Aspect Ratio and Widely Tunable Surface Plasmon Bands. *Nano Lett.* **2010,** *10* (12), 5037.
52. Zhang, Q.; Li, N.; Goebl, J.; Lu, Z.; Yin, Y., A Systematic Study of the Synthesis of Silver Nanoplates: Is Citrate a "Magic" Reagent? *J. Am. Chem. Soc.* **2011,** *133* (46), 18931.

53. Langille, M. R.; Personick, M. L.; Zhang, J.; Mirkin, C. A., Defining Rules for the Shape Evolution of Gold Nanoparticles. *J. Am. Chem. Soc.* **2012,** *134* (35), 14542.
54. Zhang, J.; Langille, M. R.; Personick, M. L.; Zhang, K.; Li, S.; Mirkin, C. A., Concave Cubic Gold Nanocrystals with High-Index Facets. *J. Am. Chem. Soc.* **2010,** *132* (40), 14012.
55. Herrero, E.; Buller, L. J.; Abruña, H. D., Underpotential Deposition at Single Crystal Surfaces of Au, Pt, Ag and Other Materials. *Chem. Rev.* **2001,** *101* (7), 1897.
56. Liu, M.; Guyot-Sionnest, P., Mechanism of Silver(I)-Assisted Growth of Gold Nanorods and Bipyramids. *J. Phys. Chem. B* **2005,** *109* (47), 22192.
57. Personick, M. L.; Langille, M. R.; Zhang, J.; Mirkin, C. A., Shape Control of Gold Nanoparticles by Silver Underpotential Deposition. *Nano Lett.* **2011,** *11* (8), 3394.
58. Liu, Y.; Pedireddy, S.; Lee, Y. H.; Hegde, R. S.; Tjiu, W. W.; Cui, Y.; Ling, X. Y., Precision Synthesis: Designing Hot Spots over Hot Spots via Selective Gold Deposition on Silver Octahedra Edges. *Small* **2014,** *10* (23), 4940.
59. Feng, Y.; He, J.; Wang, H.; Tay, Y.; Sun, H.; Zhu, L.; Chen, H., An Unconventional Role of Ligand in Continuously Tuning of Metal-Metal Interfacial Strain. *J. Am. Chem. Soc.* **2012,** *134* (4), 2004.
60. Feng, Y.; Wang, Y.; Song, X.; Xing, S.; Chen, H., Depletion sphere: Explaining the number of Ag islands on Au nanoparticles. *Chemical Science* **2017,** *8* (1), 430.
61. Wang, G.; Liu, Y.; Gao, C.; Guo, L.; Chi, M.; Ijiro, K.; Maeda, M.; Yin, Y., Island Growth in the Seed-Mediated Overgrowth of Monometallic Colloidal Nanostructures. *Chem* **2017,** *3* (4), 678.
62. Koczkur, K. M.; Mourdikoudis, S.; Polavarapu, L.; Skrabalak, S. E., Polyvinylpyrrolidone (PVP) in nanoparticle synthesis. *Dalton Trans.* **2015,** *44* (41), 17883.
63. Mdluli, P. S.; Sosibo, N. M.; Revaprasadu, N.; Karamanis, P.; Leszczynski, J., Surface enhanced Raman spectroscopy (SERS) and density functional theory (DFT) study for understanding the regioselective adsorption of pyrrolidinone on the surface of silver and gold colloids. *J. Mol. Struct.* **2009,** *935* (1), 32.
64. Zhang, Z.; Zhao, B.; Hu, L., PVP Protective Mechanism of Ultrafine Silver Powder Synthesized by Chemical Reduction Processes. *J. Solid State Chem.* **1996,** *121* (1), 105.
65. Walther, A.; Müller, A. H. E., Janus Particles: Synthesis, Self-Assembly, Physical Properties, and Applications. *Chem. Rev.* **2013,** *113* (7), 5194.

66. Guarrotxena, N.; García, O.; Quijada-Garrido, I., Synthesis of Au@polymer nanohybrids with transited core-shell morphology from concentric to eccentric Emoji-N or Janus nanoparticles. *Sci. Rep.* **2018,** *8* (1), 5721.

67. Choi, B. C.; Choi, S.; Leckband, D. E., Poly(N-isopropyl acrylamide) Brush Topography: Dependence on Grafting Conditions and Temperature. *Langmuir* **2013,** *29* (19), 5841.

68. Choueiri, R. M.; Galati, E.; Thérien-Aubin, H.; Klinkova, A.; Larin, E. M.; Querejeta-Fernández, A.; Han, L.; Xin, H. L.; Gang, O.; Zhulina, E. B.; Rubinstein, M.; Kumacheva, E., Surface patterning of nanoparticles with polymer patches. *Nature* **2016,** *538*, 79.

69. Liu, B.; Thanneeru, S.; Lopes, A.; Jin, L.; McCabe, M.; He, J., Surface Engineering of Spherical Metal Nanoparticles with Polymers toward Selective Asymmetric Synthesis of Nanobowls and Janus-Type Dimers. *Small* **2017,** *13* (20), 1700091.

70. Wang, Z.; He, B.; Xu, G.; Wang, G.; Wang, J.; Feng, Y.; Su, D.; Chen, B.; Li, H.; Wu, Z.; Zhang, H.; Shao, L.; Chen, H., Transformable masks for colloidal nanosynthesis. *Nat. Commun.* **2018,** *9* (1), 563.

71. Chen, T.; Chen, G.; Xing, S.; Wu, T.; Chen, H., Scalable Routes to Janus Au−SiO2 and Ternary Ag−Au−SiO2 Nanoparticles. *Chem. Mater.* **2010,** *22* (13), 3826.

72. Wang, F.; Cheng, S.; Bao, Z.; Wang, J., Anisotropic Overgrowth of Metal Heterostructures Induced by a Site-Selective Silica Coating. *Angew. Chem., Int. Ed.* **2013,** *52* (39), 10344.

73. Martin, C. R., Nanomaterials: A Membrane-Based Synthetic Approach. *Science* **1994,** *266* (5193), 1961.

74. Mikhailov, O. V., Molecular structure design and soft template synthesis of aza-, oxaaza- and thiaazamacrocyclic metal chelates in the gelatin matrix. *Arabian Journal of Chemistry* **2017,** *10* (1), 47.

75. Martin, B. R.; Dermody, D. J.; Reiss, B. D.; Fang, M.; Lyon, L. A.; Natan, M. J.; Mallouk, T. E., Orthogonal Self-Assembly on Colloidal Gold-Platinum Nanorods. *Adv. Mater.* **1999,** *11* (12), 1021.

76. Oh, T.; Ku, J. C.; Ozel, T.; Mirkin, C. A., Orthogonal Chemical Modification of Template-Synthesized Nanostructures with DNA. *J. Am. Chem. Soc.* **2017,** *139* (20), 6831.

77. Martin, C. R., Membrane-Based Synthesis of Nanomaterials. *Chem. Mater.* **1996,** *8* (8), 1739.

78. Liu, Y.; Goebl, J.; Yin, Y., Templated synthesis of nanostructured materials. *Chem. Soc. Rev.* **2013,** *42* (7), 2610.
79. Oldenburg, S. J.; Averitt, R. D.; Westcott, S. L.; Halas, N. J., Nanoengineering of optical resonances. *Chem. Phys. Lett.* **1998,** *288* (2), 243.
80. Wang, X.; Feng, J.; Yu, H.; Jin, Y.; Davidson, A.; Li, Z.; Yin, Y., Anisotropically Shaped Magnetic/Plasmonic Nanocomposites for Information Encryption and Magnetic-Field-Direction Sensing. *Research* **2018,** *2018*, 13.
81. Gao, C.; Zhang, Q.; Lu, Z.; Yin, Y., Templated Synthesis of Metal Nanorods in Silica Nanotubes. *J. Am. Chem. Soc.* **2011,** *133* (49), 19706.
82. Gao, C.; Lu, Z.; Yin, Y., Gram-Scale Synthesis of Silica Nanotubes with Controlled Aspect Ratios by Templating of Nickel-Hydrazine Complex Nanorods. *Langmuir* **2011,** *27* (19), 12201.
83. Zhang, Q.; Ge, J.; Goebl, J.; Hu, Y.; Sun, Y.; Yin, Y., Tailored Synthesis of Superparamagnetic Gold Nanoshells with Tunable Optical Properties. *Adv. Mater.* **2010,** *22* (17), 1905.
84. Gao, A.; Xu, W.; de Leon, Y.; Bai, Y.; Gong, M.; Xie, K.; Park, B.; Yin, Y., Controllable Fabrication of Au Nanocups by Confined-Space Thermal Dewetting for OCT Imaging. *Adv. Mater.* **2017,** *29* (26).

Chapter 2 Seed-Mediated Growth of Au Islands on Au Nanocrystals by Surface Engineering and Controlled Ripening

2.1 Introduction

It is well known that seed-mediated growth of metal nanocrystals, which involves reduction and deposition of metal precursors on the pre-existed seeds, is an effective method for the synthesis of plasmonic metal nanocrystals with well-defined geometry, size, composition, and surface properties.[1-4] Although many excellent works have been done to tune the growth pathways of metal nanocrystals and discover the chemistry behind the seed-mediated growth, it still remains a challenge to create a secondary structure on a nanocrystal in a controllable manner, which could benefit both application and fundamental study of the complicated nanostructures.

Seed-mediated growth of plasmonic nanostructures composed of Au and Ag always follows a layer-by-layer fashion, which is also known as the 'Frank-van der Merwe' (FM) mode, due to the tight match between crystal lattices.[5] To break the conformal growth pattern, the surface property of the seed and the kinetics for the metal deposition should be precisely controlled.[6] Previous research managed to adjust the interfacial strain energy during the deposition of Ag on Au by using strong ligands, which forced the deposition of Ag to follow the island-growth (Volmer-Weber, VW) mode.[7-10] In addition, partial passivation of Au surface by using inorganic solids, polymers, and metal coordinates is a straightforward method to create difference between regions, leading to the growth of secondary structures from the exposed areas. The difficulty in synthesis, and the lack of tunability in the structures and optical properties of the nanocrystals limit the application

of such methods as a general method for island-growth of plasmonic nanostructures. Therefore, it is highly important to build up a new reaction system, which is not only suitable for island-growth, but also has room for adjustment of the island nanostructures.

In this work, we design an effective route to create the secondary structure of Au on an Au nanosphere, and control the number of islands by a two-step seed-mediated growth process. The system has several degrees of freedom, and is suitable for the investigation of each of them by adjusting one variable while fixing the rests. We will analyze three important degrees of freedom: the strain energy caused by lattice mismatch, the ripening process during the seed-mediated growth and the surface diffusion of metal ions. First, the surface property of Au seed should be engineered to meet the thermodynamic requirement for the island-growth mode. Island-growth of one metal species on the other is governed by a number of physical parameters, including the mismatch of lattice constants, and the correlation of surface and interface energies. When a metal is deposited on the surface of a seed with a large lattice mismatch, the growth will be dominated by the island mode.[11] In this case, the interface strain energy could be increased by modifying the Au seeds with a thin layer of Pt, which has 4.08 % lattice mismatch with Au.[12-13] Second, a controlled oxidative ripening process, which is often neglected in previous study, should be considered during the growth of nanoislands. We employed I^- as a ligand to promote the oxidative ripening of Au. Third, control the diffusion of Au precursors on surface of the seeds should also be considered, because it influences the migration of atoms, which may lead to formation of nanoislands with different structures. Combining all of the parameters above, growth of Au nanoislands on

Au nanoparticles could be achieved in different well-controlled structures. This synthetic system has many advantages: 1) the interface strain energy can be adjusted by tuning the molar ratio of Pt/Au; 2) the AuPt nanospheres can be stable in various seeded growth reactions; 3) the ripening of deposited Au can be tuned by controlling the amount of KI; 4) Au islands with tunable structures can be obtained in the same system with minor modification of the reaction conditions. It is worth noting that although Pt is plasmonic inert in visible range, the plasmonic properties of the Au nanostructured can be retained when the Pt layer is very thin.

2.2 Materials and Methods

2.2.1 Materials

Poly(vinylpyrrolidone) (PVP, Mw=10,000), potassium iodide (KI), L-ascorbic acid (AA), sodium borohydride ($NaBH_4$, 99%), chloroauric acid ($HAuCl_4$), chloroplatinic acid ($H_2PtCl_6 \cdot 6H_2O$) and trisodium citrate (TSC) were purchased from Sigma-Aldrich. All chemicals were directly used without further purification.

2.2.2 Synthesis of AuPt Nanospheres

The AuPt nanospheres were synthesized by reducing Pt precursors in a solution containing Au nanospheres. In a typical synthesis, 20 μL of $HAuCl_4$ (0.25 M) was added to 9.5 mL of H_2O. The solution was heated to boiling, followed by injection of 0.5 mL of TSC (1 wt%) solution. After boiling for 10 minutes, the solution became wine-red. Then, 50 μL of AA (0.1 M) and 25 μL of H_2PtCl_6 (20 mM) were added to the solution for the growth of Pt. The molar ratio of AA:Pt was 10. After reacting for another 5 minutes, the AuPt nanoparticles was centrifuged at 12000 rpm for 5 minutes and redispersed in 10 mL of H2O. The amount of Pt could be tuned to adjust the ratio of Pt:Au. In this case, the molar ratio of Pt:Au was calculated to be 0.1. The sample was named as AuPt-0.1.

2.2.3 Synthesis of (AuPt-0.1)-Au Core-Satellite Nanostructure

In a typical synthesis, 500 μL of AuPt-0.1 solution, 500 μL of H_2O, 40 μL PVP (5 wt%), 2 μL of AA (0.1 M), and 2.5 μL of $HAuCl_4$ (25 mM) were added in order at room temperature. The solution was kept stirring for 10 minutes. The resulting (AuPt-0.1)-Au core-satellite nanostructures were collected by centrifugation, washed with H_2O, and redispersed in 1 mL of H_2O.

2.2.4 Synthesis of (AuPt-0.1)-Au Dimers.

A growth solution was prepared by mixing 100 μL of H_2O, 50 μL of PVP (5 wt%), 12.5 μL AA (0.1 M), 12.5 μL of KI (0.2 M), and 3 μL of $HAuCl_4$ (0.25 M). The growth solution was used within one hour after the preparation. In a typical synthesis, 500 μL of AuPt-0.1 solution, 500 μL of H_2O, and 58.3 μL of KI (0.2 M) were added in order at room temperature. 60 μL of the growth solution was added to the above solution. The molar ratio of KI: Au was 50. The Au dimers was collected after 30 minutes of the reaction, washed with H_2O and redispersed in 1 mL of H_2O.

2.2.5 COMSOL simulation of the LSPR

LSPR of the nanostructure was simulated by using COMSOL Multiphysics. The Au dimer was composed by two Au nanoparticles with size of 17 nm. A non-uniform meshing grid with smallest grid size ~ 3 nm was used. The refractive indices of gold were adopted from Palik's Handbook of Optical Constants of Solids.

2.2.6. Characterizations.

Transmission electron microscopy (TEM) images were taken with a Philips Tecnai 12 transmission electron microscope operating at 120 kV and JEOL JEM-2100 microscope operating at 200 kV (Cs 1.0 mm, point resolution 2.3 Å). The samples for TEM observation were prepared by drop casting a solution on a carbon film supported on a copper grid. Scanning transmission electron microscopy (STEM) images and energy-dispersive X-ray spectroscopy (EDS) mapping profiles were collected on a FEI Talos F200X transmission electron microscope operated at 200 kV UV-vis spectra were measured by using an Ocean Optics HR 2000CG-UV-NIR spectrometer.

2.2.5 Synthesis of (AuPt-0.1)-Au Core-Satellite Nanostructure

Deposition of Au species on Au seeds follows the layer-by-layer mode, because the lattice structure is just the same. An increase in the size from 17.0 to 28.4 nm and a slight redshift of the plasmonic extinction peak from 520 to 528 nm was observed when reducing $HAuCl_4$ on citrate capped Au nanocrystals by AA in a solution containing PVP as the surfactants (Figure 2.1 and 2.2). As described above, a mismatched interface is the sufficient condition to guide the metal deposition in the island-growth mode. Here, Pt species was introduced to modify the surface of the Au nanocrystals by reducing H_2PtCl_6 in a hot solution containing citrate capped Au nanocrystals and AA. The new seeds with Pt on the surface was names as AuPt-x, in which x indicated the molar ratio of Pt to Au. In a typical synthesis, the molar ratio of Pt to Au was fixed to 0.1. The large mismatch between Pt and Au increases the strain energy for Au deposition, which shifts the growth mode of Au from FM to VW, and hence the product from conformal nanospheres to nanoislands-on-nanospheres. Immediately after the injection of H_2PtCl_6 solution, the color of the citrate capped Au nanocrystals turned from ruby-red to burgundy, corresponding with a slight blue shift in the UV-vis spectra (Figure 2.3j) comparing with that of the citrate capped Au nanocrystals. The transmission electron microscopy (TEM) and high-angle annular dark-field scanning transmission electron microscopy (HAADF-STEM) images (Figure 2.3a and b) show that the AuPt-0.1 remained spherical with smooth surface and size of 17.3 ± 1.1 nm. Successful deposition of Pt was confirmed by X-ray spectroscopy (EDS) elemental mapping and the line elemental scan (Figure 2.3c and d), which shows the even distributions of Au and Pt elements in the AuPt-0.1. The

distribution of Au and Pt overlaps on the entire nanocrystal, indicating that the Pt layer is very thin. Seed-mediated growth of Au on AuPt-0.1 was done by reducing $HAuCl_4$ in a solution containing AA and 0.02 wt% PVP, named as (AuPt-0.1)-Au. The TEM and HAADF-STEM images (Figure 2.3e and f) show the core-satellite nanostructure of the (AuPt-0.1)-Au with an Au core of 17.2 ± 1.2 nm and Au nanoislands of 6.4 ± 1.3 nm, confirming the growth of Au species on the AuPt-0.1 nanocrystals in the VW mode. EDS elemental mapping and the line elemental scan (Figure 2.3g and h) of the (AuPt-0.1)-Au show the even distribution of Pt on the entire Au seed, and confirm that the islands are mainly composed of Au atoms. The HRTEM image in Figure 2.3i clearly shows that the small island is grown from the Au nanocrystal along the [111] direction. The stacking faults between the island and the Au nanocrystal indicate the high strain energy due to the deposition of Pt atoms. The growth of the Au nanoislands on the surface of the AuPt-0.1 nanoparticles has strong influence to their optical properties, as shown in the extinction spectra (Figure 2.3j). After the formation of Au nanoislands, the LSPR band is greatly broadened, and the peak redshifts from 512 nm to 536 nm. The redshift and broadening of the LSPR peak are due to the increase in surface roughness and anisotropy.

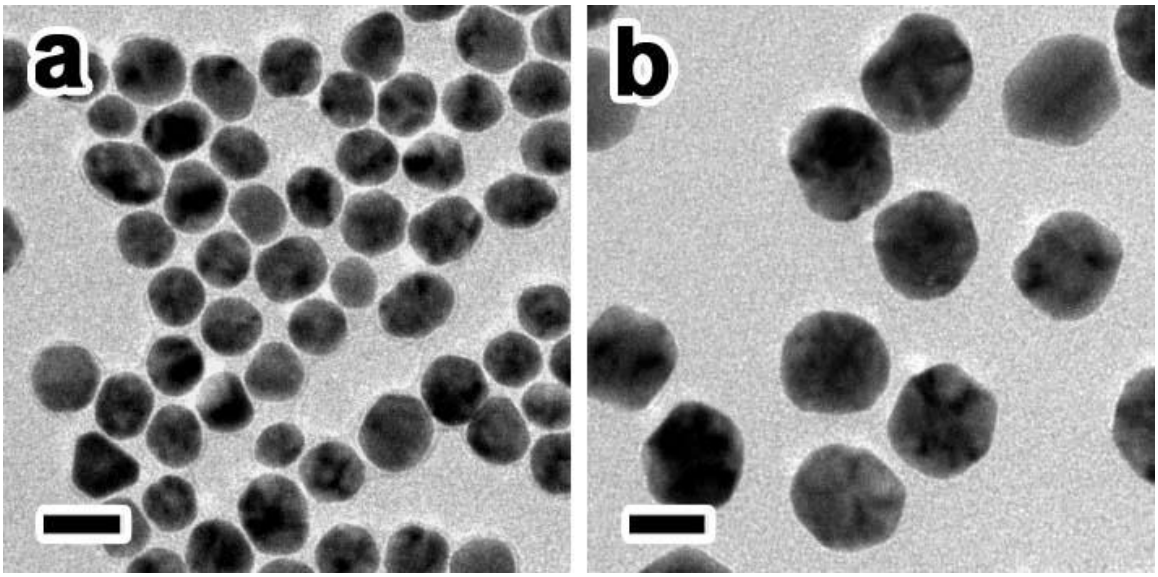

Figure 2.1 TEM images of TSC-Au seeds (a) and Au nanospheres after seeded growth (b).

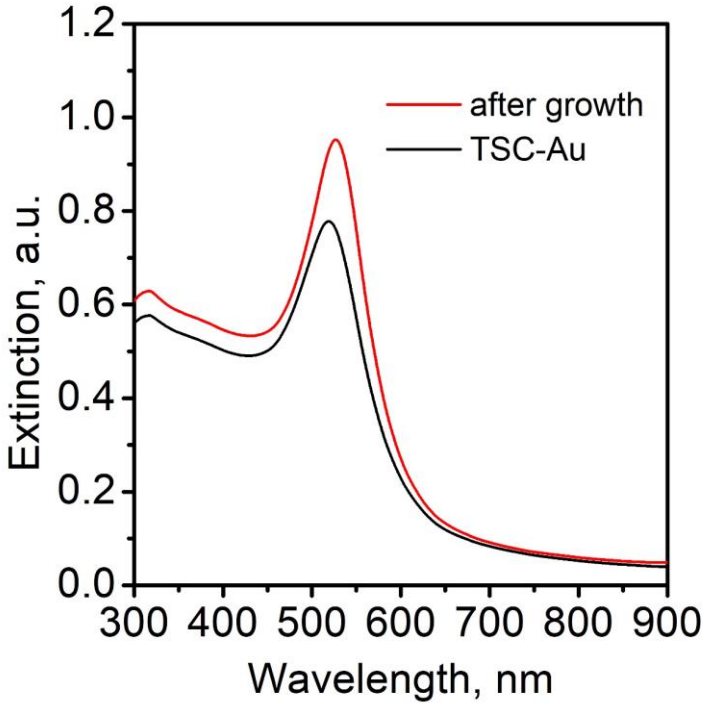

Figure 2.2 UV-vis extinction spectra of the TSC-Au seeds and Au nanospheres.

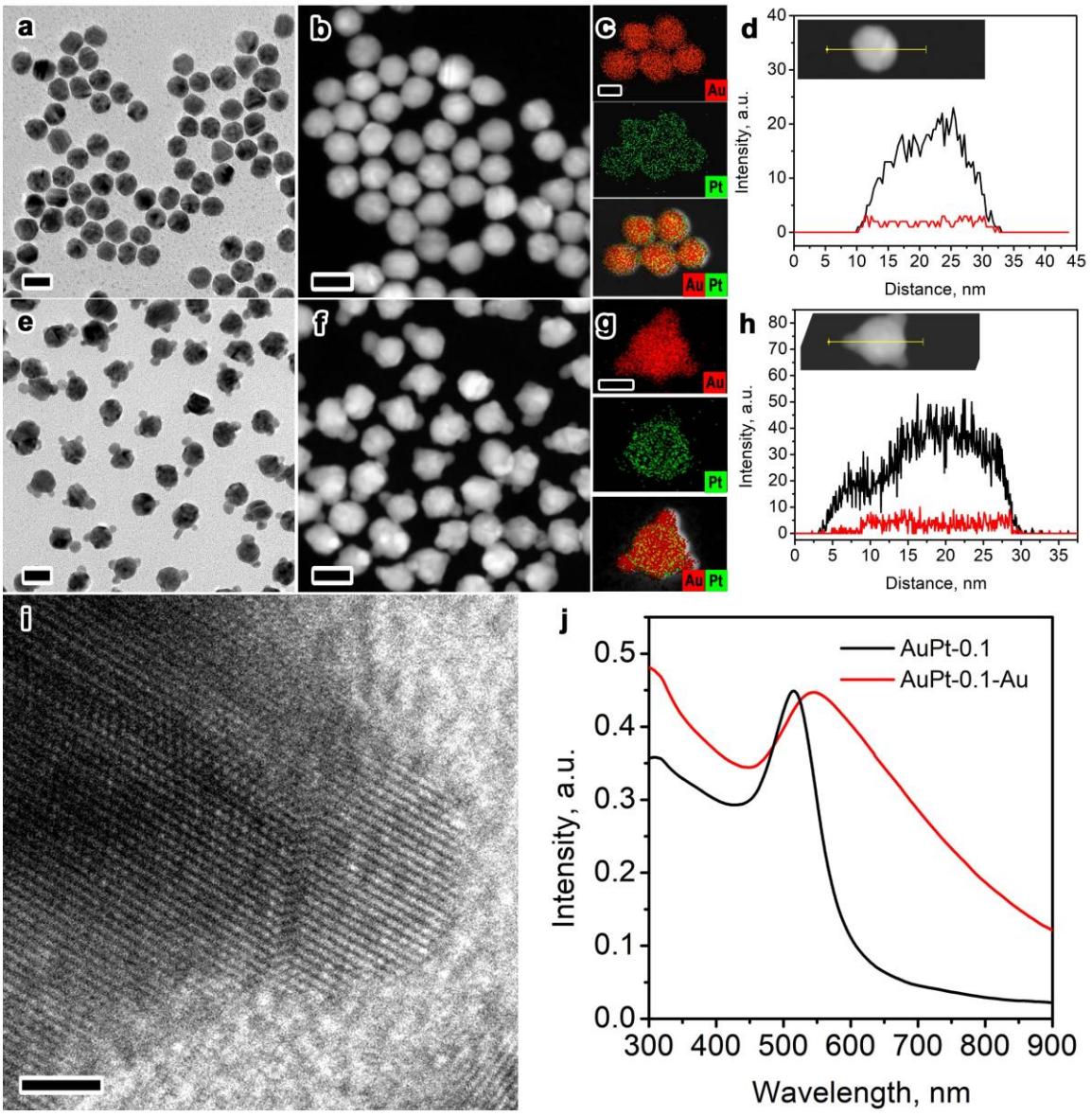
a
b
c
Au
Pt
Au Pt
d
Intensity, a.u.
Distance, nm
e
f
g
Au
Pt
Au Pt
h
Intensity, a.u.
Distance, nm
i
j
AuPt-0.1
AuPt-0.1-Au
Intensity, a.u.
Wavelength, nm

Figure 2.1 TEM images of AuPt-0.1 nanoparticles (a) and (AuPt-0.1)-Au core-satellite nanostructures (e). HADDF-STEM image and EDS elemental mapping of AuPt-0.1 nanoparticles (b, c) and (AuPt-0.1)-Au core-satellite nanostructures (f, g). EDS line scan showing the distribution of Pt (red line) on the Au (black) surface of a single AuPt-0.1 nanoparticle (d) and (AuPt-0.1)-Au nanoparticles (h). (i) HRTEM of a single Au island on AuPt-0.1. (j) UV-vis spectra of AuPt-0.1 nanoparticles and (AuPt-0.1)-Au nanoparticles. The scale bars are 20 nm in a, b, e and f, 10 nm in the EDS elemental mapping and 2 nm in i.

2.2.6 Control the Number of Islands by Ligand-Assisted Oxidative Ripening

The number of nanoislands on AuPt-0.1 should be controlled to create multiple nanostructures. Here, we managed the shape transformation from multiple islands to dimers by controlled oxidative ripening. Ripening is a phenomenon related to the energy difference of large particles and the small ones during growth crystal growth, which often results in size change and shape transformation of the nanocrystals.[14-16] In this work, oxidative etching is performed by adding I^-, which is proposed to form I_3^- to oxidize Au nanoparticles according to equations below:

$2I^- + O_2 + 4H^+ = I_2 + 2H_2O$

$I_2 + I^- = I_3^-$

$2Au + I_3^- + I^- = 2AuI_2^-$.

We show the structure transformation of (AuPt-0.1)-Au from satellite structure to dimers by adding KI into the reaction. The seed-mediated growth was done by injecting a growth solution containing PVP as surfactant, $HAuCl_4$ as the Au precursor, AA as the reducing agent and KI as the ligand to an AuPt-0.1 suspension. It appears that when the ratio of I^-/Au is fixed to 50, the dimer structure is formed (Figure 2.4). TEM images (Figure 2.4a-d) show the structure of (AuPt-0.1)-Au dimers with increasing amount of growth solution. The molar ratio of Au in growth solution (Au_{growth}) to Au in seeds (Au_{seeds}) was calculated to be 0.25, 0.5, 1, and 1.5 for sample shown in Figure 2.4a-d. Each dimer is composed of two spherical Au nanoparticles with the size of one nanoparticle fixed at around 17 nm and the other increased from 9.2 to 14.7, 18.4 and 25.1 nm with increasing amount of growth solution. A large scale TEM image (Figure

2.4e) of the sample shown in Figure 2b proves that the (AuPt-0.1)-Au dimer is of very high purity. The HAADF-STEM images and EDS mapping (Figure 2.4f) show the distribution of Au and Pt on the dimer structure. Au distributed homogeneously on the entire dimer structure, while Pt is rich on one end and rare on the other end. The inhomogeneous distribution of Pt is also confirmed by the line elemental scan (Figure 2.4g). HRTEM image in Figure 2.5 shows the stacking faults between the two spherical nanoparticles, indicating the similar island-growth mechanism with the formation of (AuPt-0.1)-Au core-satellite nanostructures.

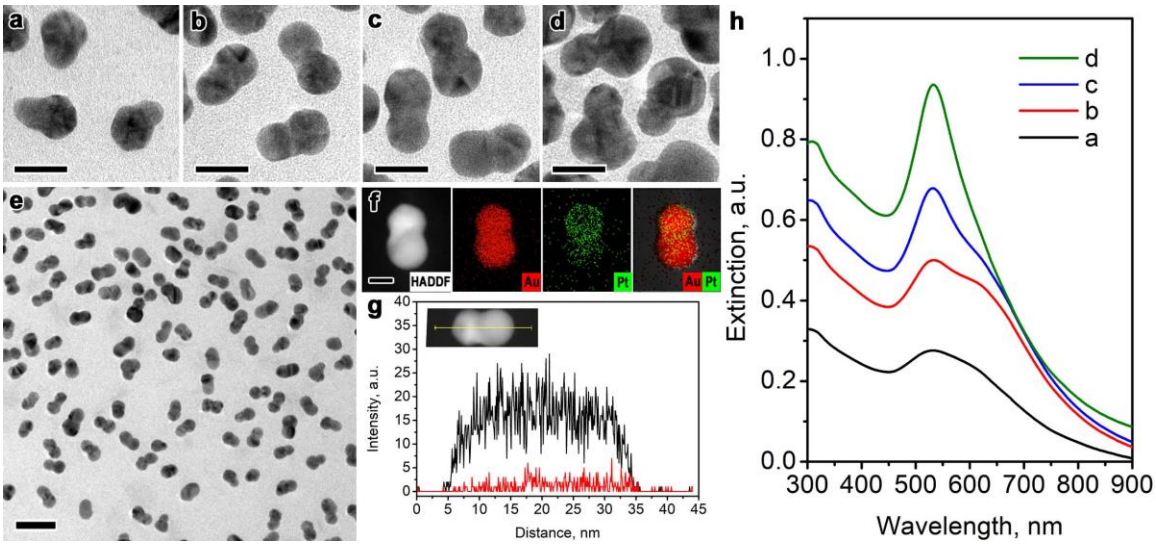

Figure 2.4 TEM images of (AuPt-0.1)-Au dimers synthesized with increasing amount of $HAuCl_4$ (a-d). (e) Large scale TEM image of sample in b. (f) HADDF-STEM image and EDS elemental mapping of the (AuPt-0.1)-Au dimer (sample in b). (g) corresponding EDS line scan showing the distribution of Pt (red line) on the Au (black) surface of a (AuPt-0.1)-Au dimer. (h) UV-vis spectra of of (AuPt-0.1)-Au dimers in a-d. The scale bars are 20 nm in (a-d), 50 nm in (e), and 10 nm in (f).

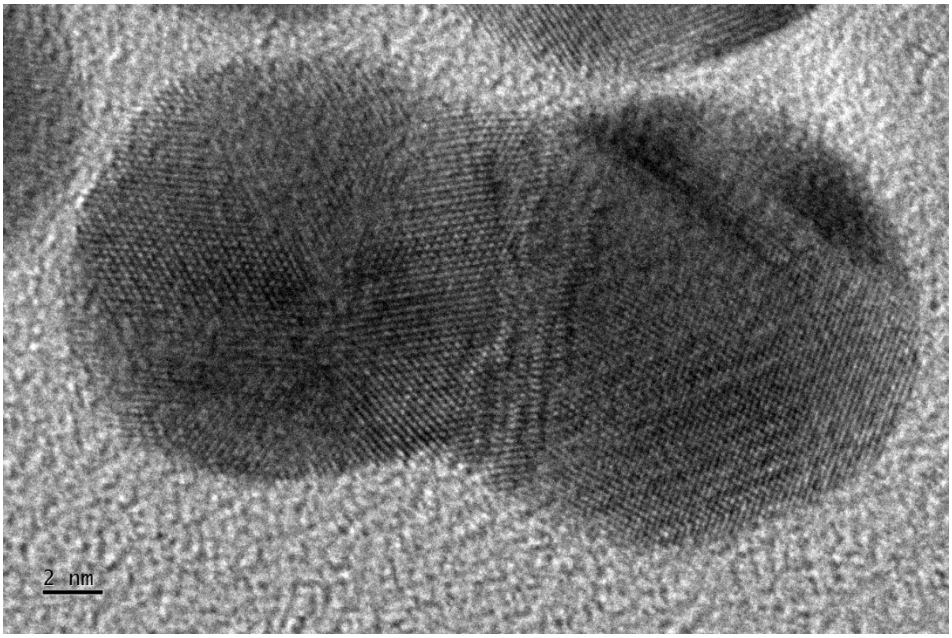

Figure 2.5 HRTEM images of (AuPt-0.1)-Au dimers.

As we have proposed, although plasmonic excitation of Au can be flattened by Pt, Au nanostructures with a very thin layer of Pt will still maintain their plasmonic properties. The UV-vis extinction spectra (Figure 2.4h) of sample a-d show dramatic changes comparing with the AuPt-0.1 nanocrystals. When the ratio of Au_{growth}/Au_{seeds} was 0.25, the extinction peak is broad, and can be split to two peaks centered at 527 and 604 nm. A more distinguishable peak appeared at 623 nm, while the peak at lower wavelength slightly redshift to 529 nm, when the ratio of Au_{growth}/Au_{seeds} increased to 0.5. Further increase the ratio of Au_{growth}/Au_{seeds} to 1 caused an increase in the intensity of the extinction peak at 529 nm, and slightly blueshift of the peak at longer wavelength to 614 nm. The intensity of the peak at lower wavelength kept increasing when the Au_{growth}/Au_{seeds} was increased to 1.5, together with slightly redshift of the peak to 531 nm. Meanwhile, the peak at longer wavelength blueshifted to 592 nm.

The plasmonic excitation of Au dimers can be understood by analyzing the excitation modes of two connected plasmonic nanoparticles. It has been reported that the plasmonic excitation of Au dimers could be split to two modes, a quadrupole resonance at lower wavelength and a dipole resonance at longer wavelength.[17-18] Here, we calculated the absorption spectra by using COMSOL Multiphysics. The scheme in Figure 2.6a shows the simulation model. The model is composed of two Au nanospheres and a tangent sphere, in which R is the radius of the Au nanosphere, r is the radius of the tangent sphere, and D is the overlapping distance. The transverse resonance and longitudinal resonance are calculated by varying the polarization direction of the incident light. When the oscillation of the electric field is polarized perpendicularly to the

interparticle axis, a transverse mode is excited, resulting in an absorption peak at short wavelength (520 nm). In contrast, when the oscillation direction of the electric field is polarized parallel to the interparticle axis, a longitudinal mode is excited, resulting in two absorption peaks at both short and long wavelength. In this case, the energy of the transverse mode is not related to the change in the shape of the dimers (Figure 2.6b and d). However, the energy of the longitudinal resonance is determined by not only the curvature of the connection (r), but also the overlapping distance (D) of the two spherical nanoparticles. As shown in Figure 2.6c, when r increases from 0.5 to 1, 5, 10, to 30 nm while D is fixed at 5 nm, the wavelength of the longitudinal resonance blueshifts from 640 to 635, 616, 605, and 595 nm. In addition, for a given r (1 nm), when D increases from 1 to 3, 5, 7, 9, and 11 nm, the wavelength of the dipole resonance blueshifts from 802 to 690, 635, 600, 575 and 560 nm. In a word, the plasmonic absorption under ordinary light is a sum of both the transverse and the longitudinal resonances, resulting in the two-peak absorption at both short and long wavelengths.

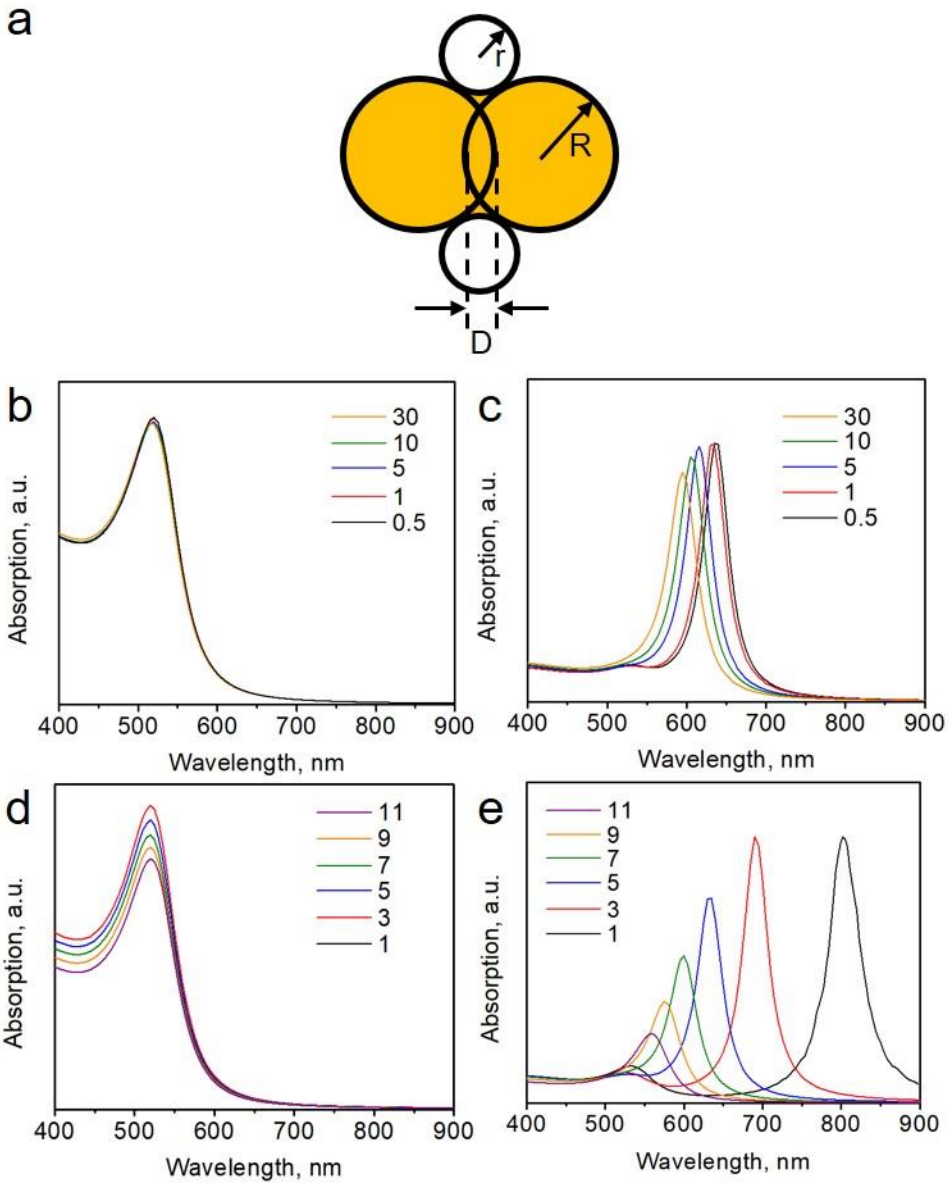
a
r
R
D
b
Absorption, a.u.
30
10
5
1
0.5
400
500
600
700
800
900
Wavelength, nm
c
Absorption, a.u.
30
10
5
1
0.5
400
500
600
700
800
900
Wavelength, nm
d
Absorption, a.u.
11
9
7
5
3
1
400
500
600
700
800
900
Wavelength, nm
e
Absorption, a.u.
11
9
7
5
3
1
400
500
600
700
800
900
Wavelength, nm

Figure 2.6 Calculated absorption spectra of Au dimers with different overlapping distances and curvatures of the connections. (a) Simulation model (r: radius of the tangent ball; R (17 nm): radius of the Au nanosphere); D: overlapping distance between two Au nanospheres); transverse (b) and longitudinal (c) absorption spectra of Au dimers with different r (D = 5 nm); transverse (d) and longitudinal (e) absorption spectra of Au dimers with different D (r = 1 nm).

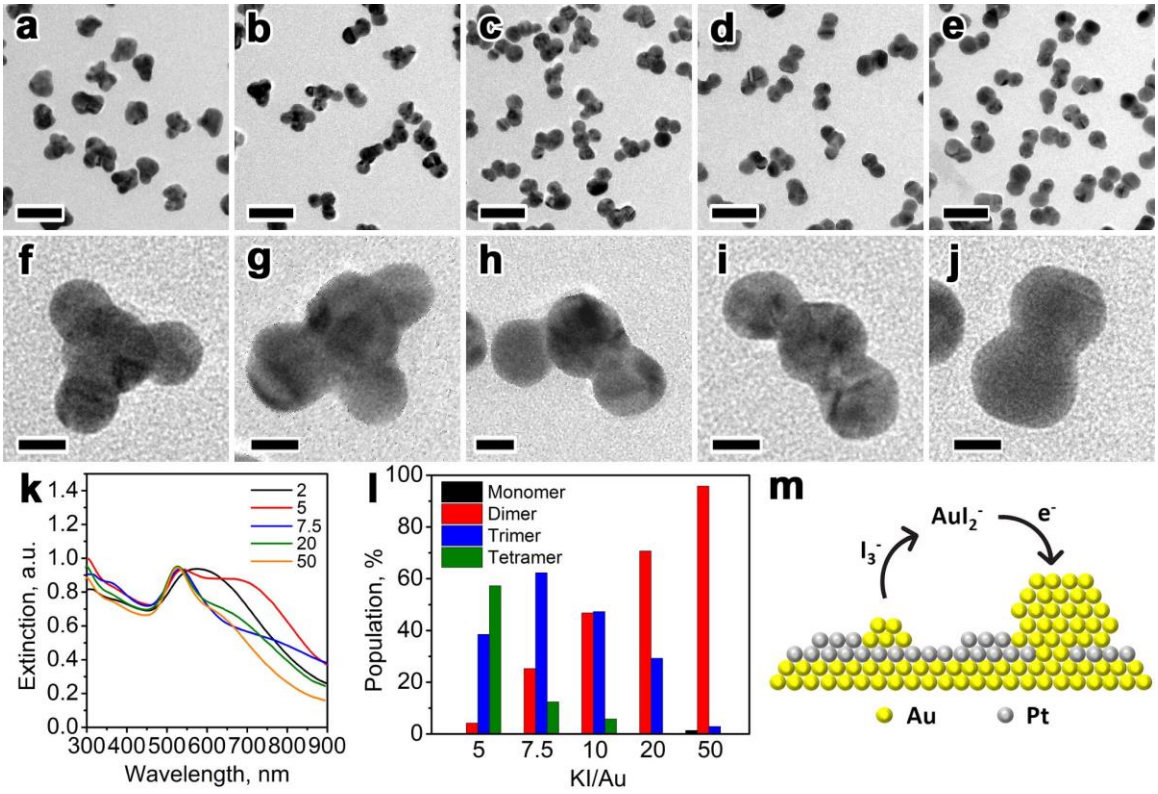

Figure 2.7 (a-e) TEM images of plasmonic nanostructures with the number of the spherical nanoparticles on the AuPt-0.1 nanospheres varying by deceasing the molar ratio of KI/$HAuCl_4$. Typical TEM images of the tetramer (f and g), trimer (h and i) and dimer (j). (k) UV-vis extinction spectra of the Au nanostructures, corresponding to (a-e). (l) Statistical analysis of the product distribution with different ratio of KI/ $HAuCl_4$. The dash line in (l) shows the trend of change in population of each nanostructure. (m) scheme illustration of ligand-assisted oxidative ripening. The scale bars are 50 nm in (a-e), and 10 nm in (f-j).

As iodide appears to be the most critical reagent for the formation of dimers, we examine its role carefully. TEM images in Figure 2.7 a-e show structure change of the (AuPt-0.1)-Au products synthesized with increasing amount of KI while the other synthetic parameters were kept exactly the same. The ratio of KI/$HAuCl_4$ in the growth solution was tuned from 2 to 5,7.5, 20 and 50 for sample shown in a-e. Some typical nanostructures, such as tetramer, trimer, and dimer (Figure 2.7f-j) can be clearly observed. It is shown that the angle between multiple Au islands are different in tetramer and trimers, indicating random distribution of the Au islands on the AuPt-0.1 nanocrystals. Statistical analysis of the product distribution (Figure 2.7l) shows that the number of Au islands on each AuPt-0.1 nanocrystal decreased with increasing the ratio of KI/$HAuCl_4$. When the ratio of KI/$HAuCl_4$ increased, the percentage of tetramers (green dashed line) decreased, while the percentage of dimers (red dashed line) increased. The shape change has significant impact to the plasmonic resonance of the (AuPt-0.1)-Au nanostructures. As shown in the UV-vis spectra, the sample synthesized with KI/$HAuCl_4$ = 2 has a broad extinction band. Increasing the ratio of KI/$HAuCl_4$ leads to exhibition of the two-band extinction. And the peak at higher wavelength redshifts when KI/$HAuCl_4$ increased from 2 to 5 and 7.5, and blueshifts when the KI/$HAuCl_4$ increased from 7.5 to 20 and 50.

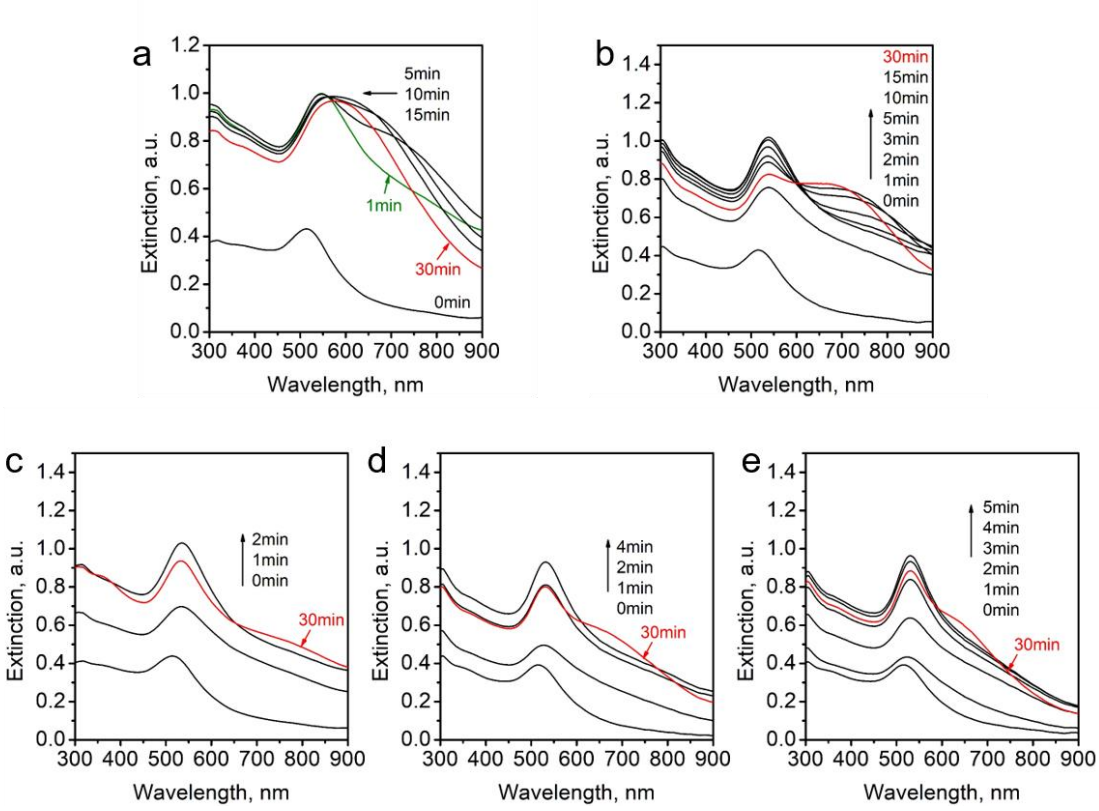

Figure 2.8 Time-dependent UV-vis spectra of plasmonic nanostructures synthesized with $KI/HAuCl_4$ = (a) 2, (b) 5, (c) 7.5, (d) 20 and (e) 50.

The reducing number of islands can be attributed to the oxidative etching of gold by iodide ions in the presence of oxygen. To further confirm the role of KI, we performed real-time UV-vis spectra (Figure 2.8) to monitor the shape transformation of the nanostructures with different KI/$HAuCl_4$. The formation of islands could be divides into two parts: initial deposition and oxidative ripening. Immediately after the injection of growth solution into the seed suspension, the plasmonic peak of Au redshifts and is greatly broadened in all of the samples, indicating the initial deposition and the formation of multiple islands on the AuPt-0.1 nanospheres. It took longer time for suspension with more KI to reach the highest extinction, indicating the lower initial deposition rate of the Au. It is worth noting that after the intensity of the plasmonic extinction at around 520 nm reaches its maximum, a second extinction peak at longer wavelength starts to emerge, and finally results in the two-band extinction for sample with higher KI/$HAuCl_4$. This process is considered a ripening process, during which the small islands dissolved and redeposited on relatively larger nanocrystals. Oxidative ripening of Au nanoparticles by KI was confirmed by adding KI in a suspension of 3-5 nm TSC capped Au nanoparticles in air. Figure 2.9 shows the real-time UV-vis spectra of sample taken at 60 minutes after the injection of KI. The broad peak at 502 nm redshifts to 525 nm, indicating an increase in size of the Au nanoparticle. And the change in peak intensity suggests dissolution and redeposition of the Au atoms. Removal of oxygen from the reaction suspension by purging N_2 leads to weakening of the shape transformation. As shown in Figure 2.9, the plasmonic resonance of Au shows almost no change under N_2 atmosphere. Here, we summarize the role of KI in two aspects, in the initial deposition step, KI is used to

coordinate with Au ions to form complex, which will lower down the reduction rate of Au. And in oxidative etching process, as shown in Figure 2.7m, the I^- ions can react with O_2 to form I_3^-, which react with Au to remove the relatively unstable small features. With increasing amount of I^-, the reaction rate for initial deposition was reduced and the etching of small Au islands was promoted, driving the reaction towards oxidative ripening.

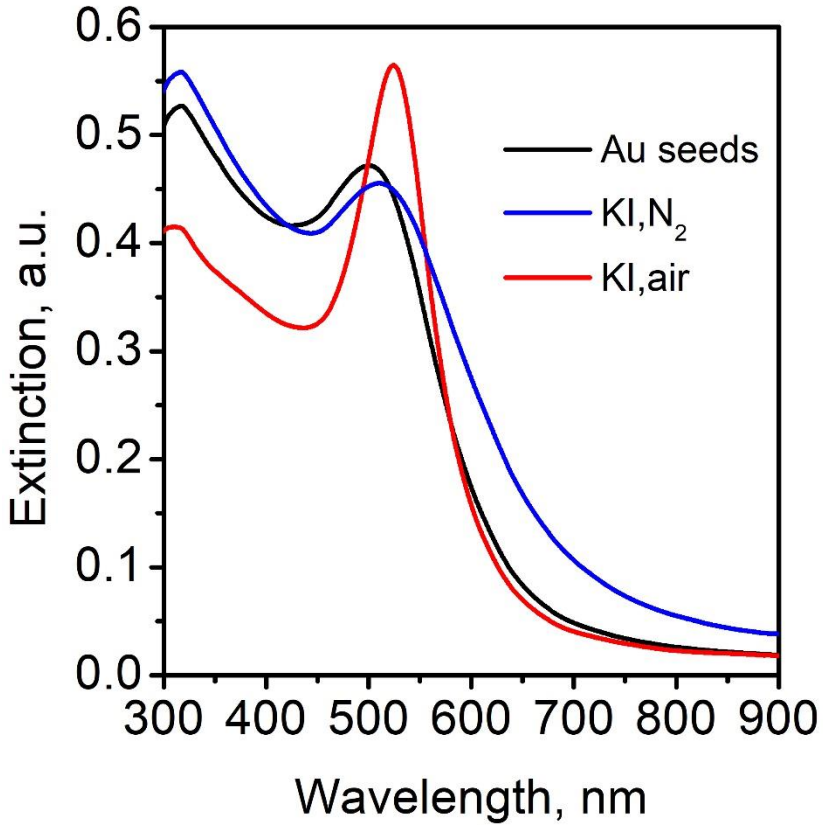

Figure 2.9 UV-vis spectra of freshly prepared Au seeds, and I^--assisted oxidative ripening products of Au seeds in air and in N_2. The products were collected after 60 minutes of the reaction.

2.2.7 Control the Number of Islands by Tuning Surface Strain

Besides the ligand-assisted oxidative ripening, there are two other important parameters need to be considered during island growth: the molar ratio of Pt/Au in the seeds and the diffusion of the precursors. The former influences the surface strain for metal deposition, while the latter determines the difficulty of the metal precursor migration on surface of the AuPt-x nanocrystals. The impact of these two parameters was studied by adjusting a single variable during the synthesis.

When the surface of Au nanocrystals is occupied by Pt atoms, the strain energy for Au deposition will increase with increasing the amount of Pt. In another word, the surface of AuPt is not friendly for Au deposition, and the degree of difficulty is elevated by modify the surface of the seeds with more Pt. Figure 2.10 shows the structure change of the AuPt-x-Au nanocrystals with Pt/Au ratio increases from 0.025 to 0.075, 0.1 and 0.25, while the other parameters were kept all the same. AuPt-x nanoparticles with different molar ratio of Pt/Au were synthesized by adjusting the injection volume of the H_2PtCl_6. The UV-vis spectra (Figure 2.11) and TEM images (Figure 2.12) of AuPt-0.025, AuPt-0.075 and AuPt-0.25 confirm the successful deposition of Pt on the Au nanocrystals. During seeded growth, the molar ratio of KI/$HAuCl_4$ in the growth solution was fixed at 10, because it gave room for the observation of the structure change. And the atomic ratio of Au in the growth solution to Au in the seeds was maintained at 1. The sample synthesized by using AuPt-0.025 as seeds still holds anisotropic nanostructure, but the morphology of the islands is not clear in the TEM images. The UV-vis extinction of sample synthesized by using AuPt-0.025 shows a broad resonance band at 566 nm

(Figure 2.10e), indicating the increase in anisotropy of the nanostructure comparing with spherical Au. However, the anisotropy is not enough for peak separation. In addition, the interfacial area between spherical nanoparticles in one nanostructure is relatively larger than the samples with higher Pt/Au ratio, due to the relatively small degree of surface strain. As the molar ratio of Pt/Au increased, the island-structure became much clearer, and the number of islands on one seed was greatly reduced. Statistical analysis of the product distribution shows a decrease from 17.6 to 8.5 and 0 % for Au tetramers, and from 56.9 to 47.3 and 18.6 % for Au trimers when the Pt/Au was increased from 0.075 to 0.1 and 0.25. Meanwhile, the percentage of Au dimers increases from 25.5 to 46.8 and 79.1 %. The shape changes also caused the change in resonance mode of the nanostructures. The two-band extinction spectra were observed for (AuPt-0.075)-Au and (AuPt-0.1)-Au (Figure 2.10e). It is worth noting that although the (AuPt-0.25)-Au is dominated by dimer structures, it shows only one extinction peak at 534 nm, which can be attributed to the plasmonic resonance of Au nanospheres. The single peak is shown because the dipole resonance of Au dimers is prohibited by the Pt layer.

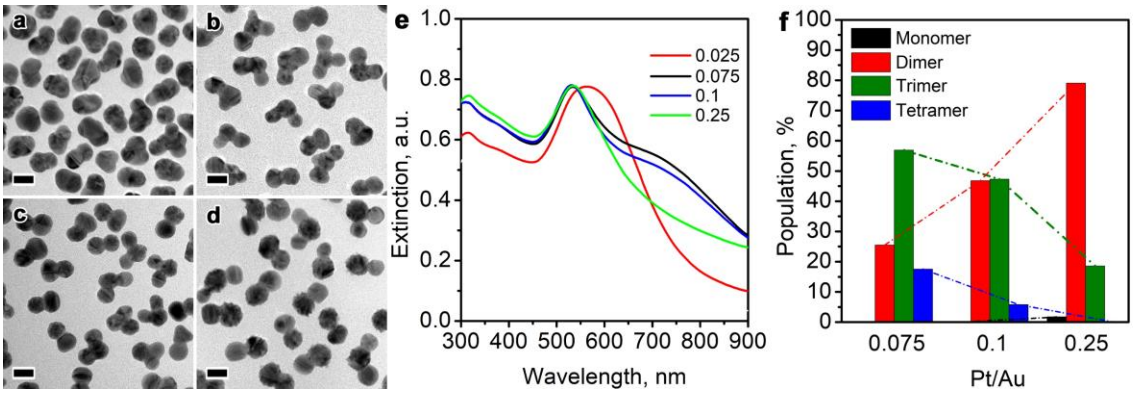

Figure 2.10 (a-d) TEM images of plasmonic nanostructures with the number of the spherical nanoparticles on the AuPt-x nanospheres varying by increasing the molar ratio of Pt/Au in the seed. (e) UV-vis extinction spectra of the Au nanostructures, corresponding to (a-d). (f) Statistical analysis of the product distribution with different ratio of Pt/Au in the seed. The dash line in (f) shows the trend of change in the population of each nanostructure. The scale bars are 20 nm in (a-d).

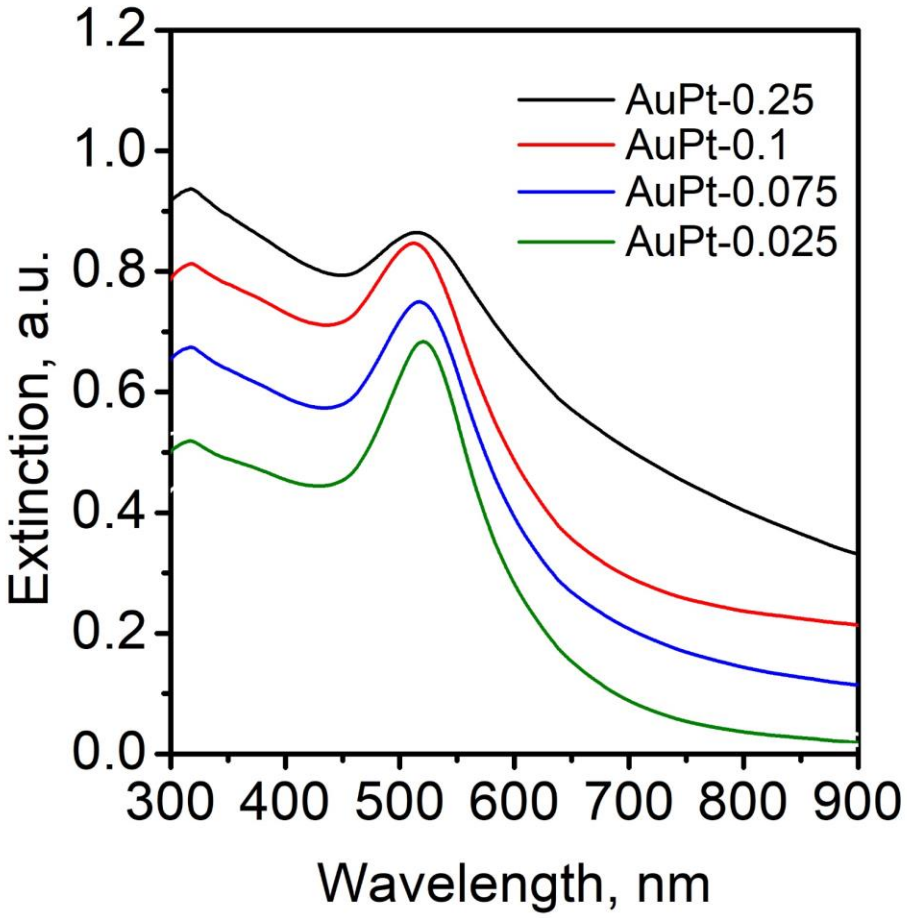

Figure 2.11 UV-vis spectra of AuPt-x nanospheres with Pt/Au = 0.025, 0.075, 0.1, 0.25.

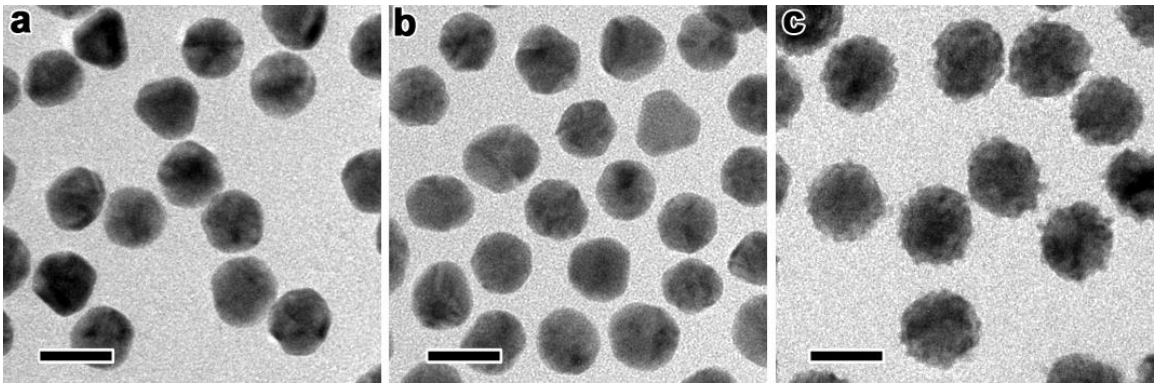

Figure 2.12 TEM images of AuPt-0.025 and AuPt-0.075, and AuPt-0.25. The scale bars are 20 nm.

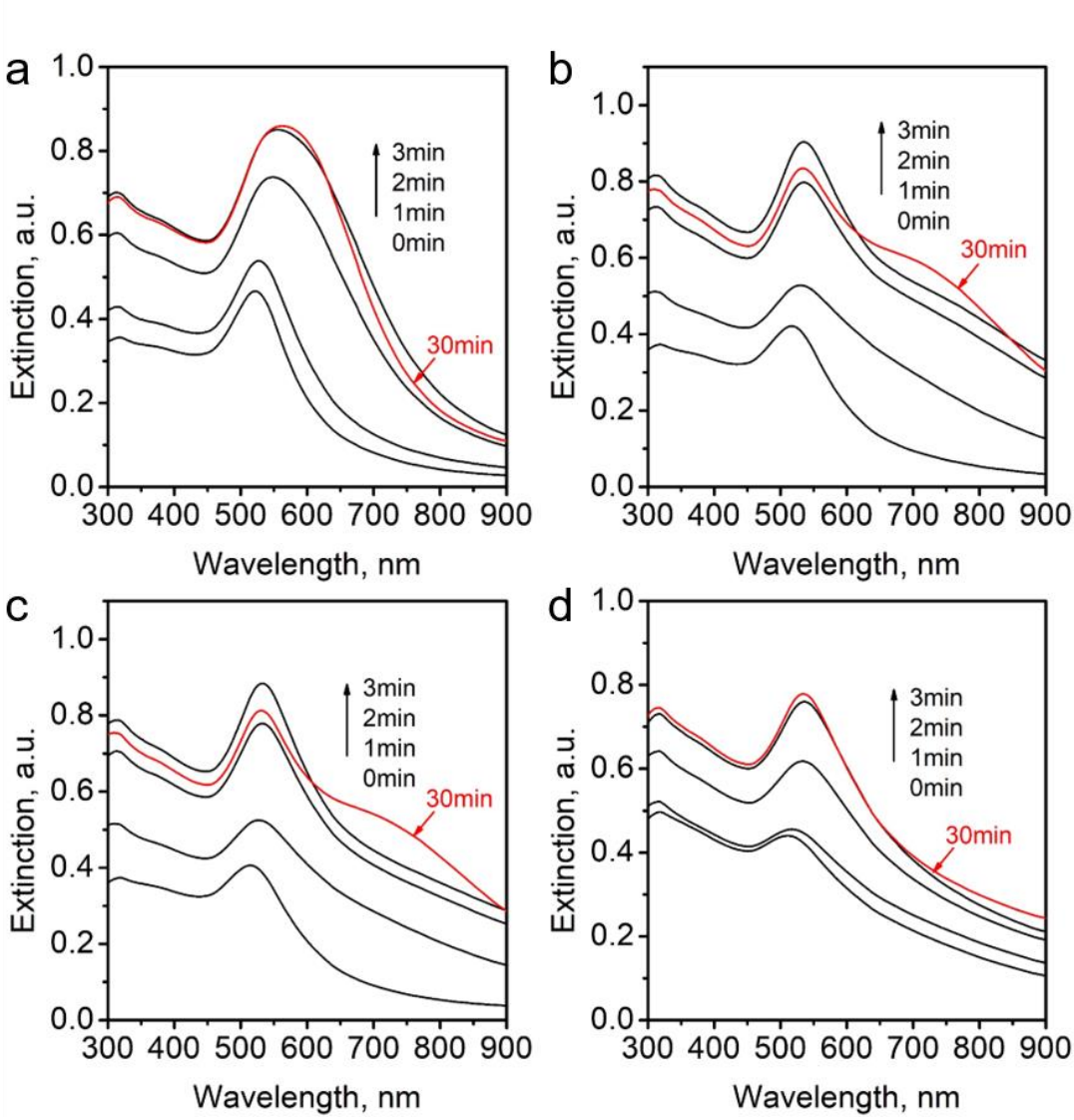

Figure 2.13 Time-dependent UV-vis spectra of the plasmonic nanostructures synthesized with Pt/Au = (a) 0.025, (b) 0.075, (c) 0.1 and (d) 0.25.

To further investigate the role of Pt, we characterized the real-time UV-vis spectra of samples shown in Figure 2.10. As it is shown in Figure 2.13, the shape evolution of all the samples follows the initial deposition and oxidative ripening process. Because the samples were synthesized with the same KI/$HAuCl_4$ ratio, the time for all the samples to reach the maximum intensity of plasmonic extinction are the same, indicating the same deposition rate for initial deposition of Au atoms. Different from the other samples, the time dependent UV-vis spectra of (AuPt-0.025)-Au (Figure 2.13a) shows slight redshift in the first 1 minute, and the peak is narrow comparing with the other samples after reaction for the same time. This feature indicates isotropic growth of Au in the early stage, which is due to the small mismatch with less Pt. With more Au deposited, the surface strain increased, leading to anisotropic growth to some extent. In addition, (AuPt-0.075)-Au and (AuPt-0.1)-Au show very broad peak for initial deposition, indicating the random distribution of Au atoms on the AuPt-x nanocrystals. These results show that the role of Pt is to create a mismatched surface for the growth of Au. Because of the strong oxidative ripening driven by KI, the randomly distributed Au nanoislands would ripen to large crystals. During this step, the growing Au tends to minimize the interfacial area with the seeds in order to reduce the total free energy. With more Pt, it is more difficult for the growing Au to “wet” the surface of the seeds. Therefore, the number of Au islands is greatly reduced.

2.2.8 Control the Number of Islands by Adjusting Diffusion of Metal Precursors

Oxidative ripening is related to the etching of metallic and redeposition of Au ions, controlling over the migration of Au ions on surface of the seed is also important to tune

the structure of the island. This tuning is realized by only adjusting the concentration of PVP during the seed-mediated growth of Au. TEM images in Figure 2.14a-d show the morphology change of (AuPt-0.1)-Au with increasing amount of PVP from 0.02 to 0.2, 2, and 4 %. It is clear that the morphology of the sample changes from dimers to trimers and tetramers. In another word, with increasing the amount of PVP, more islands are formed on the seed. The similar trend in structure change has been observed in the sample synthesized without KI. TEM image in Figure 2.17 confirms that more Au islands was formed when the concentration of PVP was elevated from 0.02 to 2 wt%. These observations agree well with our previous work on the formation of Au nanoislands on PVP modified Au nanoplates. Due to the steric hinderance caused by the large polymer molecules, the migration of Au ions on surface of the seed is greatly reduced. As a result, the oxidative ripening will happen locally, resulting in more islands on surface of the seed. The two-band extinction is observed for the sample with 0.02 wt% PVP in the UV-vis spectra (Figure 2.14e). The peak at longer wavelength redshifts with the concentration of PVP increases to 0.2 and 2 wt%, indicating an increase in the aspect ratio of the nanostructure. The sample synthesized with 4 % PVP show only one plasmonic peak, which can be attributed to the very small interface between the spherical nanoparticles. The very small connection between the spherical nanoparticles is confirmed by the HRTEM image in Figure 2.15. Due to the high concentration of PVP, the islands tend to minimize their contact with the seeds, resulting in the formation of nearly tangent island structures.

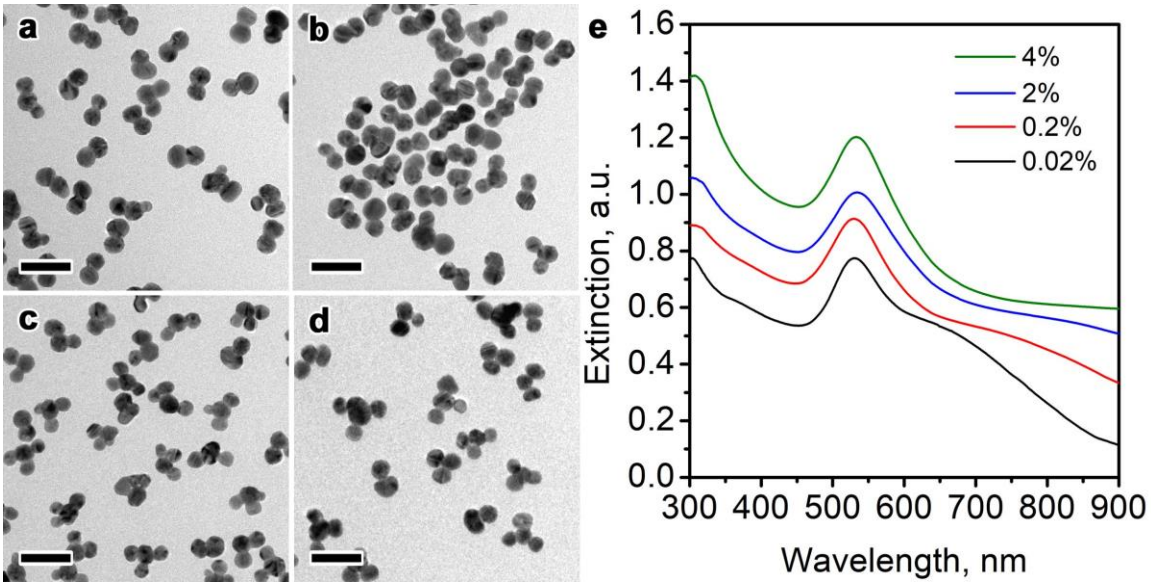

Figure 2.14 (a-d) TEM images of plasmonic nanostructures with the number of the spherical nanoparticles on the AuPt-0.1 nanospheres varying by increasing the concentration of PVP in the growth solution. (e) UV-vis extinction spectra of the plasmonic nanostructures, corresponding to (a-d).

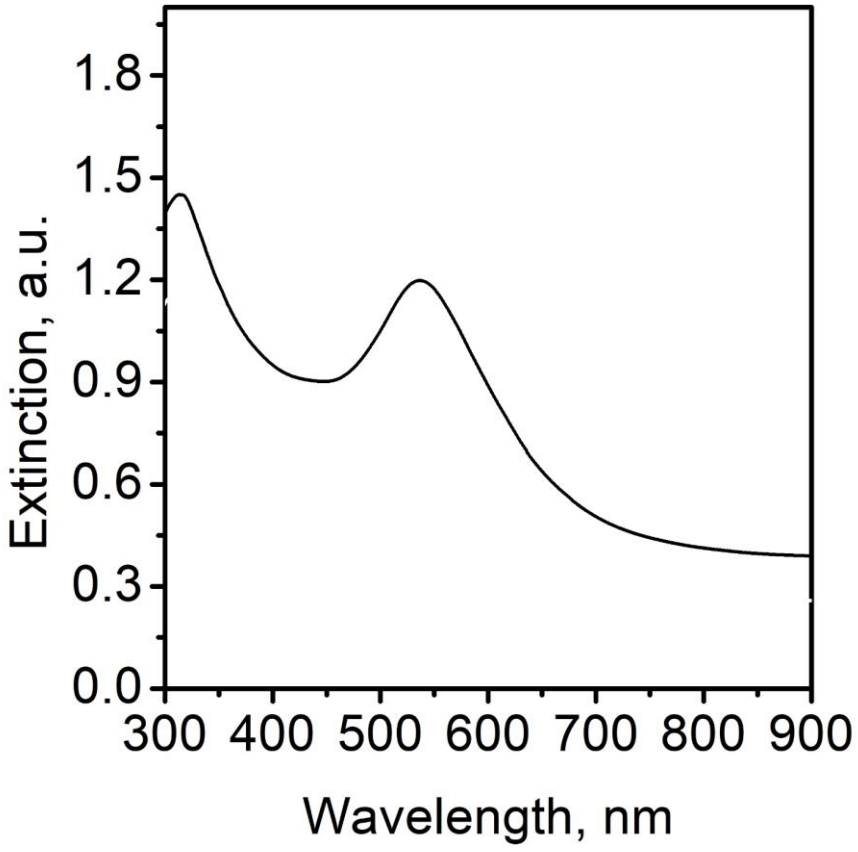

Figure 2.15 UV-vis spectra of the plasmonic nanostructures synthesized with 10 wt% PVP.

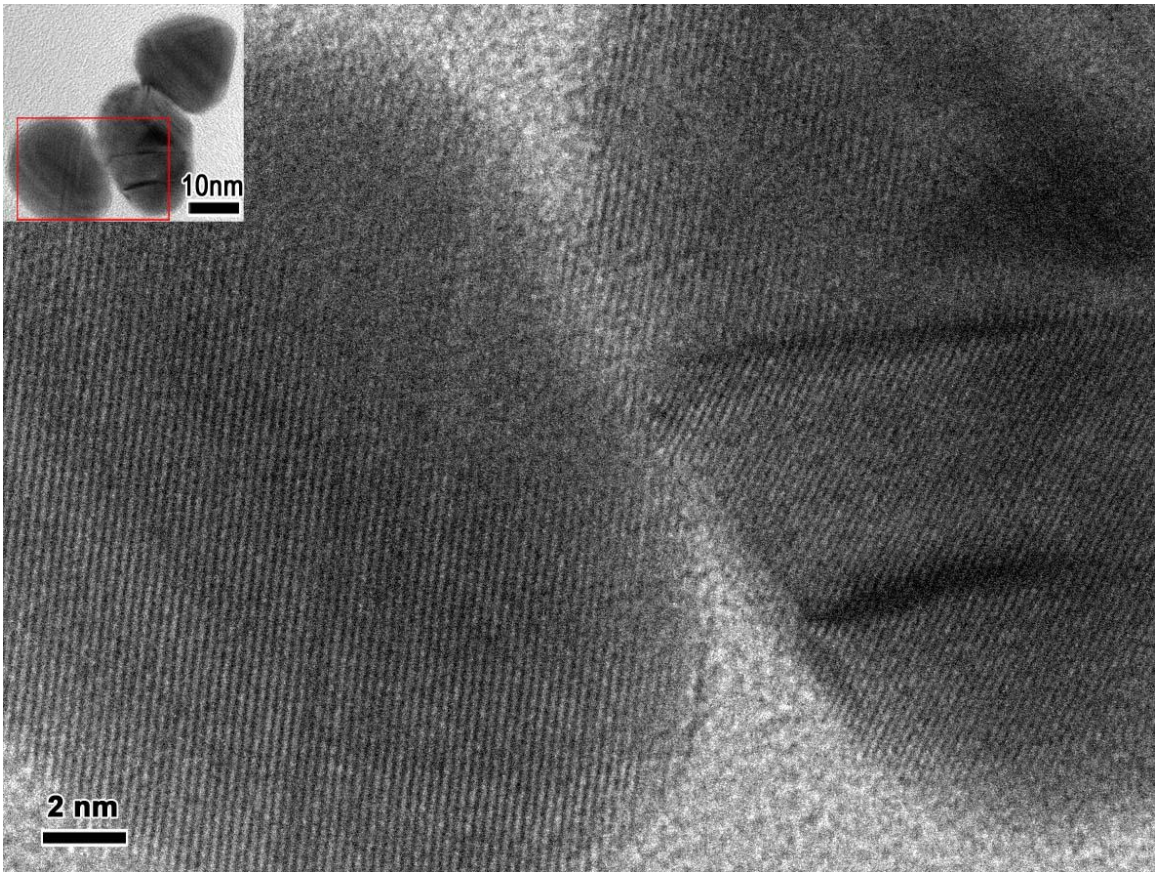

Figure 2.16 TEM images of the plasmonic nanostructures synthesized with 4 wt% PVP.

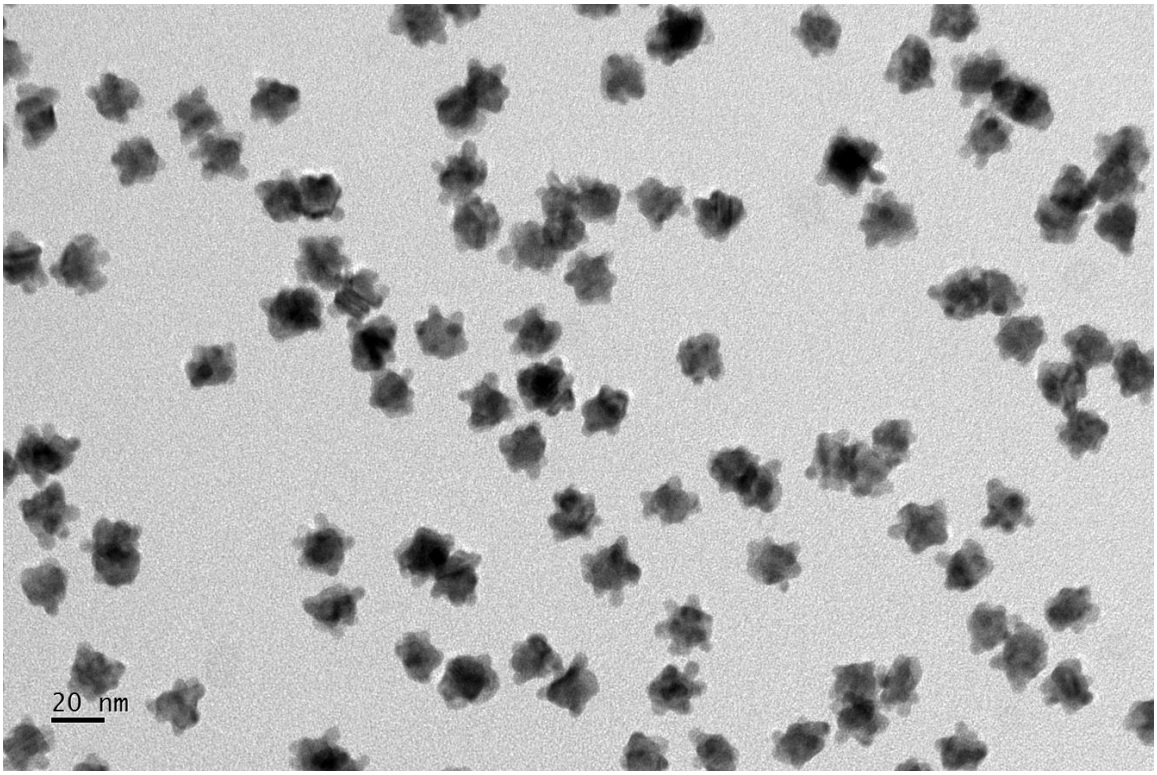

Figure 2.17 TEM images of the (AuPt-0.1)-Au satellite nanostructure synthesized in 2 % PVP.

2.3 Conclusion

In conclusion, we developed a seed-mediated growth for creating secondary structures of Au on spherical Au seeds. The formation of islands is induced by modifying the seeds with Pt to create a mismatched surface for metal deposition. The number of the islands on each seed can be controlled by adjusting the reaction parameters. Ligand assisted oxidative ripening, which is promoted by adding KI in the reaction system, drives the formation of nanostructures with less islands. In addition, increasing the degree of surface mismatch by adding more Pt also resulted in a smaller number of islands. In contrast, prohibiting surface diffusion of metal precursors by grafting the surface of the seed with more polymeric ligands can limit the oxidative ripening locally, leading to formation of more islands. By integrating all the important parameters, Au satellite structure, dimers, trimers and tetramers were obtained. It is worth noting that the Au dimers synthesized by using this method is of controllable particle size, high purity, well-defined structures and unique optical property, which has not been reported previously. The nanoparticles may have potential applications in catalysis and sensing, due to the broad absorption and enhanced electric filed in the concave structure. This synthetic method may be expended to nanostructures with different geometry, which will result in various unconventional plasmonic nanostructures.

2.4 References

1. Millstone, J. E.; Park, S.; Shuford, K. L.; Qin, L.; Schatz, G. C.; Mirkin, C. A., Observation of a Quadrupole Plasmon Mode for a Colloidal Solution of Gold Nanoprisms. *J. Am. Chem. Soc.* **2005,** *127* (15), 5312.

2. Niu, W.; Zheng, S.; Wang, D.; Liu, X.; Li, H.; Han, S.; Chen, J.; Tang, Z.; Xu, G., Selective Synthesis of Single-Crystalline Rhombic Dodecahedral, Octahedral, and Cubic Gold Nanocrystals. *J. Am. Chem. Soc.* **2009,** *131* (2), 697.

3. Zhang, J.; Langille, M. R.; Personick, M. L.; Zhang, K.; Li, S.; Mirkin, C. A., Concave Cubic Gold Nanocrystals with High-Index Facets. *J. Am. Chem. Soc.* **2010,** *132* (40), 14012.

4. Chen, H.; Shao, L.; Li, Q.; Wang, J., Gold nanorods and their plasmonic properties. *Chem. Soc. Rev.* **2013,** *42* (7), 2679.

5. Xia, Y.; Gilroy, K. D.; Peng, H.; Xia, X., Seed-Mediated Growth of Colloidal Metal Nanocrystals. *Angew. Chem., Int. Ed.* **2017,** *56* (1), 60.

6. Wang, G.; Liu, Y.; Gao, C.; Guo, L.; Chi, M.; Ijiro, K.; Maeda, M.; Yin, Y., Island Growth in the Seed-Mediated Overgrowth of Monometallic Colloidal Nanostructures. *Chem* **2017,** *3* (4), 678.

7. Feng, Y.; He, J.; Wang, H.; Tay, Y.; Sun, H.; Zhu, L.; Chen, H., An Unconventional Role of Ligand in Continuously Tuning of Metal-Metal Interfacial Strain. *J. Am. Chem. Soc.* **2012,** *134* (4), 2004.

8. Fan, Q.; Liu, K.; Feng, J.; Wang, F.; Liu, Z.; Liu, M.; Yin, Y.; Gao, C., Building High-Density Au–Ag Islands on Au Nanocrystals by Partial Surface Passivation. *Adv. Funct. Mater.* **2018,** *28* (41), 1803199.

9. Wang, Z.; He, B.; Xu, G.; Wang, G.; Wang, J.; Feng, Y.; Su, D.; Chen, B.; Li, H.; Wu, Z.; Zhang, H.; Shao, L.; Chen, H., Transformable masks for colloidal nanosynthesis. *Nat. Commun.* **2018,** *9* (1), 563.

10. Chen, T.; Chen, G.; Xing, S.; Wu, T.; Chen, H., Scalable Routes to Janus Au−SiO2 and Ternary Ag−Au−SiO2 Nanoparticles. *Chem. Mater.* **2010,** *22* (13), 3826.

11. Peng, Z.; Yang, H., Designer platinum nanoparticles: Control of shape, composition in alloy, nanostructure and electrocatalytic property. *Nano Today* **2009,** *4* (2), 143.

12. Wang, C.; Tian, W.; Ding, Y.; Ma, Y.-q.; Wang, Z. L.; Markovic, N. M.; Stamenkovic, V. R.; Daimon, H.; Sun, S., Rational Synthesis of Heterostructured Nanoparticles with Morphology Control. *J. Am. Chem. Soc.* **2010,** *132* (18), 6524.

13. Cheng, K.; Kothapalli, S.-R.; Liu, H.; Koh, A. L.; Jokerst, J. V.; Jiang, H.; Yang, M.; Li, J.; Levi, J.; Wu, J. C.; Gambhir, S. S.; Cheng, Z., Construction and Validation of Nano Gold Tripods for Molecular Imaging of Living Subjects. *J. Am. Chem. Soc.* **2014,** *136* (9), 3560.

14. Chen, L.; Ji, F.; Xu, Y.; He, L.; Mi, Y.; Bao, F.; Sun, B.; Zhang, X.; Zhang, Q., High-Yield Seedless Synthesis of Triangular Gold Nanoplates through Oxidative Etching. *Nano Lett.* **2014,** *14* (12), 7201.
15. Lou, X. W.; Yuan, C.; Rhoades, E.; Zhang, Q.; Archer, L. A., Encapsulation and Ostwald Ripening of Au and Au–Cl Complex Nanostructures in Silica Shells. *Adv. Funct. Mater.* **2006,** *16* (13), 1679.
16. Zheng, Y.; Zeng, J.; Ruditskiy, A.; Liu, M.; Xia, Y., Oxidative Etching and Its Role in Manipulating the Nucleation and Growth of Noble-Metal Nanocrystals. *Chem. Mater.* **2014,** *26* (1), 22.
17. Atay, T.; Song, J.-H.; Nurmikko, A. V., Strongly Interacting Plasmon Nanoparticle Pairs: From Dipole−Dipole Interaction to Conductively Coupled Regime. *Nano Lett* **2004,** *4* (9), 1627.
18. Romero, I.; Aizpurua, J.; Bryant, G. W.; Abajo, F. J. G. d., Plasmons in nearly touching metallic nanoparticles: singular response in the limit of touching dimers. *Opt. Express* **2006,** *14* (21), 9988.

Chapter 3 Template-Assisted Seed-Mediated Synthesis of Rod-Like Plasmonic Nanoparticles

3.1 Introduction

Control over localized surface plasmon resonance (LSPR) frequency of metal nanoparticles has attracted great attention, due to its potential application in chemical sensing, photothermal therapy and energy related area.[1-5] Because LSPR frequency is sensitive to the geometry of the nanoparticle, synthesis of anisotropic metal nanoparticles provides an access to more remarkable plasmonic absorbance and scattering phenomena that are not seen in spherical NPs.[6] Up to now, many efforts have been made to control LSPR frequency by tuning the geometry of the metal nanoparticles, as reported for nanorods, nanoshells, nanoplates and nanorings.[6-11] Among all types of metal nanostructures, the LSPR of rod-shaped nanostructures has its unique optical feature. For example, Au nanorods usually display a transverse and a longitudinal LSPR mode, which correspond to two bands of different wavelengths in extinction spectrum.[12]

In 2001, Murphy and co-workers, for the first time, discovered seeded growth method for the synthesis of Au and Ag nanorods from seeds based on Au and Ag colloidal particles.[13-15] After that, seeded growth method has been widely investigated throughout the development of colloidal chemistry for the synthesis of metal nanocrystals with well-defined shape, composition, size and structure.[16-19] Seeded growth method is performed by injecting a precursor solution of the second material into a mixture of colloidal seeds, capping ligands and reducing agents. Heterogeneous nucleation of the zero-valent metal ions on surface of the colloidal seeds, followed by continued growth of

the seeds, results in the formation of well-defined nanocrystals. The shape of a nanocrystal is determined by the internal structure of the seed and the binding affinity of the capping agent.[20] If the seed is fixed to be isotropic, controlling over surface property of the seed is necessary for the anisotropic growth of a second material. Such asymmetric surface property can be generated by either adjusting the surface constrains between metals, or creating a physical barrier to partially cover the colloidal seed. As for the former case, a high degree of lattice mismatch between different materials favors island growth of the second material and yields anisotropic heterogeneous dimers, as reported for Au-Pt.[18] Besides, anisotropic growth can be achieved by performing surface modification of the seeds. Chen et al. synthesized Au-Ag heterogeneous dimers by varying ligand conditions during the growth of Ag.[21] On the other hand, asymmetric surface can also be created by forming a physical barrier on the colloidal seed.[22-23] In this case, the surface of the seed is partially blocked by an inert material, which can direct the deposition of the second metal on the exposed surface of the seed. However, previous methods are limited to materials, and require special ligands and precise control of the reaction kinetics. In addition, conventional methods generate free standing rod-like nanoparticles, which are not suitable for the study and utilization of their angular-dependent optical property.

It is important to introduce a substrate to the synthesis of rod-like nanoparticles. A substrate can not only provide a physical barrier by contacting with the metal nanoparticles, but also alter the direction of the metal nanoparticles in response to some external stimuli. Sun et al. reported the synthesis of Au-Au homogeneous dimers and Au-

Ag heterogeneous dimers assembled on Fe_3O_4@silica nanospheres for amphiphilic asymmetric nano-assembly and catalysis.[24] The superparamagnetic property of the Fe_3O_4/SiO_2 particles facilitates the efficient purification of products with assistance of an external magnetic field. However, the two-band absorption of nanoparticle dimers is not observed because of the lack of control in the geometry of the plasmonic metal nanostructure.

In this work, we describe a template-assisted seed-mediated growth for the preparation of rod-like plasmonic nanoparticles. Colloidal silica nanospheres are employed as the substrates for illustration of the synthesis strategy. Au nanoparticles are loaded on the surface of colloidal silica as seeds through binding ligands. During seeded growth, the surface of the seed which is in contact with silica is blocked from being deposited with the second material, giving rise to anisotropic growth of the metal nanostructures. An additional layer of silica is coated on the structure through a sol-gel method to increase the contact area between the Au seed and the colloidal silica, followed by a seeded growth process. The exposure of the gold seed can be precisely tuned by adjusting the silica precursor in the sol-gel coating method without additional polymer ligands. This synthesis has several advantages: 1) the aspect ratio of the rod-like nanocrystal can be controlled by stepwise seeded growth; 2) the synthesis is easy to scale up by increasing the loading amount of Au nanoparticles; 3) the synthesis is a generalized method, which can be used for the synthesis of metal nanocrystals with different materials and shapes; 4) this template-assisted synthesis can also be used to synthesize Janus nanoparticles, such as metal-metal oxides and metal-polymer nanoparticles.

3.2 Materials and Methods

3.2.1 Materials

Tetraethylorthosilicate (TEOS), poly(vinyl pyrrolidone) (PVP, Mw~10,000), 3-Aminopropyl)triethoxysilane (APTES), potassium iodide (KI), L-ascorbic acid (AA), sodium borohydride ($NaBH_4$, 99%), sodium hydroxide (NaOH), Chloroauric acid ($HAuCl_4$), polyacrylic acid (PAA, average M.W. 1800), and trisodium citrate (TSC) were purchased from Sigma-Aldrich. For the preparation of the hydrogel film, acrylamide, 2-Hydroxy-4'-(2-hydroxyethoxy)-2-methyl-propiophe and N,N'-methylenebis(acrylamide) (purity 98%) were purchased from Sigma-Aldrich. Ammonium hydroxide ($NH_3 \cdot H_2O$, 28% by weight in water) was purchased from Fisher Scientific. Ethanol (200 proof) is purchased from Decon Laboratories Inc. All chemicals were directly used as received without further purification.

3.2.2 Synthesis of SiO_2-Au@SiO_2 seeds.

Silica nanospheres were synthesized by using a modified Stöber process. In a typical synthesis, 3 mL of $NH_3 \cdot H_2O$ was added into a mixture of 92 mL of ethanol, 16 mL of H_2O and 3.44 mL of TEOS at room temperature. The mixture was stirred for 4 hrs. Silica nanospheres were collected by centrifugation, and washed with ethanol for 3 times. The products were re-dispersed in 20 mL of ethanol. Surface modification of SiO_2 nanospheres was done by refluxing 2 mL of the dispersion of silica nanospheres in a mixture of 30 mL of ethanol and 1 mL of 3-Aminopropyltriethoxysilane (APTES) for 3 hrs. SiO_2-NH_2 was collected by centrifugation. The samples were washed with ethanol and water for 3 times, and re-dispersed in 20 mL of H_2O. According to our previous

report, Au nanoparticles were synthesized by using a seeded growth method.[25] In a typical synthesis, 1 mL of $HAuCl_4$ (5 mM) and 1 mL of TSC (5 mM) were mixed with 18 mL of H_2O under vigorous stirring. 0.6 mL of freshly made $NaBH_4$ solution (0.1 M) was quickly injected into the solution. After stirring for 4 h, 400 μL of the above solution was quickly injected into a growth solution of Au containing 2 mL of PVP (5 wt%), 1 mL of L-ascorbic acid (0.1 M), 800 μL of KI (0.2 M), 240 μL of $HAuCl_4$ (0.25M), and 4 mL of H_2O. After stirring for 10 min, the dispersion of Au nanoparticles was collected for the next step. Loading of Au nanoparticles on SiO_2-NH_2 was done by mixing one aliquot of the Au nanoparticle dispersion with 4 mL of SiO_2-NH_2. After sonicating for 10 minutes, dark red SiO_2-Au was collected by centrifugation, and washed with H_2O. The particles were re-dispersed in 20 mL of ethanol. Silica coating on SiO_2-Au was achieved by injecting TEOS into a mixture containing 10 mL of SiO_2-Au dispersion, 1 mL of H_2O and 0.5 mL of $NH_3 \cdot H_2O$. Thickness of the silica layer was controlled by adjusting the addition amount of TEOS. After sonicating for 30 minutes, the SiO_2-Au@SiO_2 was collected by centrifugation, and washed with ethanol and H_2O. The particles were re-dispersed in 2 mL H_2O as seeds solution for the growth of dimer structures.

3.2.3 Synthesis of SiO_2-Au dimer structure.

Growth of Au-Au dimer structure was achieved by using a seeded growth method. 100 μL of PVP (5 wt%), 25 μL of L-ascorbic acid (0.1 M), 20 μL of KI (0.2 M), 6 μL of $HAuCl_4$ (0.25M), and 200 μL of H_2O were mixed as a growth solution. 25 μL of the growth solution was added into 50 μL of SiO_2-Au@SiO_2 seeds and 200 μL H_2O to get the SiO_2-Au dimer structure. After stirring for 10 min, the particles were collected by

centrifugation.

3.2.4 Synthesis of heterogeneous dimers.

SiO_2-Au-Ag dimer was obtained by adding 4 μL of AA into a mixture containing 50 μL of SiO_2-Au@SiO_2 seeds, 200 μL of H_2O, 200 μL of PVP (5 wt%) and 4 μL of $AgNO_3$ (0.1 M). After stirring for 10 min, the particles were collected by centrifugation.

SiO_2-Au-Pd dimer was obtained by adding 20 μL of AA (0.1 M) into a mixture containing 50 μL of SiO_2-Au@SiO_2 seeds, 400 μL of H_2O, 10 μL of H_2PdCl_4 (20 mM) and 6 μL of NaOH (0.1 M). After stirring for 10 min, the particles were collected by centrifugation.

SiO_2-Au-Cu_2O dimer was synthesized according to a previous report.[26] Briefly, 50 μL of 0.1 M $CuCl_2$ and 0.1 g SDS were mixed in 9.475 mL H_2O to obtain a Cu^{2+} stock solution. Then, 450 μL of the stock solution was added to 25 μL of SiO_2-Au@SiO_2 seeds, followed by the addition of 3 μL of 1 M NaOH and 8.26 μL of 0.1 M $NH_2OH{\cdot}HCl$. The mixture was stirred at room temperature for 30 min for the growth of Cu_2O.

3.2.5 Characterizations

Transmission electron microscopy (TEM) images were taken with a Philips Tecnai 12 transmission electron microscope operating at 120 kV. The samples for TEM observation were prepared by drop casting a solution on a carbon film supported on a copper grid. UV-vis spectra were measured by using an Ocean Optics HR 2000CG-UV-NIR spectrometer. Optical microscopy was performed using a Zeiss Axio Imager A1m.

3.3 Results and Discussion

3.3.1 Synthesis of SiO_2-Au dimers.

The scheme for the step-wise synthesis process of Au dimers on silica nanospheres is shown in Figure 3.1a. In a typical synthesis, SiO_2 nanospheres were synthesized through a modified Stöber method, using tetrathylorthosilicate (TEOS) as the silica precursor. Then, the SiO_2 nanospheres were modified with 3-aminopropyl-triethoxysilane (APTES) to graft the surface of the nanospheres with $-NH_2$ groups. After that, gold nanoparticles, which were synthesized through a seeded growth method, were added to the SiO_2 dispersion. Due to the formation of chemical bonds between the gold atoms and the $-NH_2$ groups, the gold nanoparticles could be attached to surface of SiO_2 nanospheres, denoted as SiO_2-Au. As shown in Figure 3.2, the sizes of SiO_2 nanospheres and Au nanoparticles are 269.7 nm and 31.4 nm. In order to generate an asymmetric surface on gold nanoparticle, the SiO_2-Au was coated by a layer of silica through a sol-gel method, using TEOS as the silica precursor. Because of the different chemical nature of gold and silica, the deposition of silica could only occur on the silica nanospheres. Therefore, one part of gold nanoparticle was embedded in silica, while the other was exposed to solution. The thickness of the silica layer could be controlled at nanometer scale by adjusting the addition amount of TEOS. With an increase of the addition amount of TEOS, the exposure of the gold nanoparticle decreased. In the case of the growth for the nanoparticle dimers, the thickness of the silica layer was precisely controlled to cover most of the gold nanoparticles. The nanostructure was denoted as SiO_2-Au@SiO_2. Finally, the SiO_2-Au@SiO_2 nanostructures were used as seeds for the growth of the gold

nanoparticle dimers. Typically, a dispersion of SiO_2-Au@SiO_2 was injected to a mixture, including $HAuCl_4$, PVP, KI and AA. The reaction was maintained for 10 minutes under vigorous stirring. The color of the solution gradually changed from red to bluish-purple, indicating the formation of Au nanoparticle dimers.

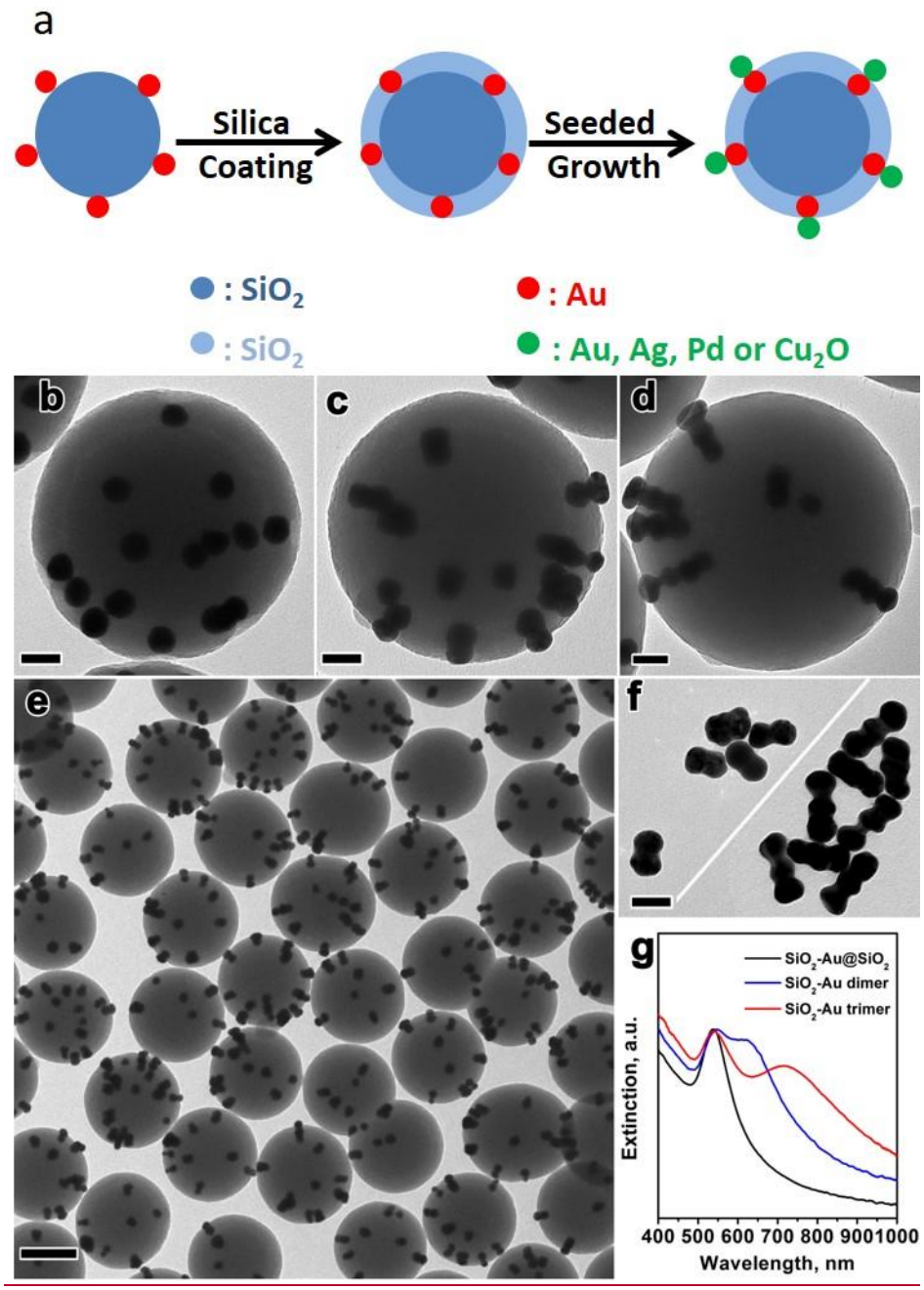
a
Silica Coating
Seeded Growth
: SiO2
: SiO2
: Au
: Au, Ag, Pd or Cu2O
b
c
d
e
f
g
SiO2-Au@SiO2
SiO2-Au dimer
SiO2-Au trimer
Extinction, a.u.
400 500 600 700 800 9001000
Wavelength, nm

Figure 3.1 A scheme illustrating the synthetic strategy. TEM images of (b) SiO_2-Au@SiO_2 nanoparticles, (c) SiO_2-Au dimers and (d) SiO_2-Au trimers. The SiO_2-Au trimers were obtained after a second round of SiO_2 coating and seeded-growth of Au. (e) Large scale TEM image of SiO_2-Au dimers. (f) Au dimers and trimers after releasing from the SiO_2 colloidal substrates. (g) UV-vis spectra of SiO_2-Au@SiO_2 nanoparticles, SiO_2-Au dimers and SiO_2-Au trimers. The scale bars in (b-d, f) and (e) are 50 and 200 nm.

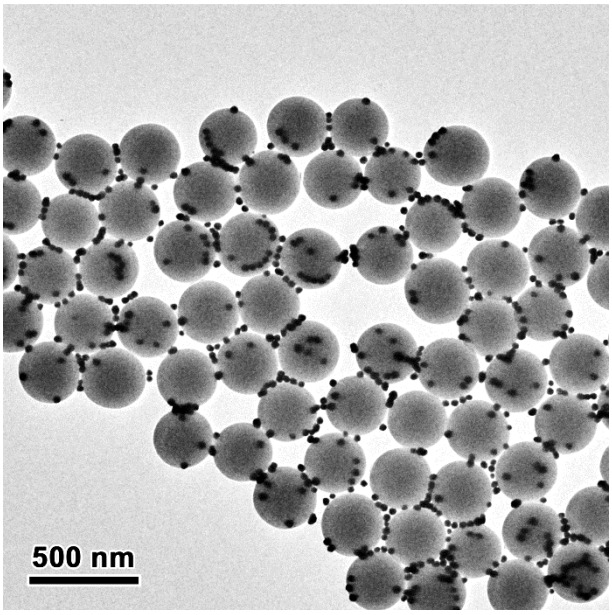

Figure 3.2 TEM image of Au nanoparticles loaded on SiO_2 nanospheres (SiO_2-Au).

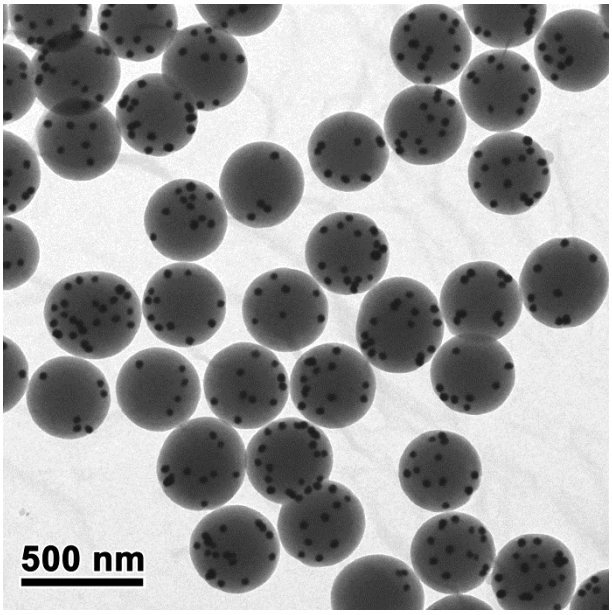

Figure 3.3 Large scale TEM image of SiO_2-Au@SiO_2.

Figure 3.1b shows the TEM image of SiO_2-Au@SiO_2 dimers. The size of SiO_2-Au@SiO_2 is measured to be 335.7 nm from the large scale TEM image (Figure 3.3). The thickness of the SiO_2 layer is calculated to be ~33.0 nm, which is about equal to the size of the Au nanoparticle. Figure 3.1c shows the nanostructure after performing seeded growth of Au on SiO_2-Au@SiO_2. The elongation of the spherical nanoparticle can be clearly observed. The large scale TEM image of the nanostructure after seeded growth (Figure 3.1e) proves that this synthesis strategy results in Au-Au nanoparticle dimers with high purity. Linear trimers made of Au could be obtained by repeating the coating and seeded growth step on the SiO_2-Au dimers (Figure 3.1d). After the removal of all the SiO_2 by HF, the free-standing Au dimers and linear trimers can be released from the substrate. As shown in Figure 3.1f, the average length and width are 56.8 and 33.5 nm of Au dimers, and 78.8 and 33.8 nm of Au linear trimers. The aspect ratios of Au dimers and Au linear trimers are calculated to be 1.7 and 2.33. Figure 3.1g shows the UV-vis extinction spectra of SiO_2-Au@SiO_2, SiO_2-Au dimers and SiO_2-Au linear trimers. SiO_2-Au@SiO_2 displays one absorption peak at 537 nm, which corresponds to the absorption of Au nanoparticles embedded in silica. Structure evolution of Au nanoparticle to Au nanoparticle dimers leads to a two-band spectrum. SiO_2-Au dimers show two absorption peaks at 544 and 621 nm, due to the transverse and longitudinal plasmonic resonance of the dimer structure. After the removal of silica, the two absorption peaks of the free-standing Au-Au nanoparticle dimers blue-shift to 536 and 598 nm due to the change in the dielectric environment (Figure 3.4). The two-peak extinction agrees with results from previous report. When two metal nanoparticles conductively contact, a transverse mode

of dipole resonance and a longitudinal mode of dipole and quadruple resonance of the nanoparticle dimers can be excited, showing two extinction bands at both shorted and longer wavelength.[27] Further elongation of the rod-like nanostructure can cause a redshift of the longitudinal mode in the UV-vis extinction. As shown in Figure 3.1f, the extinction peaks for Au linear trimers are at 540 and 719 nm.

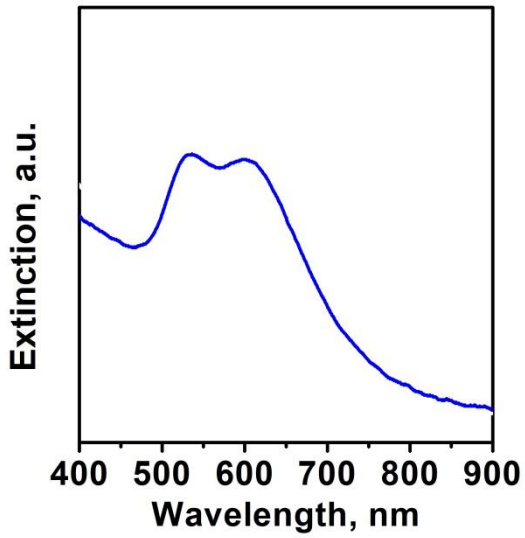

Figure 3.4 UV-vis spectrum of Au dimers after releasing form the silica substrate.

3.2.1 Key parameters in the synthesis

In this section, we will discuss the key parameters that could influence the structure of the Au nanoparticle. They are: 1) the volume ratio of $HAuCl_4$ to the seeds; 2) the thickness of the silica layer. During the seeded growth step, the volume ratio of $HAuCl_4$ to the seeds determined the size of the second Au nanoparticle. The size of the second Au nanoparticle could be enlarged with an increase of the $HAuCl_4$/seeds (v/v) ratio, leading to an elongation of the Au nanostructures. Here, we used the same SiO_2-Au@SiO_2 seeds with 31.4 nm Au nanoparticle and 33.0 nm thickness of the second silica to perform the seeded growth. By fixing the volume of the seeds at 50 μL, and adjusting the amount of growth solution of 5, 15, 25 and 35 μL, the $HAuCl_4$/seeds (v/v) ratio was changed at 10, 3.3, 2 and 1.43. Figure 3.5a-d show structure evolution of SiO_2-Au dimers with an increasing $HAuCl_4$/seeds ratio. The length of the gold nanoparticle obtained through the seeded growth process changed from 36.9, 46.2, 50.8 to 58.5 nm, resulting in a morphology change of the Au dimers from snowman-like to dumbbell-like structures. If we assume that the moles of the seeds is equal to the moles of $HAuCl_4$ that was used to prepare the seeds, the molar ratio of $HAuCl_4$/seeds during the seeded growth step can be calculated as 0.14, 0.42, 0.71 and 1.00 for samples in Figure 3.5a-d. It shows that the size of the second Au nanoparticle is about equal to the size of the Au seed, when the molar ratio of $HAuCl_4$/seeds equals to 1. Figure 3.5e shows the UV-vis spectra of SiO_2-Au nanostructures a-d. SiO_2-Au shown in Figure 3.5a has only one extinction peak, due to the relatively spherical shape of the particle. With elongation of the Au nanoparticle dimers, the dipole resonance at longer wavelength redshifts to 600, 631 and 654 nm,

resulting in a color change of the SiO_2-Au suspension from red to bluish-purple, as shown in the inset digital image of Figure 3.5e.

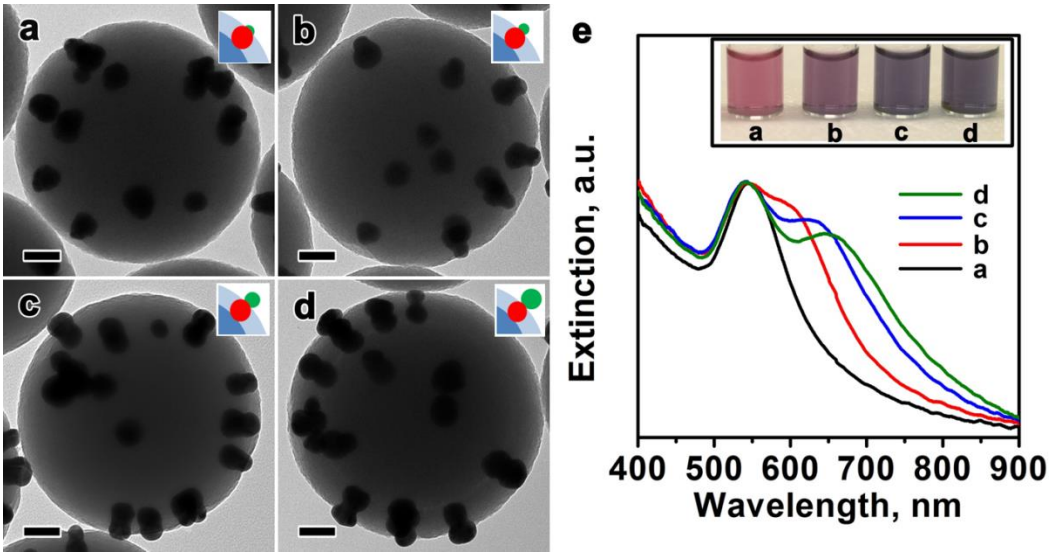

Figure 3.5 Evolution of the SiO_2-Au dimers obtained with different amount of growth solution: (a) 5, (b) 15, (c) 25, and (d) 35 μL. (e) UV-vis spectra of SiO_2-Au dimers. The inset digital image shows the corresponding color change of the solution containing SiO_2-Au nanostructures.

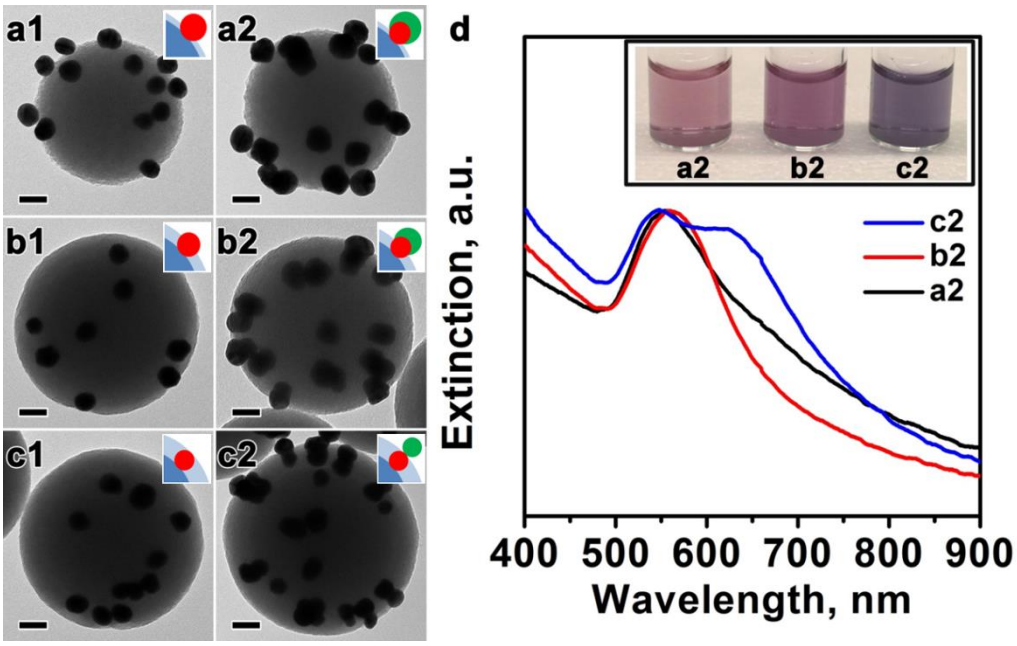

Figure 3.6 TEM images of SiO_2-Au@SiO_2 with a second layer of SiO_2 of different thickness: (a1) 6.5, (b1) 31.3, and (c1) 33.0 nm; TEM images of SiO_2-Au nanostructures after seeded-growth of Au (a2, b2 and c2); and the corresponding UV-vis spectra (d). The inset digital image in (d) shows the color of SiO_2-Au nanostructures after seeded-growth.

Besides the $HAuCl_4$/seeds ratio, the thickness of the silica layer, which covered the Au seeds, also has significant impact on the nanostructures of Au dimers. It determines the exposure of Au seeds by creating a physical barrier for seeded growth, which can further induce anisotropic growth of the nanostructure. The red and green circles on the inset scheme in Figure 3.6a-c show the Au nanostructure before and after the seeded growth step. Due to the increase of the silica layer, the shape of the Au nanostructure changes from spherical to dumbbell-like. Here, we performed seeded growth by using SiO_2-Au@SiO_2 of different thickness of silica layer. The amount of SiO_2-Au@SiO_2 and growth solution was fixed at 50 and 25 μL for all of the seeded growth steps. Figure 3.6a1, b1 and c1 show SiO_2-Au@SiO_2 seeds with silica thickness of 6.5, 31.3 and 33.0 nm, respectively. The corresponding nanostructures after seeded-growth are shown in Figure 3.6a2, b2 and c2. When the thickness of the secondary silica layer is 6.5 nm, spherical Au-Au nanostructure of 42.8 nm is formed after seeded-growth (Figure 3.6a2). With an increase in the thickness of the second silica layer, Au nanostructures with higher degree of anisotropy were observed. Rod-like Au nanostructures can be obtained when the second silica layer is 31.3 and 33.0 nm. Figure 3.6d shows the UV-vis spectra of nanostructures a2-c2. The spherical nanoparticles and short rod-like nanoparticles shows only one absorption peak at 540 and 556 nm, due to the low anisotropy of the nanostructure. The broad shoulder in the UV-vis spectrum of a2 can be attributed to free gold nanoparticle aggregates. Because the thickness of the secondary silica layer is small, some gold nanoparticles detached from the silica substrate, forming aggregates in the washing steps. The two-absorption plasmonic resonant peaks

can only be obtained when the thickness of the second silica layer reaches 33.0 nm, revealing the importance of silica thickness to the anisotropic growth of Au nanostructures.

3.2.2 Synthesis of heterodimers

The SiO_2-Au@SiO_2 seeds are versatile for the synthesis of not only homogeneous dimers, but also heterogeneous dimers, such as Au-Ag, Au-Pd and Au-Cu_2O nanoparticle dimers. Figure 3.7 shows the nanostructure and optical property of Au-Ag, Au-Pd and Au-Cu_2O nanoparticle dimers synthesized by using the same SiO_2-Au@SiO_2 seeds through different seeded-growth method. In a typical synthesis of Au-Ag nanoparticle dimers, AA was injected into an aqueous mixture containing SiO_2-Au@SiO_2 seeds, PVP and $AgNO_3$. The size of Ag was adjusted by tuning the addition amount of AgNO3, which affected the length of the particle. Figure 3.7a shows the TEM image of Au-Ag nanoparticle dimers and the corresponding UV-vis extinction spectra. The three extinction peaks at 423, 538 and 598 nm can be attributed to the absorption of Ag, Au and the dipole resonance of the rod-like nanostructure. Au-Pd nanoparticle dimers were synthesized by injecting AA into an aqueous mixture containing SiO_2-Au@SiO_2 seeds, H_2PdCl_4 and NaOH. Dandelion-like Au-Pd dimers were obtained after reaction for 10 minutes. The Au-Pd dimers show a decrease in the intensity of the plasmonic absorption. The slightly redshift and broadening of the peak indicates the connection of Au and Pd. Besides metal-metal dimers, metal-semiconductor nanoparticle dimers could also be synthesized by using SiO_2-Au@SiO_2 as seeds. For example, Au-Cu_2O dimers were synthesized by reducing $CuCl_2$ with NH_2HCl in a suspension of SiO_2-Au@Au seeds. In a

typical synthesis, $CuCl_2$ and SDS were dissolved in H_2O to obtain a stock solution. A certain amount of the stock solution was added into a mixture of SiO_2-Au@Au seeds and NaOH, followed by the addition of $NH_2 \cdot HCl$ as a reducing agent. The anisotropic growth of Cu_2O on Au results in Au-Cu_2O mushroom-like structure, which leads to a peak shift in the UV-vis spectra from 537 to 574 nm.

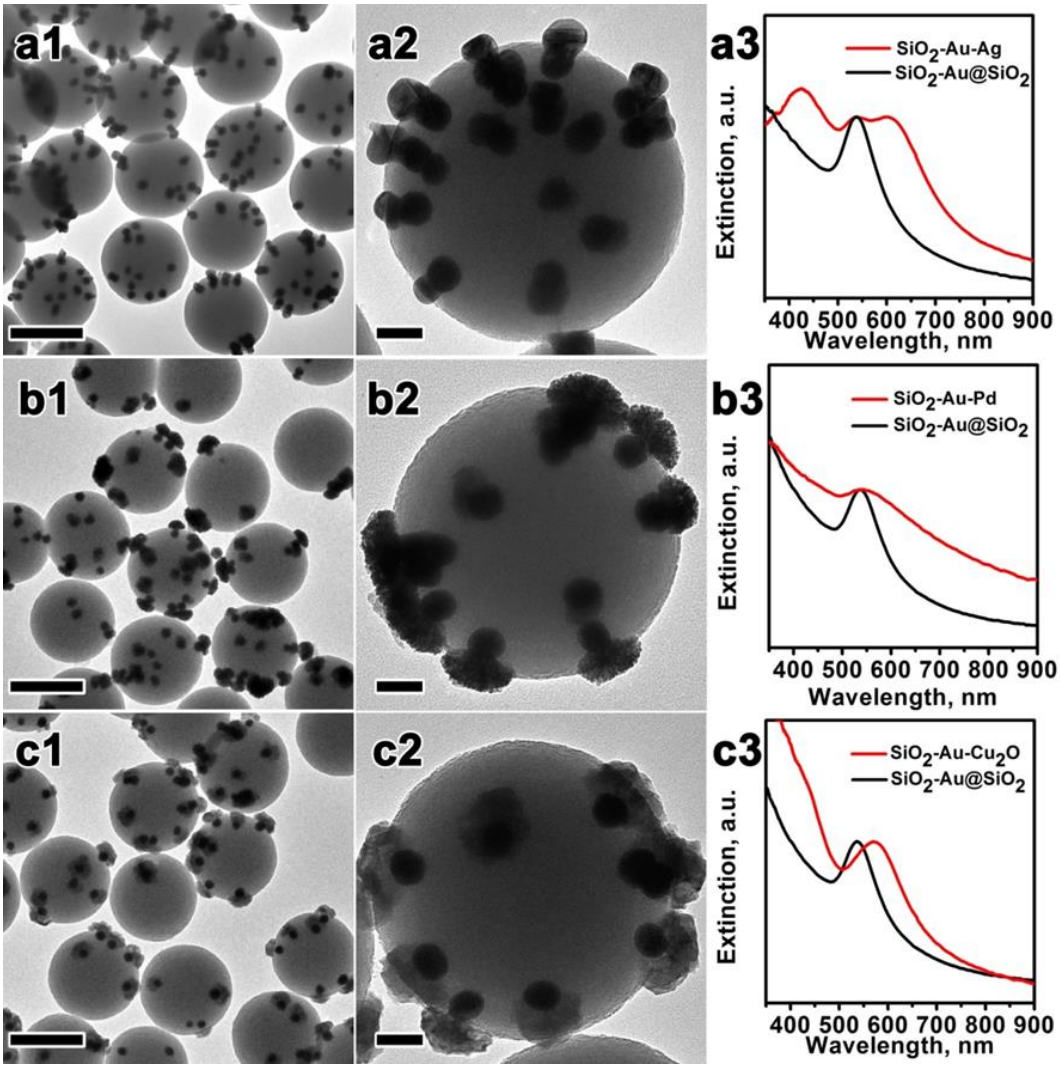

Figure 3.7 TEM images (a1, a2) and UV-vis spectra (a3) of SiO_2-Au-Ag dimers; TEM images (b1, b2) and UV-vis spectra (b3) of SiO_2-Au-Pd dimers; TEM images (c1, c2) and UV-vis spectra (c3) of SiO_2-Au-Cu_2O dimers (a1), (b1) and (c1) are large scale TEM images.

3.2.3 Optical property of Au-Cu_2O heteodimers

This SiO_2-Au@SiO_2 nanocomposites can be used as seeds for the synthesis of varies unconventional nanostructures. Because the degree of surface passivation can be precisely controlled by adjusting the amount of TEOS in the silica coating step, the exposure of Au nanoparticle is well-controlled. In addition, silica and Au are intrinsically different in chemical and physical properties. For example, silica has -OH groups which can form hydrogen bonds with other chemical species, while Au has strong coordination ability with many ligands, such as -SH, -NH_2 and -COOH. Moreover, Au is crystal, which favors the growth of crystals, while silica favors the deposition of amorphous materials because its amorphous nature. Therefore, the SiO_2-Au@SiO_2 seed can be widely applied to the synthesis of Au-X nanostructures with controlled coverage of Au nanoparticles, which is expected to show different properties than conventional core-shell nanostructures.

In this section, we show that the LSPR shift of Au-Cu_2O is related to the coverage of Cu_2O on surface of the Au nanoparticle, and the thickness of Cu_2O. We firstly prepared three types of SiO_2-Au@SiO_2 seeds with different thickness of the second silica layer. the thickness of the second silica layer is measured to be 3, 29 and 37.5 nm for SiO_2-Au@SiO_2-1, SiO_2-Au@SiO_2-2, and SiO_2-Au@SiO_2-3, respectively.

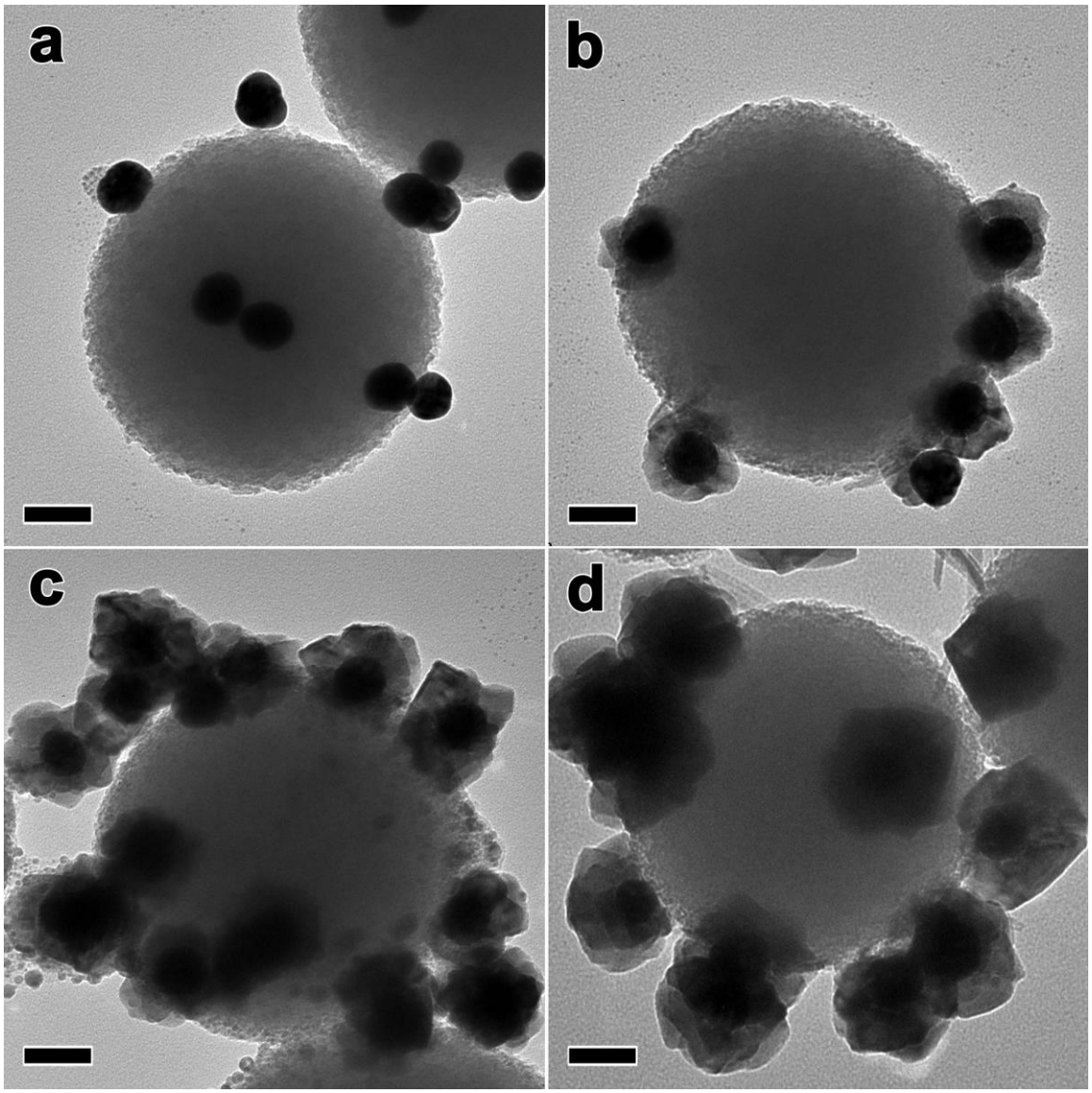

Figure 3.8 Seeded-growth of Cu_2O on SiO_2-Au@SiO_2-1 with increasing amount of $CuCl_2$. The scale bars are 50 nm.

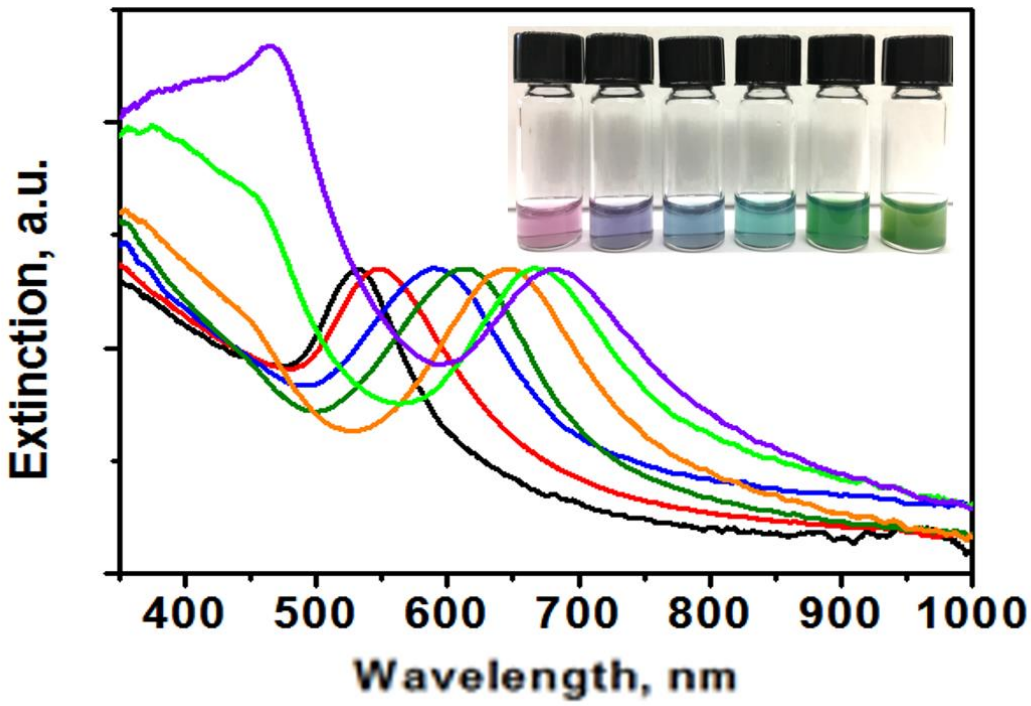

Figure 3.9 UV-vis spectra of SiO_2-Au@SiO_2-1-Cu_2O with increasing amount of $CuCl_2$. Inset is the digital image of the solution.

The growth of Cu_2O was done by reducing $CuCl_2$ with $NH_2{\cdot}HCl$ in a suspension of SiO_2-Au@SiO_2 seeds. In a typical synthesis, $CuCl_2$ and SDS were dissolved in H_2O to obtain a stock solution. A certain amount of the stock solution was added into a mixture of SiO_2-Au@SiO_2 seeds and NaOH, followed by the addition of $NH_2{\cdot}HCl$ as a reducing agent. The thickness of Cu_2O will increase with increasing the injection volume of Cu^{2+} stock solution.

The TEM images show the structure of SiO_2-Au-Cu_2O by using different SiO_2-Au@SiO_2 as seeds. For all of the three seeds, the thickness of Cu_2O increased with increasing the addition volume of the Cu^{2+} stock solution. When SiO_2-Au@SiO_2-1 was used as seeds, some Au detached from the SiO_2 substrate due to the etching effect of NaOH in the growth solution (Figure 3.8). The morphology of Cu_2O on the different SiO_2-Au@SiO_2 were slightly different in shape. When the thickness of silica was thin (SiO_2-Au@SiO_2-1 and SiO_2-Au@SiO_2-2, Figure 3.10 and 3.12), the exposure of Au nanosphere was relatively large, and the shape of Cu_2O was irregular, indicating that the structure was polycrystalline. And when the thickness of SiO_2 increased to cover most of the Au nanosphere, the Cu_2O grew to be nanoparticle with obvious edges and sharp corners, indicating that the structure may be single crystalline.

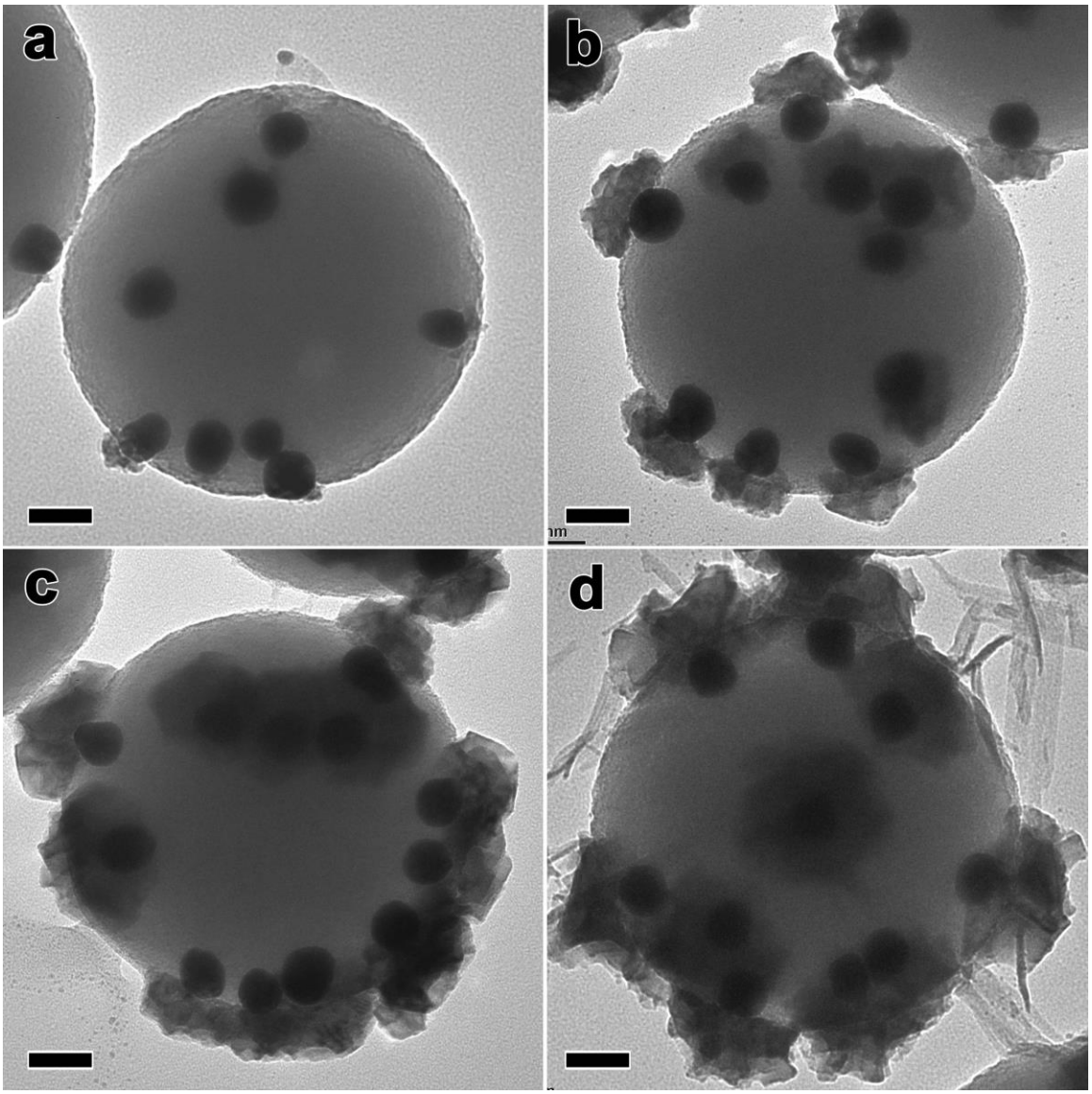

Figure 3.10 Seeded-growth of Cu_2O on SiO_2-Au@SiO_2-2 with increasing amount of $CuCl_2$. The scale bars are 50 nm.

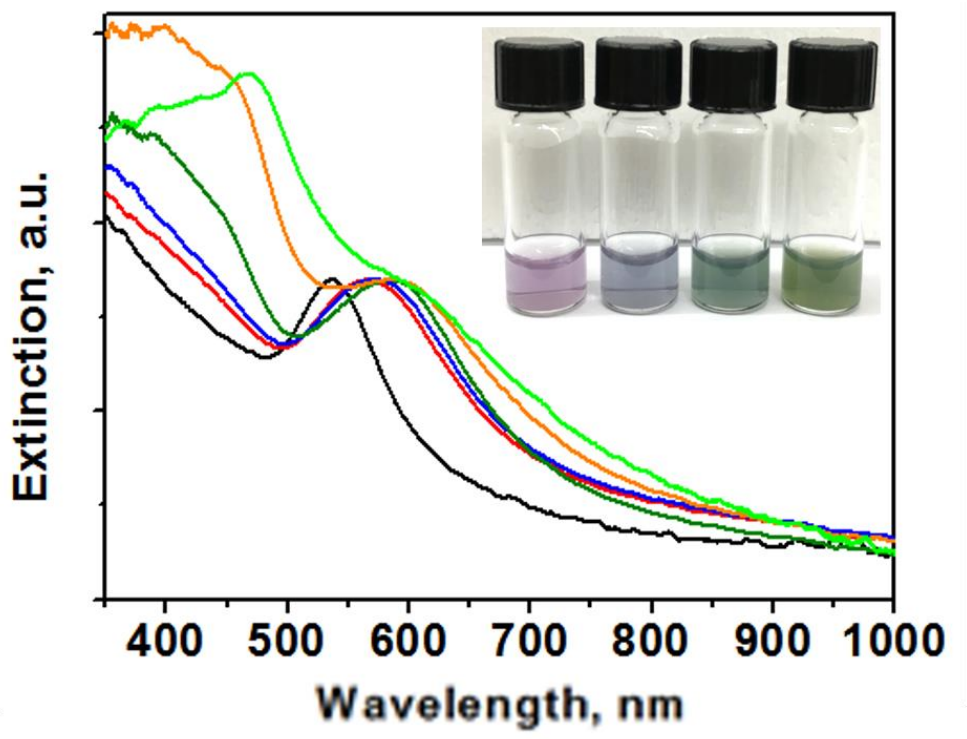

Figure 3.11 UV-vis spectra of SiO_2-Au@SiO_2-2-Cu_2O with increasing amount of $CuCl_2$. Inset is the digital image of the solution.

The UV-vis spectra show the peak-shift of the SiO_2-Au@SiO_2 after the deposition of Cu_2O. The peak-shift is due to the change in dielectric environment of the Au nanoparticles caused by the deposition of Cu_2O. When SiO_2-Au@SiO_2-1 was used as seeds, the extinction peak redshifted from 532 to 549, 590, 614, 648, 667, and 683 nm as the volume of Cu^{2+} stock solution increased from 0 to 200, 300, 450, 900, 1800 and 3600 μL, corresponding with a color change of the solution form pink to purple, bluish-purple, blue, green and yellowish-green (Figure 3.9). And when SiO_2-Au@SiO_2-1 was used as seeds, the extinction peak redshifted from 536 to 569, 577, 583, 587 and 590 nm as the volume of Cu^{2+} stock solution increased from 0 to 450, 900, 1800 and 3600 μL, corresponding with a color change of the solution form pink to bluish-purple, and yellowish-green (Figure 3.11). In contrast, when SiO_2-Au@SiO_2-3 was used as seeds, the extinction peak redshifted from 538 to 550, and 560 as the Cu^{2+} stock solution increased from 0 to 200, 450, and 1800 μL (Figure 3.13). There was no peak shift when the peak position reached 560 nm, even when the addition volume of the Cu^{2+} stock solution increased to 4 times. The color of the solution changed slightly from dark red to yellowish-red, due to the absorption of Cu_2O at around 460 nm.

Comparing the UV-vis spectra of SiO_2-Au@Cu_2O synthesized by using 1800 μL of the Cu^{2+} stock solution and different SiO_2-Au@SiO_2 seeds, the extinction peak blue-shifted from 667 to 587 and 560 nm, due to the reduced coverage of Cu_2O on the Au nanosphere.

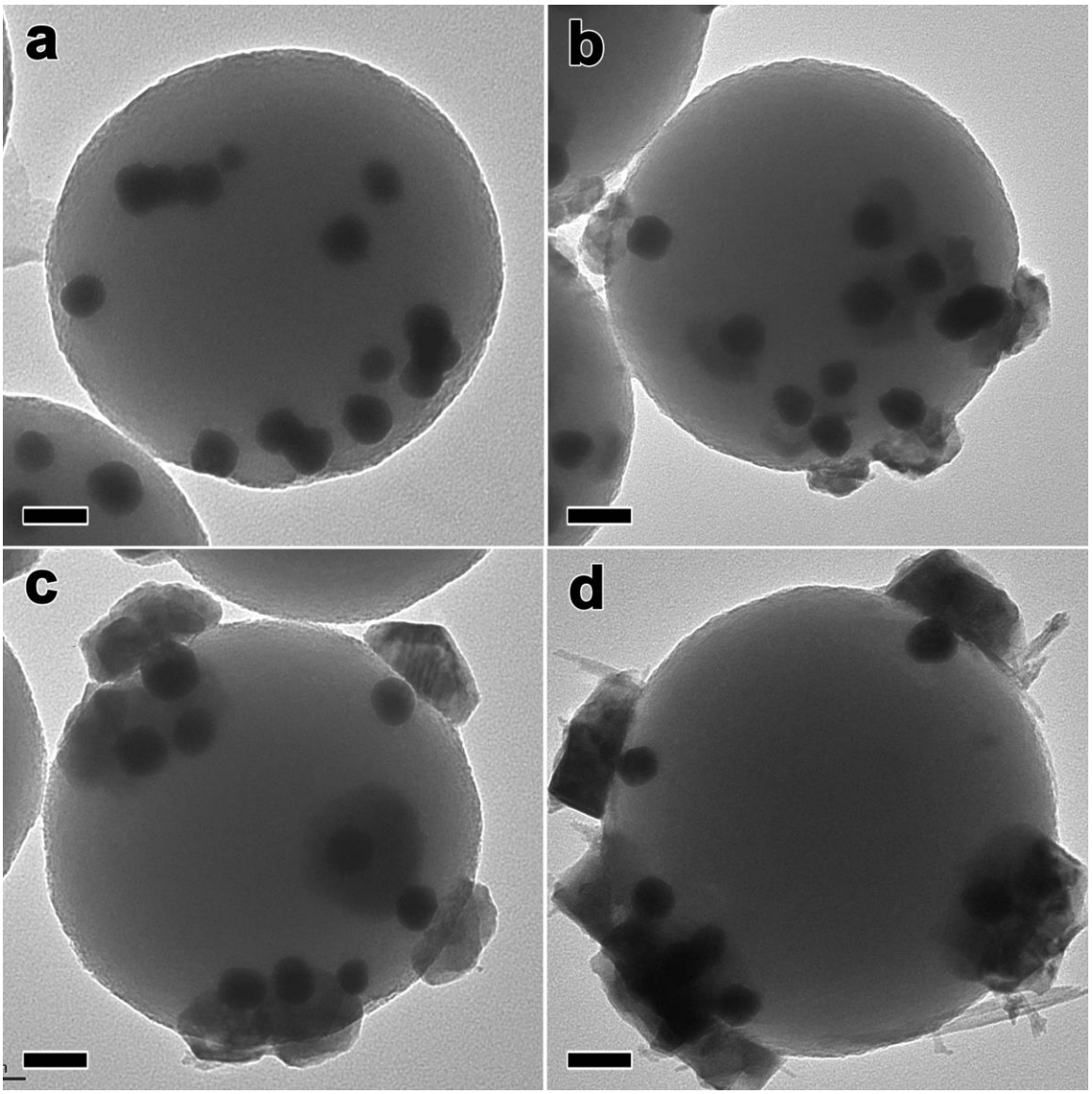

Figure 3.12 Seeded-growth of Cu_2O on SiO_2-Au@SiO_2-3 with increasing amount of $CuCl_2$. The scale bars are 50 nm.

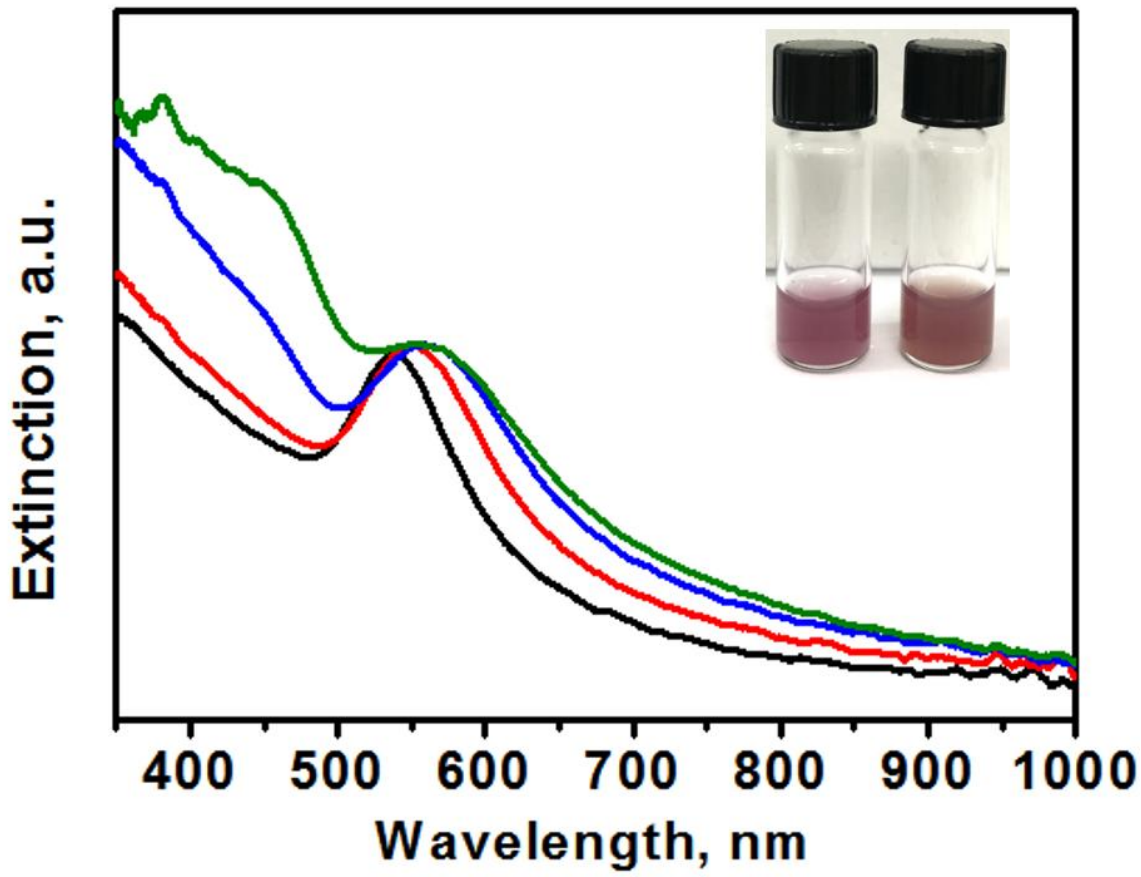

Figure 3.13 UV-vis spectra of SiO_2-Au@SiO_2-3-Cu_2O with increasing amount of $CuCl_2$. Inset is the digital image of the solution.

3.2.4 Application of SiO_2-Au@SiO_2 template for the selective deposition of polymers

In this section, we will show the application of SiO_2-Au@SiO_2 template for the selective deposition of polymers, for example, resin formaldehyde (RF) and polyaniline (PANI).

RF is a kind of synthetic polymers obtained by the reaction of phenol with formaldehyde, which has been widely used for the production of molded products including billiard balls, laboratory countertops, and as coatings and adhesives. RF nanoparticles can be synthesized by a sol-gel reaction, which includes the polymerization of phenol and formaldehyde under the catalysis of ammonia.[28] In our group, RF has been used as a sacrificial layer and protective layer to be coated on various nanostructures, such as metal nanocrystals non-medal solids and metal oxides.[29-30] Usually, the surface of the nanostructure has to be modified before the deposition of RF, because the affinity between RF and the other material is weak. For example, SiO_2 nanosphere has to be modified with PVP or CTAB before the coating of RF. It cannot be coated with RF without surface modification. On the other hand, colloidal metal nanocrystals are usually synthesized in a suspension with capping ligands, for example, PVP, which make the as-synthesized nanocrystals already a good candidate for RF coating. Therefore, when coating the SiO_2-Au@SiO_2 nanostructure with RF, only Au will be coated.

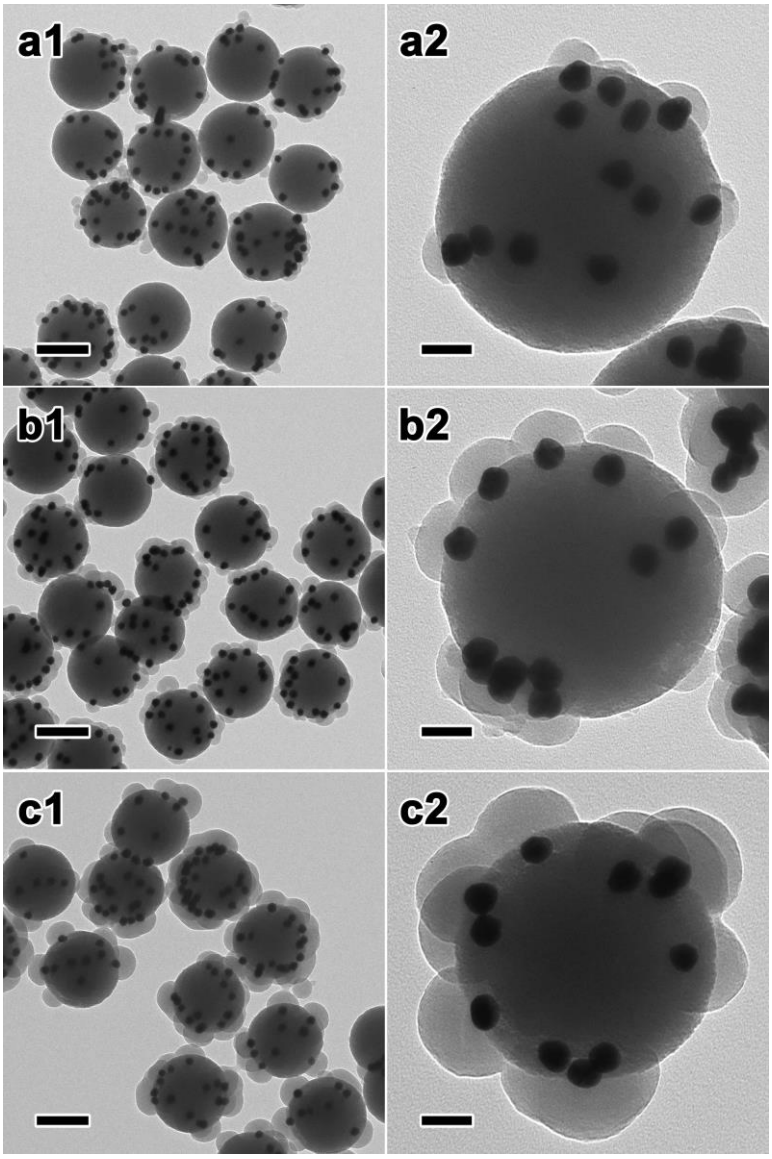

Figure 3.14 Selective deposition of RF on SiO_2-Au@SiO_2 with decreasing the amount of the seeds. The scale bars are 200 nm in a1, b1 and c1, and 50 nm in a2, b2 and c2.

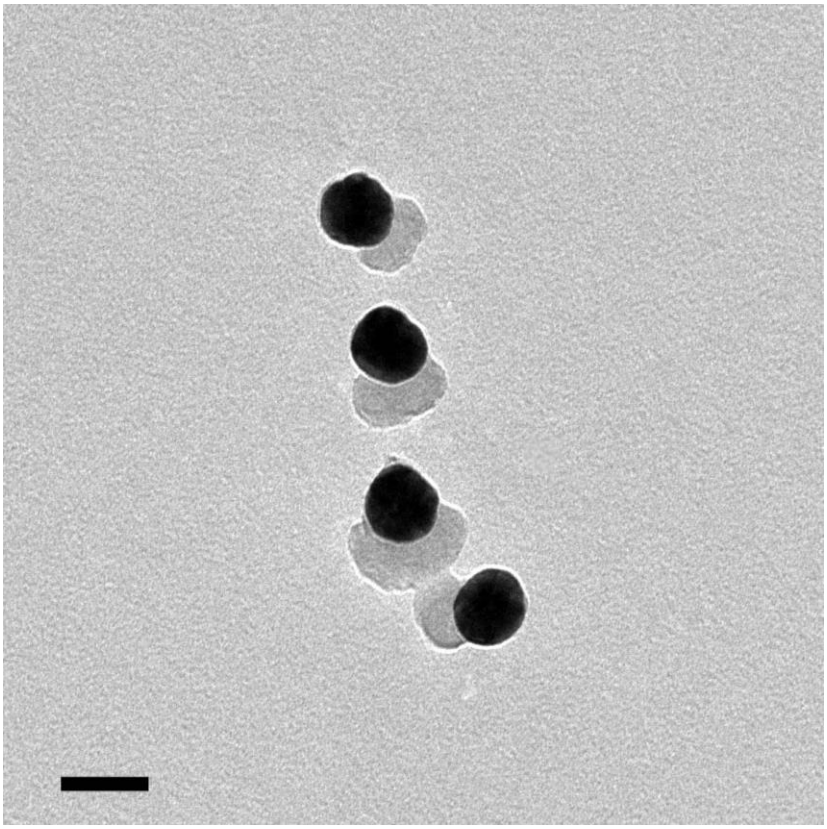

Figure 3.15 Au-RF Janus nanoparticles released from the SiO_2 substrate. The scale bar is 50 nm.

TEM images (Figure 3.14) confirm the successful deposition of RF on the SiO_2-Au@SiO_2 nanostructure. The thickness of the RF layer can be controlled by adjusting the volume ratio of SiO_2-Au@SiO_2 seed and the RF precursors. RF with increasing thickness can be achieved by decreasing the volume of the SiO_2-Au@SiO_2 seed in a fixed volume of RF precursors. It is worth noting that the Au-RF could be released from the SiO_2 substrate by removing SiO_2 with HF. The RF has to be condensed by high temperature treatment beforehand to increase its stability in the HF solution. TEM image (Figure 3.15) shows the successful preparation of Au-RF Janus nanoparticles after releasing from the substrate.

Another example is the selective coating of PANI on Au nanoparticles. In this experiment, the PANI was coated on the SiO_2-Au@SiO_2 seed by chemical oxidative polymerization of aniline monomer in sodium dodecyl sulfate (SDS) aqueous solution using ammonium persulfate as redox initiator.[31-33] It is worth noting that SDS plays a very important role in the selective deposition of PANI on Au nanoparticles. TEM images (Figure 3.16) confirm the import role of SDS as structure directing agent. When the synthesis was carried out without SDS, both SiO_2 and Au can be coated. In contrast, when a certain amount of SDS was used as surfactant, selective coating on Au rather than on SiO_2 could be achieved.

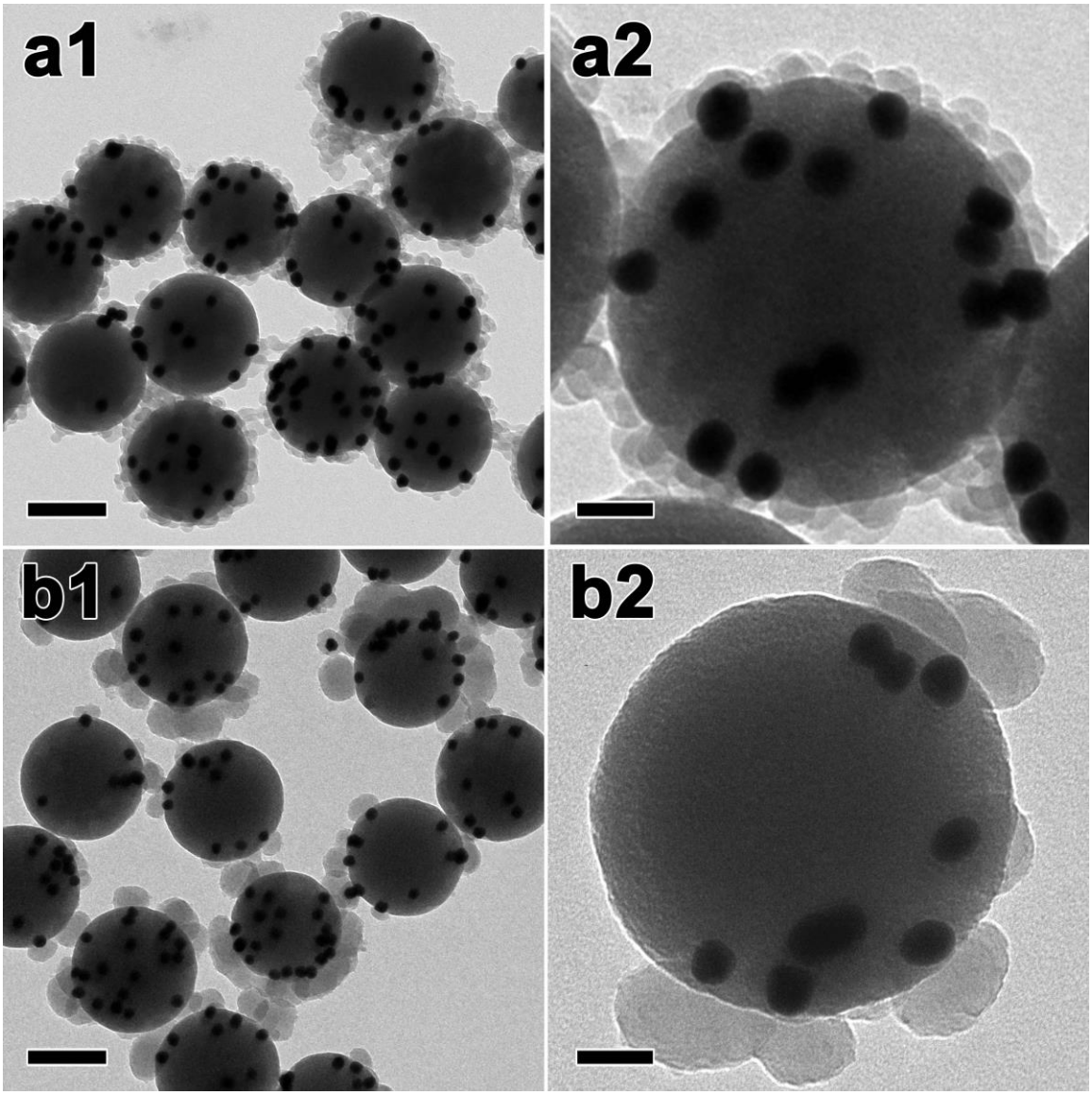

Figure 3.16 Selective deposition of PANI on SiO_2-Au@SiO_2 with increasing amount of SDS. The scale bars are 200 nm in a1 and b1, and 50 nm in a2 and b2.

The mechanism for selective deposition of PANI is shown in Figure 3.17. Because the -NH_2 groups in aniline can interact with not only the -OH groups in SiO_2 through hydrogen bonding, but also Au atoms through coordination, the deposition of PANI shouldn't have any preference. However, when the concentration of SDS was increased to a certain value, the surfactants can form micelles in the aqueous solution, which can be treated as nanoreactors with the hydrophobic tails as cores and the hydrophilic heads as shells, encapsulating the aniline molecules inside the nanoreactors. The electrostatic repulsion between the negatively charged SDS micelle and the negatively charged SiO_2 nanosphere could prevent the deposition of PANI on surface of SiO_2, resulting in selective deposition of PANI only on the Au nanospheres.

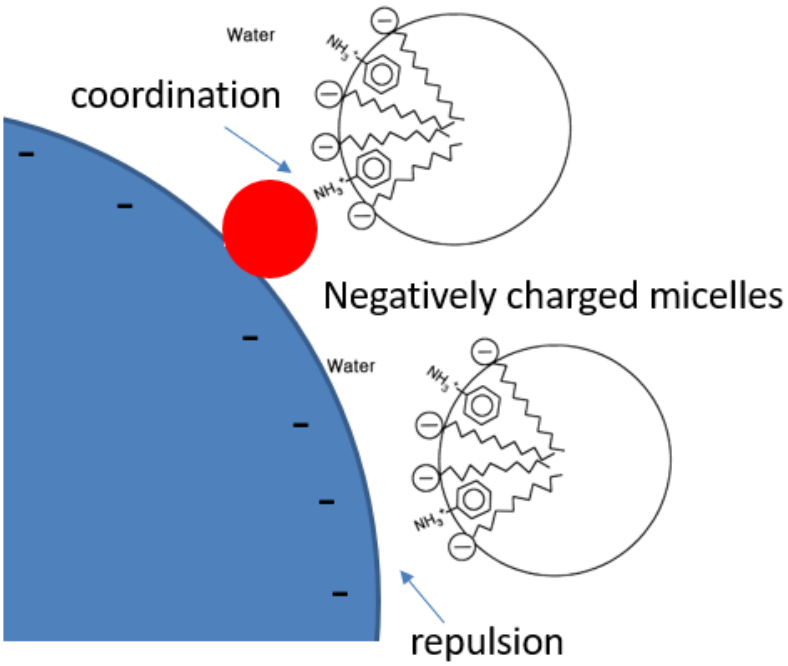

Figure 3.17 Mechanism for the selective deposition of PANI on SiO_2-Au@SiO_2.

3.2.5 Control the nanostructure of Au by ligand-assisted ripening

Besides the synthesis of Janus nanoparticles, the SiO_2-Au@SiO_2 nanostructure also provide opportunity for the growth of complicated metal nanostructures by combining the unique property of the seeds and the growth pathways. As we have introduced in Chapter 2, island growth of Au on Au nanospheres can be induced by modifying the surface of the Au nanoparticles with Pt, because the over excessive energy increase with the large mismatch between the lattice of Pt and Au. In addition, the number of islands can be controlled by ligand-assisted oxidative ripening. With more KI in the growth solution, the number of islands can be reduced. In this section, we show the unconventional Au nanostructures which could be synthesized by using SiO_2-Au@SiO_2 as seeds. The SiO_2-Au@SiO_2 seeds were modified with Pt first, followed by injecting the growth solution of Au with different amount of KI.

TEM images in Figure 3.18 show the nanostructure after the seed-mediated growth of Au with increasing amount of KI. When the synthesis was carried out without KI, multiple islands can be observed on the Au nanospheres. The number of islands was reduced by increasing the amount of KI. As shown in Figure 3.17 b, when the ratio of KI:Au^{3+} was increased to 5, the number of islands on each Au nanosphere was reduced to 2-4, corresponding with an increase in the island size. As the ratio of KI:Au^{3+} was further increased to 50, only one island could be observed.

In this synthetic system, the number of Au islands is not only related to the amounts of ligands in the synthesis, but also related to the exposed area of the Au nanosphere. Figure 3.19 shows the change in the number of islands by increasing the exposure of Au

nanosphere. When the exposed area was 27.9 % of the surface of the Au nanosphere, there were 3-4 nanoislands on each Au nanosphere. In contrast, when the exposed area increased to 56.3 %, the number of islands increased to 7-8. The surface area of a spherical cap was calculated according to $A= 2\pi rh$, where A is the surface area of the spherical cap, r is the radius of the sphere, and h is the height of the cap. After releasing from the SiO_2 substrate by adding HF, the foot-like nanostructures can be obtained.

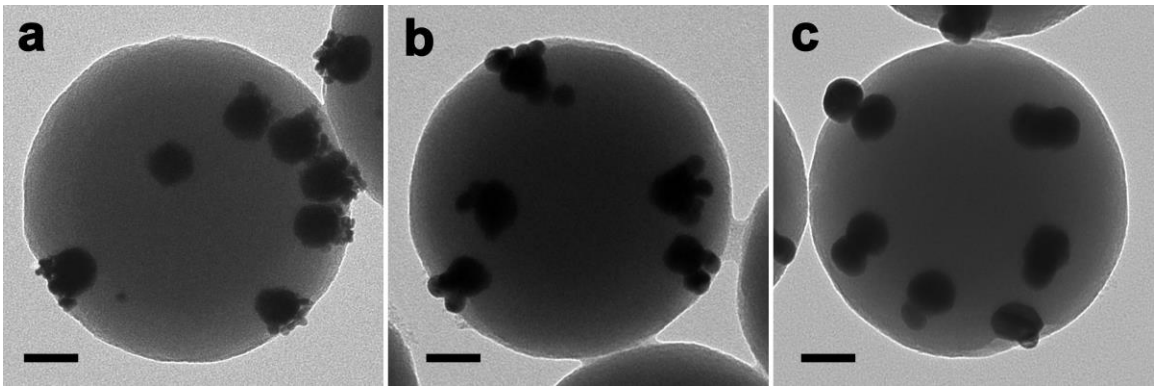

Figure 3.18 Growth of Au on Pt modified SiO_2-Au@SiO_2 seed with increasing amount of KI. The atomic ratio between KI and Au^{3+} in the growth solution were 0 (a), 5 (b) and 50 (c). The scale bars are 50 nm.

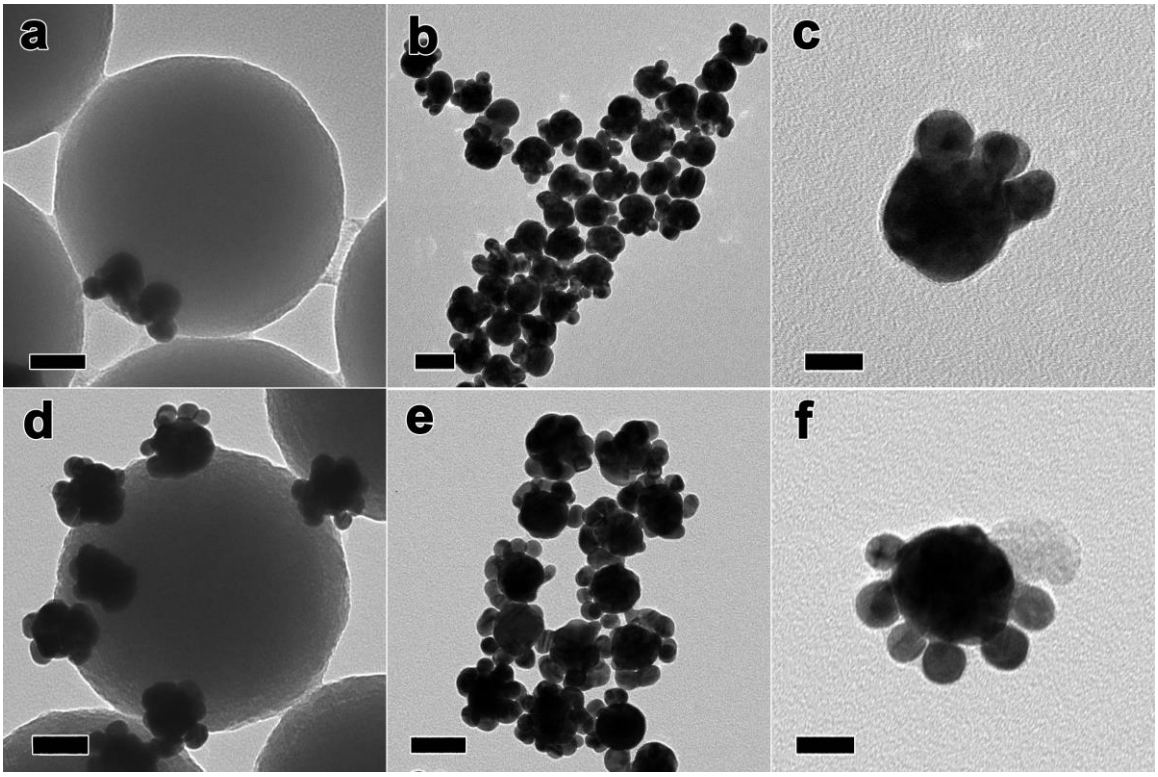

Figure 3.19 Growth of Au islands on Pt modified SiO_2-Au@SiO_2 seed. The atomic ratio of KI/Au^{3+} was 5. The scale bars are 50 nm in a and d, and 20 nm in b, c, e, and f.

3.3 Conclusion

In summary, we have developed a stepwise template-assisted seed-mediated growth method for the synthesis of rod-like plasmonic nanostructures. The synthesis requires using colloidal nanoparticle as substrates for the assembly of metal seeds, and precise control of the coverage of the metal seeds. Anisotropic growth of metal nanostructure is induced by partial passivizing the exposed area of the metal seeds. Au dimers, linear trimers and Au-Ag dimers with two distinct plasmonic excitation bands have been synthesized. Besides, this template is very versatile for the anisotropic growth of other materials, for example, Pd and Cu_2O. In addition, Au-polymer Janus nanoparticles could be obtained by selective deposition of RF and PANI on the template. Moreover, the template can be used for the synthesis of unconventional metal nanostructures by controlling the surface property of the seed and the ripening process in the seed-mediated growth step.

3.4 References

1. Hu, M.; Chen, J. Y.; Li, Z. Y.; Au, L.; Hartland, G. V.; Li, X. D.; Marquez, M.; Xia, Y. N., Gold nanostructures: engineering their plasmonic properties for biomedical applications. *Chem. Soc. Rev.* **2006,** *35* (11), 1084.
2. Chen, H. J.; Shao, L.; Li, Q.; Wang, J. F., Gold nanorods and their plasmonic properties. *Chem. Soc. Rev.* **2013,** *42* (7), 2679.
3. Liu, K.; Bai, Y.; Zhang, L.; Yang, Z.; Fan, Q.; Zheng, H.; Yin, Y.; Gao, C., Porous Au–Ag Nanospheres with High-Density and Highly Accessible Hotspots for SERS Analysis. *Nano Lett.* **2016,** *16* (6), 3675.
4. Zhang, Q.; Lima, D. Q.; Lee, I.; Zaera, F.; Chi, M. F.; Yin, Y. D., A Highly Active Titanium Dioxide Based Visible-Light Photocatalyst with Nonmetal Doping and Plasmonic Metal Decoration. *Angew. Chem., Int. Ed.* **2011,** *50* (31), 7088.
5. Bagley, A. F.; Hill, S.; Rogers, G. S.; Bhatia, S. N., Plasmonic Photothermal Heating of Intraperitoneal Tumors through the Use of an Implanted Near-Infrared Source. *ACS Nano* **2013,** *7* (9), 8089.
6. Lohse, S. E.; Murphy, C. J., The Quest for Shape Control: A History of Gold Nanorod Synthesis. *Chem. Mater.* **2013,** *25* (8), 1250.
7. Gao, A. Q.; Xu, W. J.; de Leon, Y. P.; Bai, Y. C.; Gong, M. F.; Xie, K. L.; Park, B. H.; Yin, Y. D., Controllable Fabrication of Au Nanocups by Confined-Space Thermal Dewetting for OCT Imaging. *Adv. Mater.* **2017,** *29* (26).
8. Wang, G.; Tao, S.; Liu, Y.; Guo, L.; Qin, G.; Ijiro, K.; Maeda, M.; Yin, Y., High-yield halide-free synthesis of biocompatible Au nanoplates. *Chem. Commun.* **2016,** *52* (2), 398.
9. Nikoobakht, B.; El-Sayed, M. A., Preparation and Growth Mechanism of Gold Nanorods (NRs) Using Seed-Mediated Growth Method. *Chem. Mater.* **2003,** *15* (10), 1957.
10. Chen, Y.; Yang, D.; Yoon, Y. J.; Pang, X.; Wang, Z.; Jung, J.; He, Y.; Harn, Y. W.; He, M.; Zhang, S.; Zhang, G.; Lin, Z., Hairy Uniform Permanently Ligated Hollow Nanoparticles with Precise Dimension Control and Tunable Optical Properties. *J. Am. Chem. Soc.* **2017,** *139* (37), 12956.
11. Métraux, G. S.; Cao, Y. C.; Jin, R.; Mirkin, C. A., Triangular Nanoframes Made of Gold and Silver. *Nano Lett.* **2003,** *3* (4), 519.

12. Wang, M.; Gao, C.; He, L.; Lu, Q.; Zhang, J.; Tang, C.; Zorba, S.; Yin, Y., Magnetic Tuning of Plasmonic Excitation of Gold Nanorods. *J. Am. Chem. Soc.* **2013,** *135* (41), 15302.
13. Murphy, C. J.; Jana, N. R., Controlling the aspect ratio of inorganic nanorods and nanowires. *Adv. Mater.* **2002,** *14* (1), 80.
14. Jana, N. R.; Gearheart, L.; Murphy, C. J., Wet chemical synthesis of silver nanorods and nanowires of controllable aspect ratio. *Chem. Commun.* **2001,** (7), 617.
15. Murphy, C. J.; Sau, T. K.; Gole, A. M.; Orendorff, C. J.; Gao, J.; Gou, L.; Hunyadi, S. E.; Li, T., Anisotropic Metal Nanoparticles: Synthesis, Assembly, and Optical Applications. *J. Phys. Chem. B* **2005,** *109* (29), 13857.
16. Xia, Y.; Gilroy, K. D.; Peng, H.-C.; Xia, X., Seed-Mediated Growth of Colloidal Metal Nanocrystals. *Angew. Chem., Int. Ed.* **2017,** *56* (1), 60.
17. Wiley, B.; Herricks, T.; Sun, Y.; Xia, Y., Polyol Synthesis of Silver Nanoparticles: Use of Chloride and Oxygen to Promote the Formation of Single-Crystal, Truncated Cubes and Tetrahedrons. *Nano Lett.* **2004,** *4* (9), 1733.
18. Habas, S. E.; Lee, H.; Radmilovic, V.; Somorjai, G. A.; Yang, P., Shaping binary metal nanocrystals through epitaxial seeded growth. *Nat. Mater.* **2007,** *6*, 692.
19. Langille, M. R.; Zhang, J.; Personick, M. L.; Li, S.; Mirkin, C. A., Stepwise Evolution of Spherical Seeds into 20-Fold Twinned Icosahedra. *Science* **2012,** *337* (6097), 954.
20. Xia, Y.; Xiong, Y.; Lim, B.; Skrabalak, S. E., Shape-Controlled Synthesis of Metal Nanocrystals: Simple Chemistry Meets Complex Physics? *Angew. Chem., Int. Ed.* **2009,** *48* (1), 60.
21. Feng, Y.; He, J.; Wang, H.; Tay, Y. Y.; Sun, H.; Zhu, L.; Chen, H., An Unconventional Role of Ligand in Continuously Tuning of Metal–Metal Interfacial Strain. *J. Am. Chem. Soc.* **2012,** *134* (4), 2004.
22. Crane, C. C.; Tao, J.; Wang, F.; Zhu, Y. M.; Chen, J. Y., Mask-Assisted Seeded Growth of Segmented Metallic Heteronanostructures. *J. Phys. Chem. C* **2014,** *118* (48), 28134.
23. Chen, T.; Chen, G.; Xing, S.; Wu, T.; Chen, H., Scalable Routes to Janus Au−SiO2 and Ternary Ag−Au−SiO2 Nanoparticles. *Chem. Mater.* **2010,** *22* (13), 3826.
24. Hu, Y. X.; Sun, Y. G., A Generic Approach for the Synthesis of Dimer Nanoclusters and Asymmetric Nanoassemblies. *J. Am. Chem. Soc.* **2013,** *135* (6), 2213.
25. Gao, C.; Vuong, J.; Zhang, Q.; Liu, Y.; Yin, Y., One-step seeded growth of Au nanoparticles with widely tunable sizes. *Nanoscale* **2012,** *4* (9), 2875.

26. Kuo, C.-H.; Hua, T.-E.; Huang, M. H., Au Nanocrystal-Directed Growth of Au−Cu2O Core−Shell Heterostructures with Precise Morphological Control. *J. Am. Chem. Soc.* **2009,** *131* (49), 17871.
27. Romero, I.; Aizpurua, J.; Bryant, G. W.; Abajo, F. J. G. d., Plasmons in nearly touching metallic nanoparticles: singular response in the limit of touching dimers. *Opt. Express* **2006,** *14* (21), 9988.
28. Liu, J.; Qiao, S. Z.; Liu, H.; Chen, J.; Orpe, A.; Zhao, D.; Lu, G. Q., Extension of The Stöber Method to the Preparation of Monodisperse Resorcinol–Formaldehyde Resin Polymer and Carbon Spheres. *Angew. Chem., Int. Ed.* **2011,** *50* (26), 5947.
29. Li, N.; Zhang, Q.; Liu, J.; Joo, J.; Lee, A.; Gan, Y.; Yin, Y., Sol–gel coating of inorganic nanostructures with resorcinol–formaldehyde resin. *Chem. Commun.* **2013,** *49* (45), 5135.
30. Liu, H.; Joo, J. B.; Dahl, M.; Fu, L.; Zeng, Z.; Yin, Y., Crystallinity control of TiO2 hollow shells through resin-protected calcination for enhanced photocatalytic activity. *Energy Environ. Sci.* **2015,** *8* (1), 286.
31. Kim, B.-J.; Oh, S.-G.; Han, M.-G.; Im, S.-S., Synthesis and characterization of polyaniline nanoparticles in SDS micellar solutions. *Synth. Met.* **2001,** *122* (2), 297.
32. Jiang, N.; Shao, L.; Wang, J., (Gold Nanorod Core)/(Polyaniline Shell) Plasmonic Switches with Large Plasmon Shifts and Modulation Depths. *Adv. Mater.* **2014,** *26* (20), 3282.
33. Lu, W.; Jiang, N.; Wang, J., Active Electrochemical Plasmonic Switching on Polyaniline-Coated Gold Nanocrystals. *Adv. Mater.* **2017,** *29* (8), 1604862.

Chapter 4 Magnetic Tuning of Plasmonic Excitation of Au-Au and Au-Ag Dimers

4.1 Introduction

It is known that the plasmonic properties of metal nanostructures are mainly related to their sizes, shapes and surrounding medium.[1-5] Many efforts have been devoted to tuning the plasmonic property of metal nanocrystals by shape-controlled synthesis or by assembling them into defined structures.[6-10] Compared to isotropic spherical particles, anisotropic nanostructures like nanorods, which have two plasmonic resonant modes in responds to light polarized along different directions, could offer plasmonic tunability by controlling their alignment in the optical field.[11-16] Magnetic field is an ideal tool for this purpose because it can be applied instantly and remotely. Another important advantage of magnetic control is the anisotropic nature of magnetic interactions, which allow effective alignment of magnetic dipoles along the external fields. However, as Au is nonmagnetic, additional magnetically active material needs to be incorporated to enable the desired magnetic orientational control of Au nanorods.[17] Our group has successfully demonstrated that the orientation of gold nanorods could be dynamically controlled by binding them parallelly to the surface of superparamagnetic iron oxide nanorods. As shown in Figure 4.1, when applying an external magnetic field, the angle between the field direction and the direction of polarization of the incident light could be readily adjusted, thus resulting in the selective excitation of either transverse or longitudinal mode of the gold nanorods.

Similar as Au nanorods, Au dimers which are composed of two Au nanoparticles show the polarization dependent optical properties.[18-22] Atay et al. has studied the plasmonic

excitation modes of Au dimers composed of two Au disks with size of 130 nm and tunable interparticle distance under polarized light.[23] As shown in Figure 4.2 (a), when the incident light was polarized perpendicular to the dimers, a transverse mode was excited, resulting in one plasmonic peak at around 700 nm. In contrast, when the incident light was polarized parallel to the Au dimers, a longitudinal mode was excited, resulting in a two-band absorption at both shorter and longer wavelength. The polarization dependent plasmonic property of Au dimers provide opportunity for dynamic tuning.

The result of our template-assisted seed-mediated growth results in self-registered rod-like Au nanoparticles assembled along the surface normal of the colloidal substrates. this structure makes it convenient to manipulate the orientation of the nanorods and consequently their plasmonic properties by controlling the orientation of the colloidal substrates rather than the nanorods themselves. To demonstrate this unique advantage, we adopted this strategy for growing Au nanorods on the surface of magnetic iron oxide nanorods and nanoplates to produce magnetic/plasmonic nanocomposites whose plasmonic bands can be selectively excited by controlling the orientation of the magnetic components using external magnetic fields. The convenient magnetic control further enabled the creation of thin polymer films containing Au nanorods with defined orientations at different locations, producing polarization dependent color displays that may find potential applications in many areas such as information encryption.

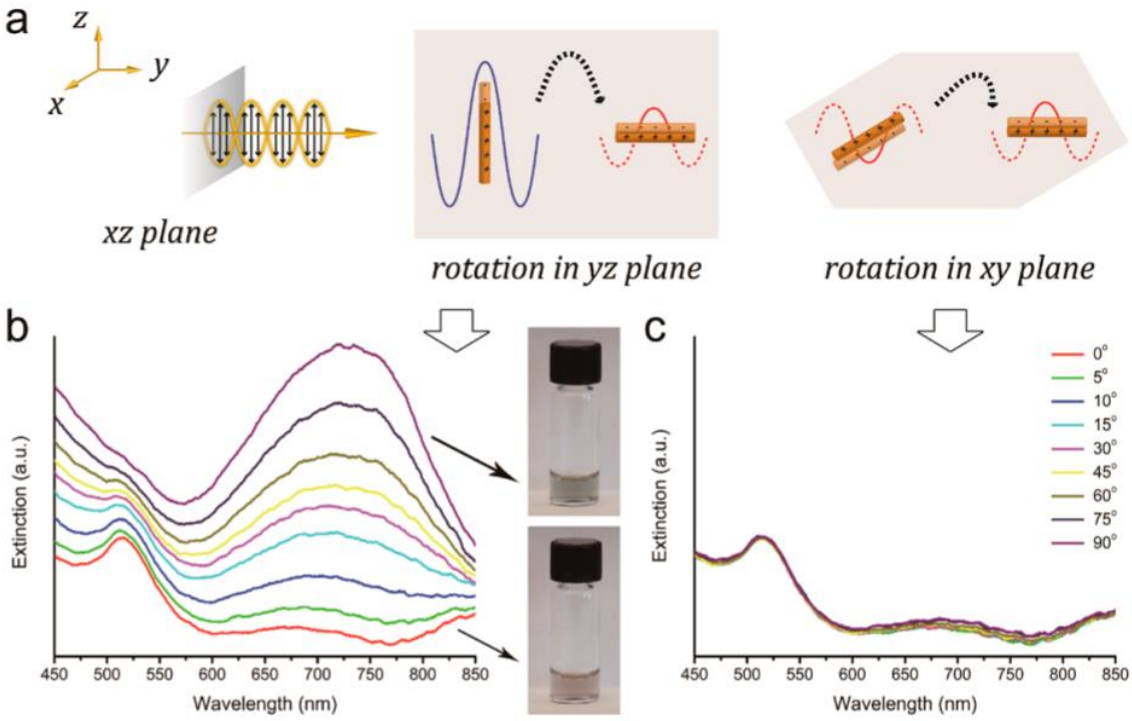

Figure 4.1 (a) Scheme showing the plasmon excitation of AuNRs under polarized light. (b) Spectra of a dispersion of the hybrid nanostructures under a magnetic field with its direction varying from perpendicular to parallel within the yz plane relative to the incident light. The incident light is polarized along the z axis. The inset shows digital images of the dispersion under a magnetic field with its direction parallel (bottom) and perpendicular (up) to the incident beam. (c) Spectra of the dispersion under a magnetic field with its direction varying within the xy plane from perpendicular to parallel relative to the incident light. Copyright © 2013 American Chemical Society.[17]

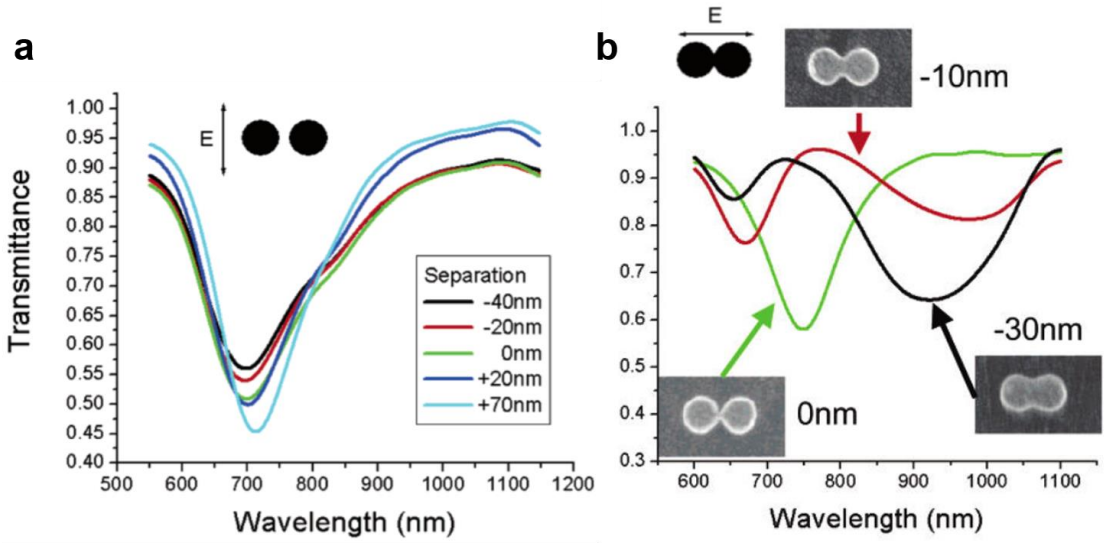

Figure 4.2 (a) Spectra for perpendicular polarization over the entire pair separation regime. (b) Spectra for parallel polarization over the entire pair separation regime. Increasing the particle overlap from point contact and the widening of the interconnection "neck" into an eventually single ellipsoidal single (anisotropic) plasmonic particle. Copyright © 2004 American Chemical Society.[23]

4.2 Materials and Methods

4.2.1 Materials

Tetraethylorthosilicate (TEOS), poly(vinyl pyrrolidone) (PVP, Mw~10,000), 3-Aminopropyl)triethoxysilane (APTES), potassium iodide (KI), L-ascorbic acid (AA), sodium borohydride ($NaBH_4$, 99%), sodium hydroxide (NaOH), $FeCl_3$, $CoCl_2$, Chloroauric acid ($HAuCl_4$), polyacrylic acid (PAA, average M.W. 1800), and trisodium citrate (TSC) were purchased from Sigma-Aldrich. For the preparation of the hydrogel film, acrylamide, 2-Hydroxy-4'-(2-hydroxyethoxy)-2-methyl-propiophe and N,N'-methylenebis(acrylamide) (purity 98%) were purchased from Sigma-Aldrich. Ammonium hydroxide ($NH_3 \cdot H_2O$, 28% by weight in water) was purchased from Fisher Scientific. Ethanol (200 proof) is purchased from Decon Laboratories Inc. All chemicals were directly used as received without further purification.

4.2.2 Synthesis of Au Dimers-on-Magnetic Nanorods

(1) Synthesis of FeOOH@SiO_2 Nanorods

The synthesis of FeOOH nanorods was based on a previous report with some modifications.[24] Typically, 19.464 g of anhydrous $FeCl_3$ were dissolved in 80 mL of water. The solution was added into 1.166 mL of concentrated HCl and then centrifuged at 11000 rpm for 5 min for the removal of unsolvable precipitates. The purified solution was diluted to 200 mL and heated to 98 ºC for 24 hrs. The solid product was collected by centrifugation and washed with water twice. The FeOOH nanorods were dispersed in 40 mL of DI water. The nanorods were modified with PAA before silica coating. 40 mL of FeOOH nanorods dispersion was added to 160 mL of 0.1M PAA solution. Ammonia was

added to adjust the pH of the solution to 8-9. After overnight stirring, the nanorods were recovered by centrifugation and were redispersed in 200 mL H_2O. Silica coating on FeOOH nanorods was done by adding 150 μL TEOS to 10 mL FeOOH nanorods, 100 mL of ethanol and 5 mL of ammonia. After stirring for 40 min, the products was centrifuged, washed with Ethanol twice and redispersed in 10 mL Ethanol.

(2) Reduction of FeOOH@SiO_2 Nanorods

FeOOH@SiO_2 nanorods and were heated at 360 ºC for 2 h in a flow of forming gas to convert the FeOOH nanorods to the magnetic phase.

(3) Au Seeds Loading

After forming gas reduction, the Fe_3O_4@SiO_2 nanorods were dispersed in 30 mL of ethanol and 1 mL of APTES. The suspension was heated at 80 ºC for 3 hrs, isolated by centrifugation, washed with ethanol and water for three times, and redispersed in 10 mL H_2O. The Au nanoparticles were synthesized by injecting 1 mL of the Au seeds solution into a growth solution containing 5 mL of PVP (5 wt%), 2.5 mL of L-ascorbic acid (0.1 M), 2 mL of KI (0.2 M), 600 μL of $HAuCl_4$ (0.25M), and 10 mL of H_2O. After stirring for 10 min, the Au suspension was mixed with the APTES modified Fe_3O_4@SiO_2 nanorods.

(4) Silica Coating

For silica coating, 2 mL of Fe_3O_4@SiO_2-Au was added to 18 mL of ethanol, 2 mL of water and 1 mL of $NH_3 \cdot H_2O$ with sonication. 40 μL of TEOS was added to the above solution under sonication for 5 minutes, and leave on vortex for 40 minutes to achieve Fe_3O_4@SiO_2-Au@SiO_2. The nanocomposites were washed with Ethanol twice, and redispersed in 4 mL of water.

(5) Seeded Growth of Au Dimers

For the growth of Au, an Au growth solution was prepared by mixing 1.5 mL of PVP (5 wt%), 375 μL of L-ascorbic acid (0.1 M), 300 μL of KI (0.2 M), 90 μL of $HAuCl_4$ (0.25M), and 3 mL of H_2O. Then, 4 mL of Fe_3O_4@SiO_2-Au@SiO_2 was added to 4 mL of the Au growth solution, and stirred for 10 minutes. The Au dimers-on-magnetic nanorods were collected by centrifugation, and washed with water for 3 times.

(6) Seeded Growth of Au-Ag Dimers

For the growth of Ag, 4 mL of Fe_3O_4@SiO_2-Au@SiO_2 was added to 6 mL of H_2O, 10 mL of PVP (5 wt%), 50 μL of $AgNO_3$ (0.1 M) and 100 μL of AA (0.1 M), and stirred for 10 minutes. The same procedure was repeated for 6 times. The nanocomposites were washed with water and ethanol to remove the excess reagents.

4.2.3 Synthesis of Au Dimers-on-Magnetic Nanoplates

(1) Synthesis of $Co(OH)_2$@SiO_2 Nanoplates

$Co(OH)_2$ nanoplates were synthesized based on a previous report with some modifications.[25] Typically, 0.48 g of $CoCl_2$ was dissolved in 0.2 g of PVP (Mw=55,000) and 72 mL of H_2O, followed by adding 56 g of hexamethylenetetramine and 8 mL of ethanol. The mixture was heated at 95 ºC for 2 hrs. The products were collected by centrifugation, washed with H_2O and redispersed in 40 mL of H_2O. For silica coating, 50 μL TEOS was added to a mixture contains 2 mL of the $Co(OH)_2$ dispersion, 20 mL of ethanol and 1 mL of ammonia. The solution was sonicated for 30 min. After silica coating, the particles were isolated by centrifugation, and redispersed in 20 mL ethanol.

(2) Reduction of $Co(OH)_2$@SiO_2 Nanoplates

$Co(OH)_2$@SiO2 nanoplates and were heated at 360 ºC for 2 h in a flow of forming gas to convert the $Co(OH)_2$ nanoplates to the magnetic phase.

(3) Au Seeds Loading

After forming gas reduction, the $Co(OH)_2@SiO_2$ nanoplates were dispersed in 20 mL of ethanol. 2 mL of the $Co(OH)_2@SiO_2$ nanoplates were mixed with 1 mL of APTES, and heated at 80 ºC for 3 hrs, isolated by centrifugation, washed with ethanol and water for three times, and redispersed in 5 mL H_2O.

The Au nanoparticles were synthesized by injecting 200 mL of the Au seeds solution into a growth solution containing 1 mL of PVP (5 wt%), 500 μL of L-ascorbic acid (0.1 M), 400 μL of KI (0.2 M), 120 μL of $HAuCl_4$ (0.25M), and 2 mL of H_2O. After stirring for 10 min, the Au suspension was mixed with the APTES modified $Co(OH)_2@SiO_2$ nanoplates. The nanocomposites were collected, and redispersed in 5 mL of H_2O.

(4) Silica Coating

For silica coating, 1 mL of $Co(OH)_2@SiO_2$-Au was added to 10 mL of ethanol and 0.5 mL of $NH_3 \cdot H_2O$ with sonication. 20 μL of TEOS was added to the above solution under sonication for 40 minutes to achieve $Co(OH)_2@SiO_2$-Au@SiO_2. The nanocomposites were washed with Ethanol twice, and redispersed in 2 mL of water.

(5) Seeded Growth of Au Dimers

For the growth of Au, an Au growth solution was prepared by mixing 1.5 mL of PVP (5 wt%), 375 μL of L-ascorbic acid (0.1 M), 300 μL of KI (0.2 M), 90 μL of $HAuCl_4$ (0.25M), and 3 mL of H_2O. Then, 1 mL of $Co(OH)_2@SiO_2$-Au@SiO_2 was added

to 120 μL of the Au growth solution, and stirred for 10 minutes. The Au dimers-on-magnetic nanoplates were collected by centrifugation, and washed with water for 3 times.

4.2.4 Fabrication of Polymer Film for Anti-Counterfeiting Display

Polyacrylamide precursor was prepared by mixing 0.5 g of acrylamide, 0.007 g of N,N'-methylenebis(acrylamide) and 2 mL of ethylene glycol. Then, one batch of nanorods-Au dimers was dispersed in 1 mL mixture of the hydrogel precursor, followed by sonication for 5 min. The dispersion was sandwiched between two clean glass slides to form a liquid film. The liquid film was solidified under UV irradiation (365 nm) for 1 min.

4.3 Results and Discussion

4.3.1 Magnetic Tuning of Plasmonic Excitation of Au-Au Nanoparticle Dimers

Plasmonic excitation of nanoparticle dimers is angular dependent. Study of two Au nanodisks in contact reveals that when the optical field is polarized perpendicular to the interparticle axis, only a transverse mode of dipole resonance is excited, resulting in one absorption peak at a shorter wavelength. In contrast, an optical field polarized along the interparticle axis can excite a longitudinal mode of dipole and quadrupole resonance of the nanoparticle dimers, showing two absorption peaks at both shorter and longer wavelength.

The stepwise template-assisted seed-mediated growth method we discussed in Chapter 3 brings plasmonic nanostructure with two unique features: 1) the rod-like nanostructure has two distinct extinction bands at both lower and higher wavelength; 2) the rod-like nanostructures are perpendicularly assembled to the surface of the substrate. These two features give an opportunity for the study and dynamic tuning of the plasmonic excitation of the rod-like plasmonic nanostructures. Study of the angular dependent plasmonic excitation is realized by changing the substrate to anisotropic magnetic nanoparticles, for example, magnetic nanorods and nanoplates. It is known that anisotropic magnetic nanoparticle will orient parallel to the external magnetic field to minimize the magnetic potential energy and dipole-dipole interaction. When the polarization direction of the incident light is fixed, the angular-dependent plasmonic excitation of the rod-like nanostructures can be studied by tuning the direction of the magnetic field.

In the following section, we will use Au dimers-on-magnetic nanorods as an example to show the dynamic tuning of plasmonic excitation of the rod-like plasmonic structures. FeOOH nanorods were chosen as the substrates, because they are anisotropic nanoparticles, and can be reduced to their magnetic counterparts. The FeOOH nanorods were coated with silica, reduced in forming gas, and modified with APTES for the attachment of Au nanoparticles. After loading Au nanoparticles, the nanocomposites were coated with another layer of silica to expose only the tips of the Au nanoparticles. Finally, a seeded growth process was performed to achieve Au dimers-on-magnetic nanorod. We show the XRD patterns for the phase change of FeOOH nanorods after reduction by forming gas in Figure 4.3. It is clear that the nanorods were reduced from β-FeOOH (JCPDS No. 34-1266) to Fe_3O_4 (JCPDS No. 19-0629).[26]

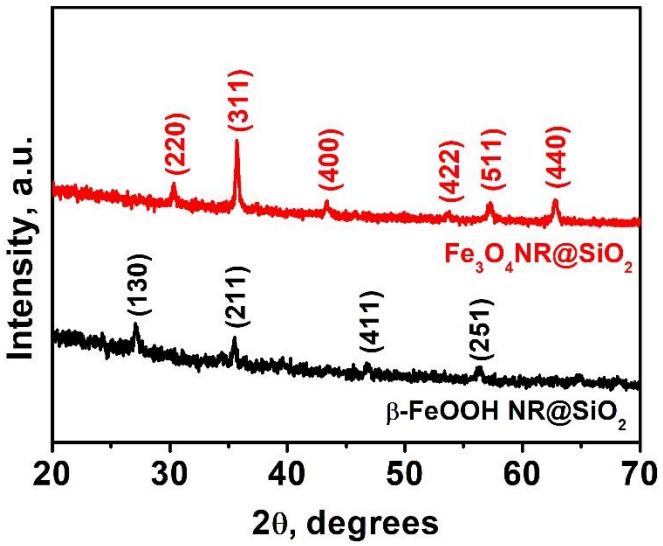

Figure 4.3 XRD patterns of $FeOOH@SiO_2$ and $Fe_3O_4@SiO_2$.

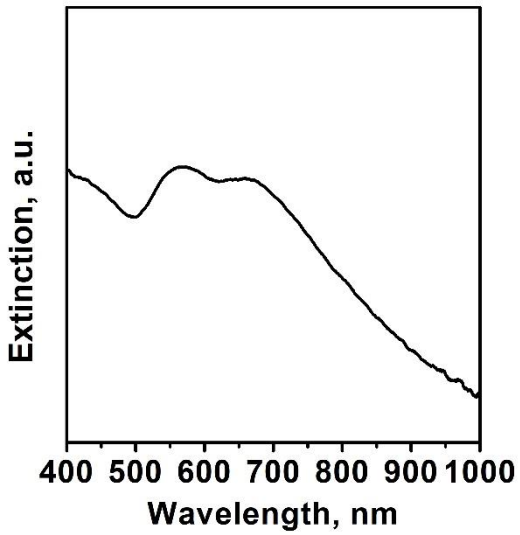

Figure 4.4 UV-vis spectrum of Au dimers-on-magnetic nanorods.

The structure of the Au dimers-on-magnetic nanorod is shown in Figure 4.5a. The nanocomposite is composed of Fe_3O_4 nanorod with ~2 μm in length and ~100 nm in width. The Au dimers are very densely distributed on the surface of the Fe_3O_4 nanorod with their long sides perpendicularly to the long side of the nanorod. The extinction spectrum of Au dimers-on-magnetic nanorod under ordinary light shows two distinct peaks at 568 and 660 nm (Figure 4.4). The angular-dependent plasmonic excitation can be studied by tuning the direction of the magnetic field. As shown in Figure 4.5b, when the direction of the magnetic field changes (black arrow), the magnetic nanorod will orient parallel to the direction of the magnetic field to minimize the magnetic potential energy and dipole-dipole interaction. Because the long sides of the Au dimers orient perpendicularly to the long sides of the magnetic nanorods, the long sides of the Au dimers will always be perpendicular to the direction of the magnetic field. Therefore, dynamic tuning of the plasmonic excitation of Au dimers can be achieved by tuning the direction of the magnetic field. To be more specific, we herein employed z-polarized light incident along y-axis as the light source for the dynamic tuning of the plasmonic excitation of Au dimers. When the magnetic field is along x and y-axis, both the longitudinal mode and the transverse mode of the Au dimers can be excited, showing two-bands extinction spectra. In contrast, when the magnetic field is along z-axis, only the transverse mode of the Au dimers will be excited, resulting in only one extinction band. Figure 4.5c shows the change of the extinction spectra of Au dimers under magnetic field along x, y and z-axis. When the magnetic nanorods are aligned in x-axis, both the longitudinal mode and the transverse mode of the Au dimers are excited,

showing two-bands extinction at 544 and 660 nm, exhibiting a dark bluish-purple color. In contrast, when the rods are aligned along z-axis, only the transverse mode is excited, showing a single extinction peak at 559 nm, showing red color. When the rods are aligned along y-axis, the extinction at shorter wavelength maintained, and redshift to 560 nm, together with the emerging of a broad absorption band centered at 727 nm, displaying a blue color. Dynamic tuning of Au dimers with more orientations of the magnetic field is shown in Figure 4.6. When the direction of the magnetic field was tuned from 0-90° in the X-Y plane, the spectra show a gradual decrease in the extinction intensity at a shorter wavelength and an increase at a longer wavelength. Both extinction peaks at short and long wavelength redshift. Tuning the direction of magnetic field in the X-Z plane resulted in an increase in the extinction intensity at lower wavelength. The evolution of extinction peak at 727 nm for PzBy could be attributed to the polarization dependent absorption of the nanorods. As shown in Figure 4.7, when the nanorods are aligned along y-axis, which is parallel to the direction of the incident light, a broad extinction peak appears due to the change in absorption cross-section of the nanorods in the light field. In addition, we demonstrated the synthesis of Au-Ag dimers-on-magnetic nanorods and characterized their optical property under magnetic field and polarized light. The structure of the nanocomposite is shown in Figure 4.8. Under ordinary light without a magnetic field, the Au-Ag dimers show three well-resolved peaks at 435, 535 and 637 nm (Figure 4.8b). Same as the optical property of Au dimers-on-magnetic nanorods, only the transverse plasmonic resonance of Au-Ag dimers could be excited when the nanorods are aligned with the long sides in the same direction as the light

polarization direction (Figure 4.9). Shifting the Au-Ag dimers to x or y-direction caused a decrease in the intensity of the transverse plasmonic resonance. Arranging Au-Ag dimers in the direction of the incident light generated a broad peak around 710 nm. The broad extinction agrees with the case of Au dimer when being aligned along the y axis, which should be attributed to the absorption of Fe_3O_4.

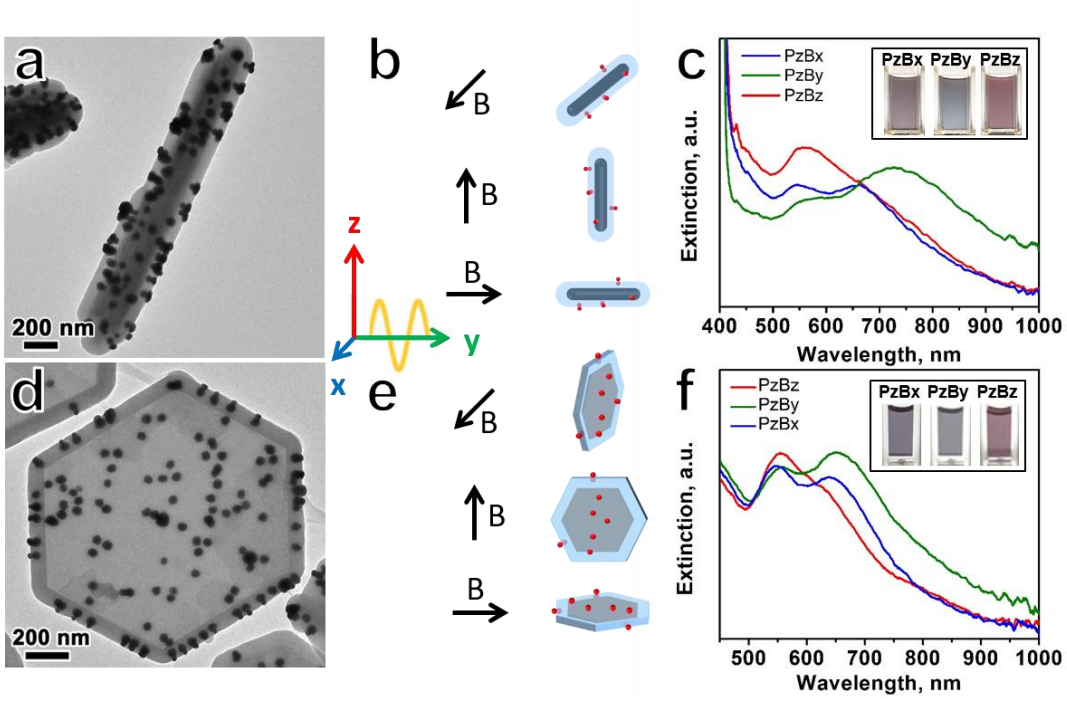

Figure 4.5 TEM images of Au dimers on the (a) magnetic nanorod and (d) nanoplate; scheme showing the orientation of (b) magnetic nanorod and (e) nanoplate under magnetic field; UV-vis spectra of Au dimers on the (c) magnetic nanorod and (f) nanoplate under a magnetic field with its direction varying along x, y and z axis. A z-polarized light incident along y direction is used as the light source for characterization. The inset digital images in (c) and (f) show the color of solution with a magnetic field along x, y and z directions.

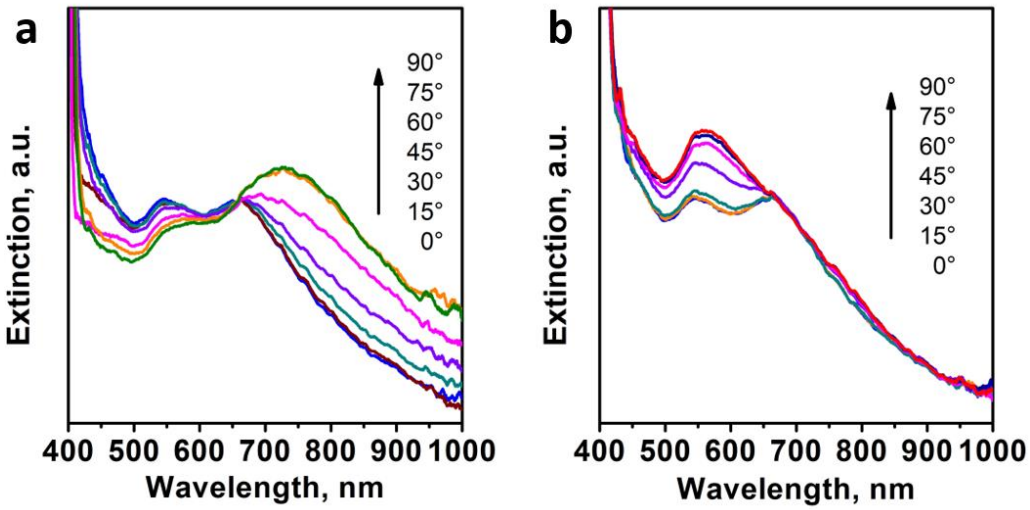

Figure 4.6 Spectra of a dispersion of the Au dimers-on-magnetic nanorod under magnetic fields with different directions in (a) xy plane and (b) xz plane. The degree inset indicate the angle relative to x axis.

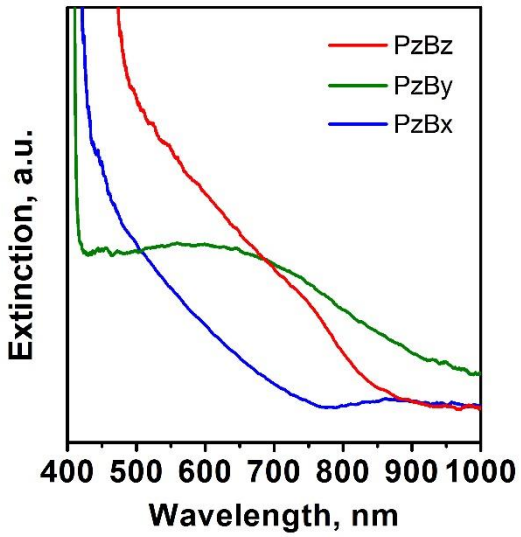

Figure 4.7 Spectra of a dispersion of the magnetic nanorod under magnetic field with different directions.

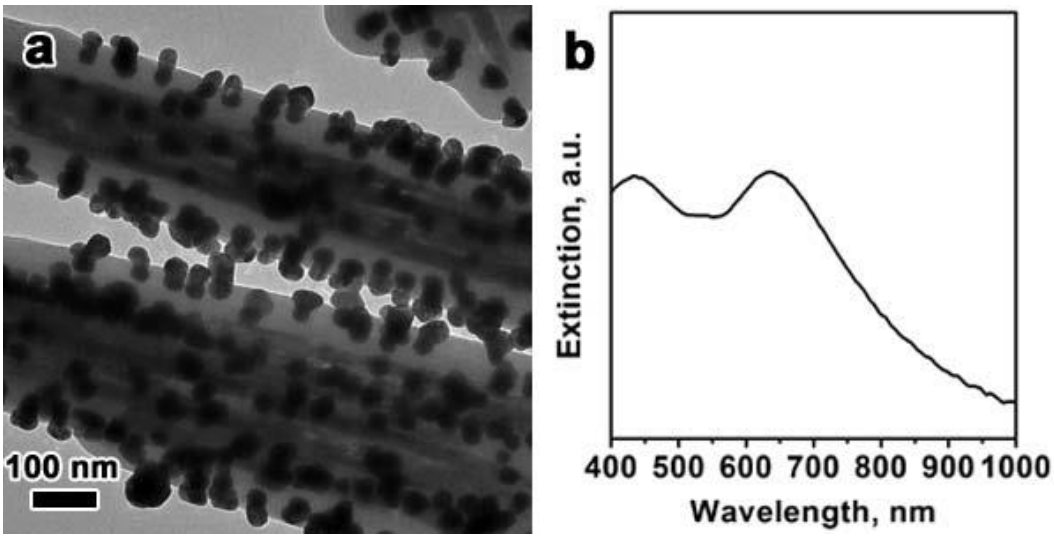

Figure 4.8 TEM image and extinction spectra of Au-Ag dimers-on-magnetic nanorods.

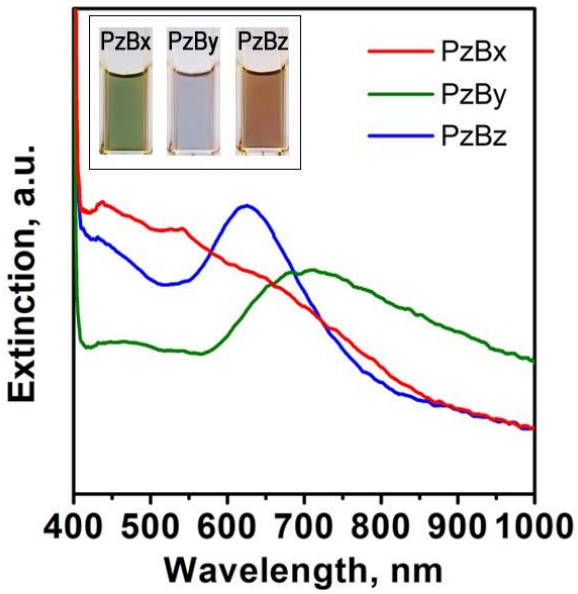

Figure 4.9 Dynamic tuning of Au-Ag dimers-on-magnetic nanorods.

Besides magnetic nanorods, we demonstrate dynamic tuning of the plasmonic excitation by employing magnetic nanoplates as substrates for the assembly of Au dimers. The synthesis of Au dimers-on-magnetic nanoplates was quite similar with the synthesis of Au dimers-on-magnetic nanorods, except switching the starting material from FeOOH nanorods to $Co(OH)_2$ nanoplates. As shown in Figure 4.10 and 4.11, reduction in a flow of forming gas could successfully covert α-$Co(OH)_2$ to CoO_x. The three predominant diffraction peaks in Figure 4.11 can be attributed to the (111), (200) and (220) planes of CoO (JCPDS No. 43-1004), which is known to be magnetic.[27] The structure of Au dimers-on-magnetic nanoplate is shown in Figure 4.5d, with most of the Au dimers assembled on the plane of the nanoplate. Under a magnetic field, the nanoplate will arrange with its plane parallel to the magnetic field (Figure 4.5e), shifting the alignment of the Au dimers. Seeded-growth of Au dimers leads to emerging of the two-bands plasmonic extinction bands at 553 and 638 nm (Figure 4.12). Dynamic tuning of the plasmonic excitation of Au dimers is shown in Figure 4.5f. Similar with the magnetic tuning behavior of Au dimers-on-magnetic nanorods, we observe a single plasmonic extinction peak at a shorter wavelength (555 nm) when the direction of the magnetic field is parallel to the light polarization direction. In addition, when the direction of the magnetic field is the same as the light incident direction, the peak at both shorter and longer wavelength redshift. The color of the Au dimers-on-magnetic nanoplate suspension under a magnetic field of different direction was shown in the inset of Figure 4.5f. When the magnetic field was tuned from x to y and z-axis, the color of the suspension changes from purple to greyish blue and red.

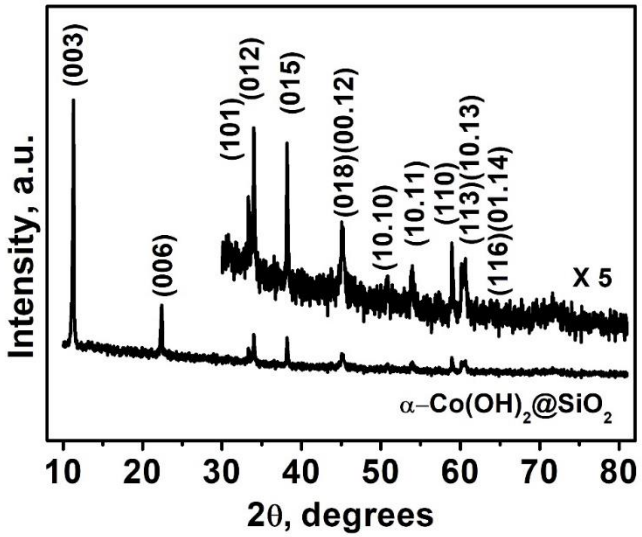

Figure 4.10 XRD pattern of $Co(OH)_2@SiO_2$.

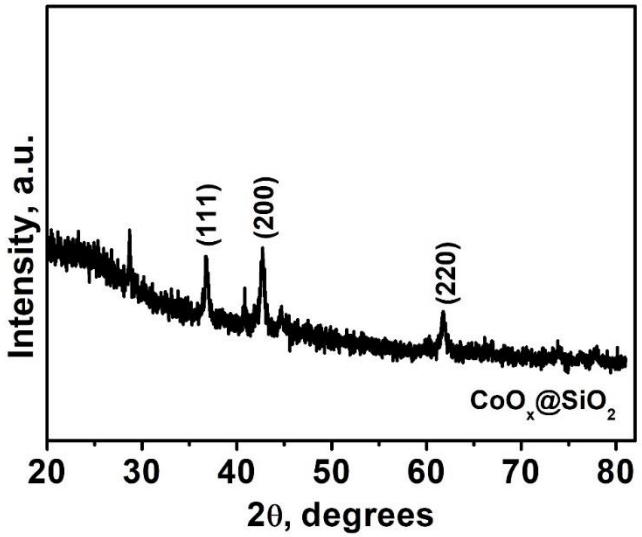

Figure 4.11 XRD pattern of $CoO_x@SiO_2$.

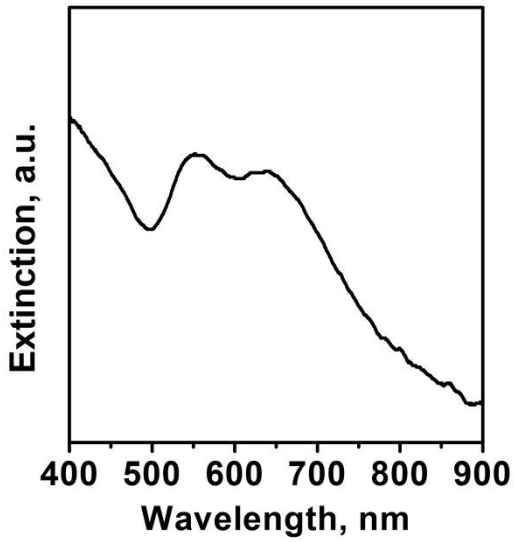

Figure 4.12 UV-vis spectrum of Au dimers on magnetic nanoplates.

4.3.2 Polarization dependent color display and anti-counterfeiting pattern

Due to the magnetic tunable plasmonic excitation of the Au dimer-magnetic nanoparticle nanocomplex, we developed a polarization dependent color display by fixing the nanocomplex in a thin film. Here, we use the nanocomplex, which has Au dimers on magnetic nanorods, as an example to demonstrate the fabrication of the polarization dependent thin film. Thin films patterned with different optical polarizations can be conveniently produced by combining the nanocomplex with lithography processes. Polyacrylamide hydrogel was chosen as the medium of the film because the nanocomposites can be dispersed very well in the hydrogel precursor. In addition, the polymerization of acrylamide can be initiated by UV light within a few minutes.

The fabrication steps are shown in Figure 4.13. The nanocomplex was first mixed with the hydrogel precursor to produce a homogeneous solution. Then, the mixture was sandwiched between two glass slides to form a liquid film. A photomask, which was printed by an ink-jet printer, was placed on top of the glass slide. The lower right corner of the photomask was black, which could prevent the covered area from being irradiated by the UV light. A magnetic field along x-axis was applied to the sample, while the exposed area was cured by UV light (365 nm). Then, the photomask was removed, and the sample was again exposed to UV light in the presence of a magnetic field along y-direction. After all these steps, the alignment of the magnetic nanorods could be separated into two areas. In area I and II, the orientation of magnetic nanorods are along x- and y-axis, respectively. These two regions display different colors in response to polarized light. Under polarized light, the region with the magnetic nanorods aligned in

the same direction as the polarized light will show a red color, which corresponds with the transverse plasmonic excitation. Meanwhile, the region with the magnetic nanorods aligned perpendicular to the polarized light will show a bluish-purple color, which corresponds with the overall plasmonic excitation of the Au dimers. Figure 4.13b and c show the optical microscopy images of the polarized patterns for Au dimers. Under the x-polarized light, the color of the region I and II are red and bluish-purple, respectively. An inverse color of the region I and II can be observed when the polarized light is rotated to the y-axis. A similar observation was found for magnetic plasmonic nanocomplex with Au-Ag dimers. As shown in Figure 4.13d and e, the color of the region I and II are red and green under the x-polarized light and inversed under the y-polarized light.

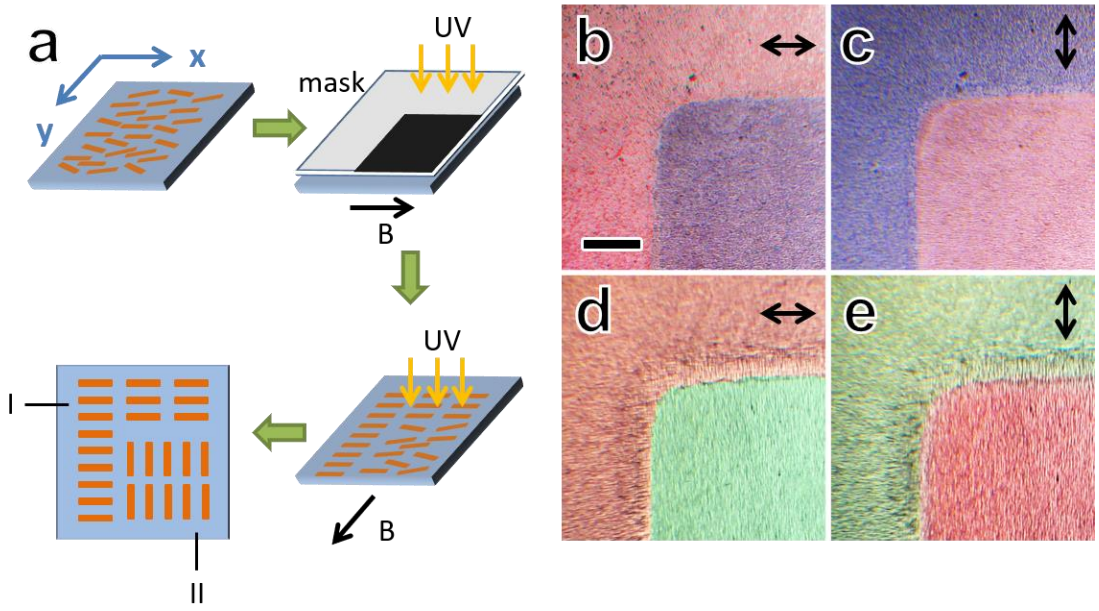

Figure 4.13 (a) Scheme showing the lithography process for the fabrication of thin films with patterns of different polarizations; optical microscopy images of patterns with (b and c) SiO_2-Au dimers and (d and e) SiO_2-Au-Ag dimers under light with different polarization directions. The scale bar in (b-e) is 500 μm.

This polarization-dependent color display can be further applied for the anti-counterfeiting pattern. Here, we fabricate a 0.7 cm×0.7 cm film by using a transparent photomask with a black clover pattern (Figure 4.14a). The orientation of the magnetic nanorods is fixed along x-axis and y-axis in the black and transparent area. Fig. 4.14b to g shows digital images of patterns having Au dimers and Au-Ag dimers under ordinary light, x-polarized light, and y-polarized light. Under the ordinary light, the pattern is invisible, because both transverse and longitudinal modes of the plasma resonance are excited. However, when a polarized light was applied, the area which has nanorods being oriented parallel to the oscillation of light wave shows a red-pink color, because the transverse mode is split from the plasmonic excitation of the dimers. In this way, the latent information of the graphic sequence was decoded and can be used for authentication purposes.

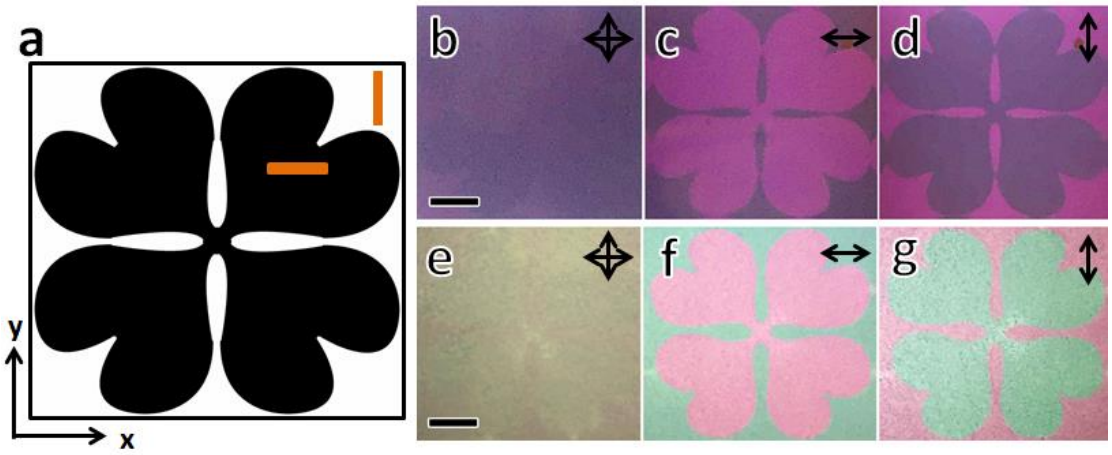

Figure 4.14 (a) Scheme showing the pattern of clover with magnetic plasmonic nanocomplex oriented along different directions; digital images of patterns with SiO_2-Au dimers and SiO_2-Au-Ag dimers under (b and e) ordinary light; (c and f) x-polarized light and (d and g) y-polarized light. The scale bar in (b-g) is 1.5 mm.

4.4 Conclusion

In summary, we reported dynamic tuning of the plasmonic excitation of Au and Au-Ag dimers by controlling their orientation relative to the incident lights for the first time. Such tuning is enabled by switching the substrate to anisotropic magnetic nanoparticles, whose orientation can be magnetically controlled. By tuning the direction of magnetic field, we are then able to control the excitation of plasmonic modes of Au dimers and Au-Ag dimers under the incidence of polarized light. The optical switching of Au and Au-Ag dimers shows colors with high contrast, which can be fixed in a hydrogel as polarization dependent color display.

4.5 References

1. Wang, H., Plasmonic refractive index sensing using strongly coupled metal nanoantennas: nonlocal limitations. *Sci. Rep.* **2018,** *8* (1), 9589.
2. Stockman, M. I., Nanoplasmonic sensing and detection. *Science* **2015,** *348* (6232), 287.
3. Mesch, M.; Metzger, B.; Hentschel, M.; Giessen, H., Nonlinear Plasmonic Sensing. *Nano Lett.* **2016,** *16* (5), 3155.
4. Millstone, J. E.; Hurst, S. J.; Métraux, G. S.; Cutler, J. I.; Mirkin, C. A., Colloidal Gold and Silver Triangular Nanoprisms. *Small* **2009,** *5* (6), 646.
5. Mark, W. K.; Naomi, J. H., Nanoshells to nanoeggs to nanocups: optical properties of reduced symmetry core–shell nanoparticles beyond the quasistatic limit. *New Journal of Physics* **2008,** *10* (10), 105006.
6. Nehl, C. L.; Liao, H.; Hafner, J. H., Optical Properties of Star-Shaped Gold Nanoparticles. *Nano Lett.* **2006,** *6* (4), 683.
7. Nikoobakht, B.; El-Sayed, M. A., Preparation and Growth Mechanism of Gold Nanorods (NRs) Using Seed-Mediated Growth Method. *Chem. Mater.* **2003,** *15* (10), 1957.
8. Sánchez-Iglesias, A.; Pastoriza-Santos, I.; Pérez-Juste, J.; Rodríguez-González, B.; García de Abajo, F. J.; Liz-Marzán, L. M., Synthesis and Optical Properties of Gold Nanodecahedra with Size Control. *Adv. Mater.* **2006,** *18* (19), 2529.
9. Jones, M. R.; Osberg, K. D.; Macfarlane, R. J.; Langille, M. R.; Mirkin, C. A., Templated Techniques for the Synthesis and Assembly of Plasmonic Nanostructures. *Chem. Rev.* **2011,** *111* (6), 3736.
10. Liu, N.; Liedl, T., DNA-Assembled Advanced Plasmonic Architectures. *Chem. Rev.* **2018,** *118* (6), 3032.
11. Dirix, Y.; Bastiaansen, C.; Caseri, W.; Smith, P., Oriented Pearl-Necklace Arrays of Metallic Nanoparticles in Polymers: A New Route Toward Polarization-Dependent Color Filters. *Adv. Mater.* **1999,** *11* (3), 223.
12. Murphy, C. J.; Orendorff, C. J., Alignment of Gold Nanorods in Polymer Composites and on Polymer Surfaces. *Adv. Mater.* **2005,** *17* (18), 2173.
13. Ng, K. C.; Udagedara, I. B.; Rukhlenko, I. D.; Chen, Y.; Tang, Y.; Premaratne, M.; Cheng, W., Free-Standing Plasmonic-Nanorod Superlattice Sheets. *ACS Nano* **2012,** *6* (1), 925.

14. Nikoobakht, B.; Wang, Z. L.; El-Sayed, M. A., Self-Assembly of Gold Nanorods. *J. Phys. Chem. B* **2000,** *104* (36), 8635.
15. Pérez-Juste, J.; Rodríguez-González, B.; Mulvaney, P.; Liz-Marzán, L. M., Optical Control and Patterning of Gold-Nanorod–Poly(vinyl alcohol) Nanocomposite Films. *Adv. Funct. Mater.* **2005,** *15* (7), 1065.
16. van der Zande, B. M. I.; Pagès, L.; Hikmet, R. A. M.; van Blaaderen, A., Optical Properties of Aligned Rod-Shaped Gold Particles Dispersed in Poly(vinyl alcohol) Films. *J. Phys. Chem. B* **1999,** *103* (28), 5761.
17. Wang, M.; Gao, C.; He, L.; Lu, Q.; Zhang, J.; Tang, C.; Zorba, S.; Yin, Y., Magnetic Tuning of Plasmonic Excitation of Gold Nanorods. *J. Am. Chem. Soc.* **2013,** *135* (41), 15302.
18. Lassiter, J. B.; Aizpurua, J.; Hernandez, L. I.; Brandl, D. W.; Romero, I.; Lal, S.; Hafner, J. H.; Nordlander, P.; Halas, N. J., Close Encounters between Two Nanoshells. *Nano Lett.* **2008,** *8* (4), 1212.
19. Esteban, R.; Borisov, A. G.; Nordlander, P.; Aizpurua, J., Bridging quantum and classical plasmonics with a quantum-corrected model. *Nat. Commun.* **2012,** *3*, 825.
20. Gunnarsson, L.; Rindzevicius, T.; Prikulis, J.; Kasemo, B.; Käll, M.; Zou, S.; Schatz, G. C., Confined Plasmons in Nanofabricated Single Silver Particle Pairs: Experimental Observations of Strong Interparticle Interactions. *J. Phys. Chem. B* **2005,** *109* (3), 1079.
21. Pérez-González, O.; Zabala, N.; Borisov, A. G.; Halas, N. J.; Nordlander, P.; Aizpurua, J., Optical Spectroscopy of Conductive Junctions in Plasmonic Cavities. *Nano Lett.* **2010,** *10* (8), 3090.
22. Scholl, J. A.; García-Etxarri, A.; Koh, A. L.; Dionne, J. A., Observation of Quantum Tunneling between Two Plasmonic Nanoparticles. *Nano Lett.* **2013,** *13* (2), 564.
23. Atay, T.; Song, J.-H.; Nurmikko, A. V., Strongly Interacting Plasmon Nanoparticle Pairs: From Dipole−Dipole Interaction to Conductively Coupled Regime. *Nano Lett.* **2004,** *4* (9), 1627.
24. Wang, M.; He, L.; Zorba, S.; Yin, Y., Magnetically Actuated Liquid Crystals. *Nano Lett.* **2014,** *14* (7), 3966.
25. Liu, Z.; Ma, R.; Osada, M.; Takada, K.; Sasaki, T., Selective and Controlled Synthesis of α- and β-Cobalt Hydroxides in Highly Developed Hexagonal Platelets. *J. Am. Chem. Soc.* **2005,** *127* (40), 13869.

26. Wang, X.; Feng, J.; Yu, H.; Jin, Y.; Davidson, A.; Li, Z.; Yin, Y., Anisotropically Shaped Magnetic/Plasmonic Nanocomposites for Information Encryption and Magnetic-Field-Direction Sensing. *Research* **2018,** *2018*, 13.
27. Xu, W.; Lyu, F.; Bai, Y.; Gao, A.; Feng, J.; Cai, Z.; Yin, Y., Porous cobalt oxide nanoplates enriched with oxygen vacancies for oxygen evolution reaction. *Nano Energy* **2018,** *43*, 110.

Chapter 5 Conclusion and Outlook

5.1 Conclusion of this Dissertation

Unconventional seed-mediated growth aims to create plasmonic nanostructures with tunable geometry and LSPR frequency. Although some excellent work has been done to control the growth pathway of plasmonic nanostructures, it still remains a challenge to create a second nanostructure on Au and Ag nanoparticles, due to the tight lattice match in between the seed and the growing material. In addition, previous work, which focuses on tuning the growth modes of nanostructures to VW mode, is lack of structural tunability. Either multiple islands or just a single island on the seed could be obtained. Moreover, dynamic LSPR tuning of anisotropic nanoparticles, for example, Au dimers, can lead to the development of new smart optical devices. It is important to design a method to not only prepare anisotropic nanoparticles with high purity, but also give orientation control to the nanostructures. This Dissertation has discussed our efforts in the development of unconventional seed-mediated growth strategies to nanostructures with tunable geometry and optical properties. In addition, dynamic tuning of the polarization dependent optical property of anisotropic plasmonic nanostructures has been studied and applied as the key component for data encryption. We are trying to shed some light on the development of nanotechnology.

By analyzing the growing pathways of Au nanocrystals on different metal surface, we developed a seed-mediated growth for creating secondary structures of Au on spherical Au seeds by modifying the seeds with Pt to create a mismatched surface for metal deposition. We also show that it is possible to tune the structure of the islands by

adjusting the reaction parameters. We show the influence of three key parameters to the geometry of the nanostructures: ligand-assisted oxidative ripening, interfacial strain energy, and surface diffusion of the metal precursors. By integrating all the important parameters, Au core-satellites, dimers, trimers and tetramers with tunable LSPR frequencies were obtained.

Analysis of the LSPR of Au dimers with different geometries by simulation show that the LSPR frequency is not only related to the overlapping distance of the two spherical nanoparticles, but also the curvature at the connection part. To better control the geometry of the nanostructures, we have developed a stepwise template-assisted seed-mediated growth method for the synthesis of rod-like plasmonic nanostructures. The synthesis requires using colloidal nanoparticle as substrates for the assembly of metal seeds, and precise control of the coverage of the metal seeds. Anisotropic growth of metal nanostructure is induced by partial passivizing the exposed area of the metal seeds. We show the successful synthesis of Au dimers and linear trimers with high purity and uniformity.

Based on the successful synthesis of Au dimers by using the stepwise template-assisted seed-mediated growth method, we developed dynamic tuning of the plasmonic excitation of Au and Au-Ag dimers by combining the plasmonic nanostructures with anisotropic magnetic nanoparticles. The orientation of the nanostructures relative to the incident lights could be controlled by applying a magnetic field. By tuning the direction of magnetic field, we are able to control the excitation of plasmonic modes of Au dimers and Au-Ag dimers under the incidence of polarized light. The optical switching of Au-Au

and Au-Ag dimers shows different colors with high contrast, which can be fixed in a hydrogel for information encryption.

5.2 Outlook and Future Work

There are still room for the development of unconventional seed-mediated growth to plasmonic nanostructures. In this section, we proposed the future research directions in several aspects.

First, as shown in Chapter 2, surface modification of the Au seed with Pt results in a shift of the growth mode of Au from the FM mode to the VW mode. This method should be applied to Au seeds with other geometries, for example, Au nanorods and Au nanoplates. By adjusting the reaction parameters, for example, the ligand-assisted oxidative ripening, Au islands with different structures should be expected to grow on the Au nanorod/nanoplate. It will be very interesting to study the location of Au islands on the Au nanorod/nanoplate. And the LSPR corresponding to different geometries is also worth to be studied. We can even change the material of the seed from Au to Ag, which has stronger LSPR to see if this method is applicable. In addition, as we presented in the discussion, the reason why Pt is an effective material to induce island growth is due to the lattice mismatch between Pt and Au. It will be very interesting to see if other materials of high lattice mismatch with Au, for example, Pd and Cu, have the same effect in seed-mediated growth. Moreover, from the application aspect, the nanoparticles may have potential applications in catalysis and sensing, due to the broad absorption and enhanced electric filed in the concave structure.

In Chapter 3, we discussed the successful synthesis of rod-like Au nanostructures by using SiO_2-Au@SiO_2 nanostructures as templates. The template is versatile for the synthesis of Ag, Pd, Cu_2O and polymers. There are more opportunities based on this template. Taking advantages of the difference in intrinsic chemical nature of SiO_2 and Au, selective deposition of other materials should be studied. In addition, this method results in precise control of the exposure of Au nanoparticles. This property can open up new research areas, which will focus on the influence of the exposed area of Au to the property of the nanocomposites. For example, by coating the SiO_2-Au@SiO_2 nanostructures with a layer of TiO_2, Au@TiO_2 can be obtained as a photocatalyst after removal of the SiO_2. The contact area of Au and TiO_2 can be controlled by adjusting the thickness of the SiO_2 layer to get a series of photocatalysts. These nanoparticles can be used to study the influence of contact area between Au and TiO_2 to the catalytic performance of the nanocomposites. Moreover, the amount of Au and the sizes of Au could also be adjusted to achieve better catalytic performance.

In a word, there's still plenty of room at the bottom. We look forward to exploring the beauty of nano-world, and contributing more to the development of nanotechnology.